Initiating polar growth in plant cells

Functions of RopGEFs during root hair development in *Arabidopsis thaliana*

Anna Denzler

2021

DISSERTATION

submitted to the

Combined Faculty of Natural Sciences and Mathematics

of the Ruperto Carola University Heidelberg, Germany

for the degree of

Doctor of Natural Sciences

Presented by

Anna Denzler, M.Sc.

Born in Mosbach, Germany

Oral examination: 12th May 2021

Initiating polar growth in plant cells

Functions of RopGEFs during root hair development in *Arabidopsis thaliana*

Referees:

Prof. Dr. Karin Schumacher

Prof. Dr. Guido Grossmann

ABSTRACT

Cell polarity is a prerequisite for the formation of distinct cell shapes, which allow different cell types to fulfill their specialized functions. In plants, the family of Rho-Of-Plants (ROPs) controls cellular pathways required for the initiation symmetry breaking including cytoskeleton rearrangements and targeted vesicle transport. Because of their decisive role in these fundamental processes, the spatio-temporal regulation of ROP activation is a delicate task. Efficient ROP activation is mediated by plant-specific ROP guanine nucleotide exchange factors (RopGEFs), which share the central Plant-specific Rop Nucleotide Exchanger (PRONE) domain. While the PRONE domain of RopGEFs is conserved, the flanking N- and C-termini are variable in sequence and do not contain known functional domains.

In this PhD thesis, selected RopGEFs were studied for their roles in the establishment of cell polarity during root hair development in the model plant *Arabidopsis thaliana*. I investigated the functions and regulation of RopGEFs, which were reported to polarize at the Root Hair Initiation Domain (RHID) early (RopGEF3, RopGEF14) or during the onset of polar growth (RopGEF4). In this thesis, I showed that the early polarizing RopGEF3 is crucial for early events including ROP2 recruitment and timing of growth initiation, while the late polarizing RopGEF4 is required for root hair elongation. Furthermore, the unrelated N-termini of early and late polarizing RopGEFs were characterized by exchange of N-termini in RopGEF3. I showed that the N-termini of early polarizing RopGEFs are functionally related in distinction to the N-terminus of RopGEF4. While N-termini of RopGEF3 and RopGEF14 promote RopGEF removal from the RHID, absence of these N-termini or presence of RopGEF4 N-terminus resulted in root hair phenotypes reminiscent of ROP overexpression as well as protein stabilization at the RHID. Cross-species and pairwise RopGEF N-termini sequence alignments combined with *in silico* prediction for phosphorylation sites in the RopGEF3 N-terminus revealed promising candidate amino acid residues possibly being involved in RopGEF3 regulation at the RHID. Taken together, in this PhD thesis evidence is provided for a putative task-sharing mechanism of early and late polarizing RopGEFs during root hair development as well as for the involvement of RopGEF N-termini in RopGEF protein abundance regulation at the RHID most likely involving regulatory phosphorylations.

ZUSAMMENFASSUNG

Zellpolarität ist die Voraussetzung für die Bildung verschiedener Zellformen, die es unterschiedlichen Zelltypen ermöglichen, ihre speziellen Funktionen zu erfüllen. In Pflanzen kontrolliert die Familie der Rho-of-Plants (ROPs) die zellulären Prozesse, die für den Symmetriebruch erforderlich sind, einschließlich der Reorganisation des Zytoskeletts und des gezielten Vesikeltransports. Aufgrund ihrer entscheidenden Rolle in diesen grundlegenden Prozessen, ist die Regulation der räumlich-zeitlichen ROP-Aktivierung eine empfindliche Aufgabe. Die effiziente Aktivierung von ROPs wird durch pflanzenspezifische ROP Guanin-Nukleotid-Austauschfaktoren (RopGEFs) vermittelt, die die zentrale pflanzenspezifische ROP-Nukleotid-Austauscher (PRONE) Domäne gemein haben. Während die PRONE-Domäne konserviert ist, sind die flankierenden N- und C-Termini variabel in ihrer Sequenz und enthalten keine bekannten funktionellen Domänen.

In dieser Doktorarbeit wurden ausgewählte RopGEFs auf ihre Rollen bei der Etablierung von Zellpolarität während der Wurzelhaarentwicklung in der Modellpflanze *Arabidopsis thaliana* untersucht. Ich untersuchte die Funktionen und Regulation jener RopGEFs, für die gezeigt wurde, dass sie früh (RopGEF3 und RopGEF14) oder spät, während des Beginns des polaren Wachstums, (RopGEF4) an der Wurzelhaarinitiationsdomäne (RHID) polarisieren. Ich konnte zeigen, dass das früh polarisierende RopGEF3 für frühe Ereignisse wie die Rekrutierung von ROP2 und dem Timing der Wachstumsinitiation entscheidend ist, während das spät polarisierende RopGEF4 für die Wurzelhaarverlängerung erforderlich ist. Darüber hinaus wurden die wenig verwandten N-termini der früh und spät polarisierenden RopGEFs durch den Austausch von N-termini in RopGEF3 funktionell charakterisiert. Ich konnte zeigen, dass die N-Termini der früh polarisierenden RopGEFs im Unterschied zu dem N-Terminus von RopGEF4 funktionell verwandt sind. Die N-Termini von RopGEF3 und RopGEF14 fördern den Abtransport von RopGEF aus der RHID. Dagegen führte das Fehlen dieser N-Termini oder die Anwesenheit des N-Terminus von RopGEF4 zu Wurzelhaarphänotypen, die an die Überexpression von ROP erinnern, sowie zur Stabilisierung von RopGEF an der RHID. Speziesübergreifende und paarweise Abgleichungen von RopGEF N-Termini-Sequenzen in Kombination mit *in silico* Vorhersagen für Phosphorylierungsstellen im N-Terminus von RopGEF3 gaben vielversprechende Aminosäurereste-Kandidaten preis, die möglicherweise an der Regulation von RopGEF3 an der RHID beteiligt sind. Zusammenfassend werden in dieser Doktorarbeit Belege für einen mutmaßlichen Mechanismus zur Aufgabenverteilung unter früh und spät polarisierenden RopGEFs während der Wurzelhaarentwicklung geliefert. Zudem wurden Belege erbracht, die auf die Beteiligung der N-Termini von RopGEFs an der Regulierung der RopGEF-Proteinmenge an der RHID hinweisen, die höchstwahrscheinlich regulatorische Phosphorylierungen involviert.

PUBLICATION & CONTRIBUTIONS

Part of the data presented in this thesis is published in the following publication:

Denninger, P., Reichelt, A., Schmidt, V. A. F., Mehlhorn, D. G., Asseck, L. Y., Stanley, C. E., Keinath N. F., Evers J. F., Grefen C. and Grossmann, G. (2019). Distinct RopGEFs Successively Drive Polarization and Outgrowth of Root Hairs. *Current Biology*, *29*(11), 1854-1865.e5. https://doi.org/10.1016/j.cub.2019.04.059

Parts of this thesis were done with the contribution of co-workers, which are specified in the following:

Dr. Philipp Denninger cloned the ROP2 rescue construct used for the generation of the *rop2/4* + mCitrine-ROP2 rescue line (Fig. 3) as well as the constructs for mCitrine-RopGEF3, mCitrine-RopGEF4 and mCitrine-RopGEF14 (genomic) used for RopGEF expression in *rop2/4* mutant and *ropgef3-1* mutant background (Fig. 9). Furthermore, he generated the stable *Arabidopsis thaliana* line expressing mCitrine-RopGEF3 inducibly and mTurquoise-ROP2 under its endogenous promoter (Fig. 8).

Dr. Milan Župunski wrote the R script used for the ANOVA test (see section 4.2.3.5)

CONTENTS

I. INTRODUCTION

Polarity is a basic feature of all living systems and implicates the presence of at least two sides with different characteristics. It becomes most obvious when macroscopically visible differences in shape and structure prevail at the distinct poles. For example, plants usually exhibit morphological polarity along their growth axis with the green shoot at one end and the root at the other end. Polarity on such a scale largely relies on polarization of smaller entities, such as organs, tissues and – as the smallest living units – single cells. The polarization of cells, a feature referred to as cell polarity, involves the asymmetric distribution of cellular structures and functions along a spatial axis within a cell.

A prominent example from the plant kingdom demonstrating the relevance of cell polarity is the plant mutant *gnom*. In this mutant, the first cell division of the zygote cannot happen asymmetrically due to disturbed vesicle transport to the cell poles resulting in impaired cell polarity. As a consequence, the asymmetry along the shoot-to-root axis cannot be established and the resulting plants can develop strong phenotypes such as a ball- or cone-shaped overall structure without distinct leaves or roots (Mayer *et al.,* 1993; Vroemen *et al.,* 1996; Geldner *et al.,* 2003). This example shows that the unsuccessful polarization of one individual cell can impact the whole organism.

Obviously, cell polarity is not only crucial for plants; instead, it represents a common feature of almost all eukaryotic cells and is considered a prerequisite for numerous vital cellular processes including cell differentiation, cell migration and directed cell growth (Drubin & Nelson, 1996; Muroyama & Bergmann, 2019). There are many examples of specialized cell types within multicellular organisms, which require distinct polar morphologies to fulfill their biological functions (Nelson, 2003): Neurons, which have a cell body at the one end and form synapses with other neurons at the other end in order to propagate neurological signals over long distances; migrating cells such as immune cells require cell polarity to establish a leading edge, which allows them to push forward; epithelial cells, which are integrated into a specific tissue on one side providing cell-cell-contacts, while the other cell pole is exposed to the surface and requires different cellular functions. In the plant kingdom, polar growth of pollen tubes is required for the delivery of sperm cells to egg cells enabling fertilization and plant reproduction. Root hairs, which penetrate the soil to promote nutrient uptake, also rely on polarized growth. These examples show that cell polarization manifests in very diverse shapes, which allow the development of highly specialized cell types. How are these various

cellular morphologies created? Which cellular mechanisms enable and regulate shaping of these different cell types as it is needed for their distinct biological functions?

Despite this variety in morphology, the molecular mechanisms establishing and maintaining cell polarity are shared among eukaryotes. The establishment of cell polarity includes three stages: (1) Definition of the site of symmetry breaking upon the perception of an external or internal polarity cue, (2) amplification of the signal and (3) signal propagation and implementation (Fig. 1; Drubin and Nelson, 1996; Asnacios & Hamant, 2012). The cue to establish a new polarity axis can be of different natures in different contexts.For example, the cue can be a landmark protein like it is found at bud scars in yeast, a chemical stimulus such as hormones or other chemoattractants, a mechanical cue like tension gradients (Asnacios & Hamant, 2012) or an electrochemical signal such as intracellular ion gradients (Campetelli *et al.,* 2012). Upon perception of the cue at a specific site of the plasma membrane, the polarity signal is amplified by local accumulation and activation of small guanosine triphosphatases (GTPases) of the Rho-type family.

Rho GTPases and their regulators are conserved and considered central regulators of cell polarization throughout the eukaryotic kingdom (Etienne-Manneville, 2004; Craddock *et al.,* 2012; Asnacios & Hamant, 2012). As molecular switches, Rho GTPases exist in two conformational states: In the inactive state, guanosine diphosphate (GDP) is bound and in the active state, GDP is exchanged by guanosine-5'-triphosphate (GTP; Fig. 1). The cycling between these two states is facilitated by the interaction with GTPase-regulating factors. Guanine nucleotide exchange factors (GEF) promote the transition from the inactive to the active state by accelerating GDP dissociation from the GTPase allowing a new round of GTP binding. Once activated, Rho GTPases adopt a specific conformation enabling them to interact with effector proteins, which regulate required downstream pathways to establish cellular polarity. These include among others cytoskeletal reorganization, membrane trafficking and polarity-enforcing feedback loops. Inactivation of Rho GTPases involves the hydrolysis of the bound GTP, an intrinsically slow process. GTPase-activating proteins (GAPs) accelerate GTP hydrolysis, which induces another conformational switch and eventually the inactivation of the GTPase (Vetter & Wittinghöfer, 2001; Schmidt & Hall, 2002; Etienne-Manneville & Hall, 2002). The third class of GTPase-regulating proteins comprises guanine nucleotide-dissociation inhibitors (GDIs). Rho GTPases with certain C-terminal lipid modifications can interact with GDIs, which sequester inactive GTPases in the cytosol by burying the hydrophobic membrane anchor and inhibition of nucleotide release (Vetter & Wittinghöfer, 2001; Dovas & Couchman, 2005).

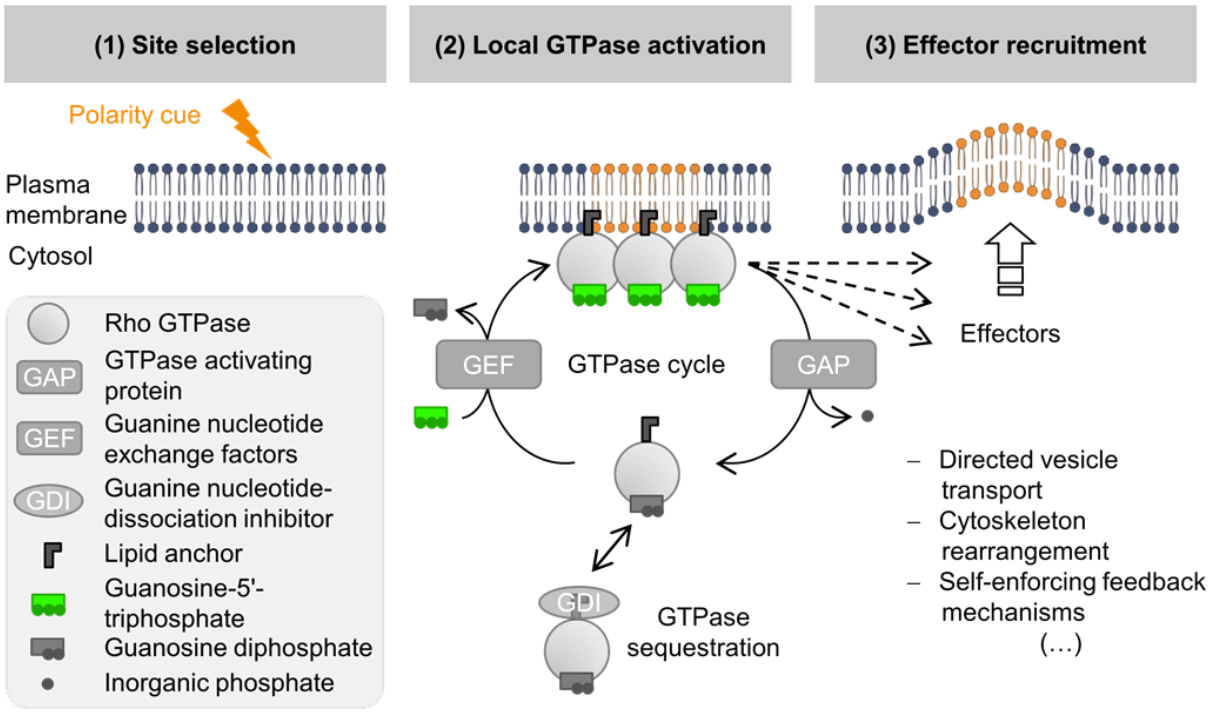

Fig. 1: Phases of cell polarity establishment and Rho GTPase cycle. The establishment of a new polarity axis starts with the perception of a polarity cue, which defines the site of the future symmetry breaking. In a next step, key regulators of cell polarity, the Rho-type GTPases, are recruited to the selected site. Rho GTPases cycle between an active, GTP-bound and an inactive, GDP-bound state. The transition between these two states is accelerated by the interaction with GEFs and GAPs. GEFs activate Rho GTPases by acceleration of GDP dissociation from the inactive GTPase. In the active state, Rho GTPases interact with effector proteins regulating downstream pathways required for the establishment of cell polarity. GAPs promote GTP hydrolysis rendering the GTPase inactive. Inactive GTPases with lipid anchors interact with GDIs resulting in sequestration of the inactivated GTPases in the cytosol.

In the present thesis, GTPase-activating GEFs were the central subject of research. The aim of this project was to understand the molecular mechanisms underlying GEF function and regulation in cell polarity establishment with focus on early events preceding GTPase activation. This process was studied in root hairs of the model plant *Arabidopsis thaliana*. Therefore, essential information on cell polarity and involved molecular players in plants is provided in the next section.

1.1 Cell polarity in plants

Establishing polarity on both, the tissue as well as the cellular level, is of particular importance for plants due to their sessile lifestyle as well as the presence of the cell wall. The immobility of plants demands the constant adaptation to varying environmental conditions involving the continuous regulation of plant growth and development. The stiff cell wall limits cell migration resulting in the necessity to realize tissue patterning differently than animals. These plant-specific conditions led to the independent evolution of polarity regulatory mechanisms in multicellular plants (Dettmer & Friml, 2011; Kania *et al.,* 2014). On the scale of the plant as a whole, apical/ basal polarity and specific tissue patterning is largely coordinated by the plant hormone auxin (Berleth & Sachs, 2001; Kleine-Vehn & Friml, 2008;

Leyser, 2011). The differential auxin distribution throughout the plant, which enables the coordination of morphogenesis on different levels and in various tissues is mainly mediated by polarly localized auxin transporters (Vieten *et al.,* 2007; Grunewald & Friml, 2010). The prominent role in directing auxin fluxes is assigned to auxin efflux carriers of the PIN-FORMED (PIN) protein family (Gälweiler *et al.,* 1998; Luschnig *et al.,* 1998; Chen *et al.,* 1998; *Wiśniewska et al.,* 2006; Petrášek *et al.,* 2006). Depending on the cell type and developmental stage, PIN proteins are polarly deposited at the apical, basal or lateral plasma membrane of the cells (Kleine-Vehn & Friml, 2008) thereby regulating local auxin levels and providing a quantitative positional cue, which translates into specific developmental programs (e.g. Dubrovsky *et al.,* 2008). The best-studied auxin response is the transcriptional regulation of auxin-responsive genes involving the de-repression of these genes by the auxin-dependent degradation of responsible translational repressors. Depending on the context, downstream target genes are involved in different developmental processes including embryo development, root development, stress responses, stomata development and more (Salehin *et al.,* 2015).

It is well established that auxin is central to almost all processes involved in plant development and growth, even though the complex network of auxin-related processes is clearly not characterized in every detail yet. Despite the increasing evidence for auxin-mediated regulation of polarization also on the level of single cells, the specific molecular mechanisms by which auxin contributes to cell morphogenesis and cell polarity remain largely obscure (Leyser, 2018). However, this field of research is being investigated actively providing increasing insights into the molecular nature of these processes.

1.1.1 Rho-of-Plants (ROPs) and ROP interactors

Hazak *et al.* (2010) revealed a molecular link between auxin and the subcellular polarization of PIN proteins via Rho-of-Plants GTPases (ROPs), which are well established master regulators of cell morphogenesis and polar growth in plant cells. This unique subfamily of Rho-type GTPases, which is most similar to the animal Cdc42 and Rac subfamilies (Nagawa *et al.,* 2010), consists in *Arabidopsis thaliana* (*At*) of 11 functionally diverse family members (Vernoud *et al.,* 2003). Major features of ROP proteins are the catalytic G-domain at the N-terminus, which is required for nucleotide and effector binding as well as GTP hydrolysis, and the C-terminal hypervariable region (HVR), which contains posttranslational lipid modifications required for ROP membrane association. Based on C-terminal differences in sequence and modifications, ROPs are grouped into type I ROPs (*At*ROP1-8) and type II ROPs (*At*ROP9-11). Type I ROPs are prenylated at a C-terminal cysteine, which is a prerequisite for RhoGDI interaction, while type II ROPs are S-acylated (Zheng & Yang, 2000; Feiguelman *et al.,* 2019).

Similar to animal Rho-type GTPases, ROPs are negatively regulated by guanine nucleotide dissociation inhibitors (GDIs) and GTPase-activating protein (GAPs). Plant RopGAP proteins are unique, because besides the GAP domain they contain a Cdc24/ Rac-Interactive Binding (CRIB) motif, which was found to be specific for Rac and Cdc42 effectors in animals (Hoffman & Cerione, 2000). In plants, the CRIB motif in RopGAPs was shown to be involved in the regulation of their GAP activity and their binding affinity to ROPs (Borg *et al.,* 1999; Wu *et al.,* 2000). Besides RopGAPs, plants possess a second type of GAP proteins, which are known as ROP1 ENHANCER (REN) GAPs. RENGAPs are characterized by a N-terminal Pleckstrin Homology (PH) domain (Hwang *et al.,* 2008), which contributes to membrane association by binding to phosphoinositides and is found among others in animal RhoGEFs and RhoGAPs (Lemmon *et al.,* 2002). Plant RhoGDIs regulate ROPs with C-terminal prenylation by cytosolic sequestration and share high similarity with animal RhoGDI. In *Arabidopsis thaliana*, three RhoGDI homologs are encoded including RhoGDI1 (also known as SUPERCENTIPEDE1 (SCN1)), RhoGDI2a and RhoGDI2b (Brembu *et al.,* 2006). Positive regulators of ROP activity are guanine nucleotide exchange factors (GEFs), two types of which can be found in plants: The plant-specific RopGEFs, which contain a highly conserved Plant-specific ROP Nucleotide Exchanger (PRONE) domain (Berken *et al.,* 2005; Gu *et al.,* 2006), are central for this thesis and therefore introduced in detail in section 1.2. In *Arabidopsis thaliana*, SPIKE1 (SPK1) is the only representative of the second type of plant RhoGEFs and is a homolog of the animal Dock family RhoGEFs (Qiu *et al.,* 2002; Basu *et al.,* 2008). These lack the Diffuse B-cell lymphoma (Dbl) homology (DH) domain, which is usually found in animal Dbl-related RhoGEFs. Instead, SPK1 and Dock RhoGEFs are characterized by the conserved Dock homology region (DHR) 1 and 2, which provide GEF activity (Rossmann *et al.,* 2005; Basu *et al.,* 2008).

Despite regulating similar cellular pathways, no homologs of animal effector proteins of Rho-type GTPases are found in plants. Instead, plants evolved specific ROP effector proteins, which include the following two protein families: The ROP-INTERACTIVE CRIB MOTIF-CONTAINING (RIC) proteins (Wu *et al.,* 2001) and INTERACTOR OF CONSTITUTIVELY ACTIVE ROP1 (ICR1/ ICR1-like) proteins (Lavy *et al.,* 2007). The 11 members of the RIC protein family share the central CRIB motif, which is required for the interaction with active, GTP-bound ROPs; but besides this exhibit only little sequence similarity. Also, subcellular localization and functions of RICs appear to be distinct (Wu *et al.,* 2001; Gu *et al.,* 2005; Fu *et al.,* 2005). Well established is the link of certain RICs to cytoskeletal rearrangements. For example, in pollen tubes, RIC3 and RIC4, both ROP1 targets, act antagonistically to regulate actin dynamics during polar growth (Gu *et al.,* 2005). The jigsaw puzzle morphology of leaf pavement cells is realized by the concerted action of two pathways involving ROP2/4-RIC4 for actin coordination in lobes, while ROP6-RIC1 organize microtubules in indentations (Fu *et*

al., 2005; Fu *et al.,* 2009). ICR1 is a representative of the second ROP effector protein family and is a coiled-coiled domain protein. It was identified as a ROP effector as it preferentially interacted with constitutively active ROP. Due to its interaction with the exocyst complex subunit SEC3A, ICR1 is proposed to act as scaffold in targeted vesicle trafficking mediating protein recruitment to a polar plasma membrane domain (Lavy *et al.,* 2007). Indeed, for PIN1 it was shown that ICR1 loss results in reduced polar localization and membrane association providing a link between cellular polarity, ROPs and auxin transport as mentioned above (Hazak *et al.,* 2010; Hazak *et al.,* 2014).

Similar to other Rho-type GTPases, ROPs are crucial in a multitude of cellular processes in which they act as molecular switches (Fig. 1) including the establishment and maintenance of cell polarity (Yang, 2008). More specifically, ROP1 to ROP6 were implicated in cell polarity establishment (Yang, 2002). Polar growth involving these ROP GTPases has been studied well in several plant model systems such as leaf pavement cells, guard cells and tip-growing cells such as pollen tubes and root hairs (Yang, 2008). In this PhD thesis, *Arabidopsis thaliana* root hairs were the model system of choice to study the molecular mechanisms underlying cell polarity establishment. Therefore, these structures and their unique features rendering them a valuable cell polarity model system are introduced in more detail in the following section.

1.1.2 Root hairs as model system to study cell polarity establishment

Arabidopsis thaliana root hairs are cylindrical protrusions from root epidermal cells growing perpendicular to the primary root (Fig. 2). Root hair-forming cells are referred to as trichoblasts in distinction to root epidermal cells, which do not grow such structures, called atrichoblasts (Peterson & Farquhar, 1996). Per trichoblast one root hair grows out, which on average has a diameter of approximately 10 µm and can reach a length of 1 mm or more depending on growth conditions (Grierson *et al.,* 2014). A major function of root hairs is to enlarge the root surface area and to invade a larger volume of soil thereby promoting nutrient and water uptake (Jungk, 2001). Furthermore, root hairs are thought to improve plant anchorage in the soil (De Baets *et al.,* 2020) and to contribute to plant-microbe interactions (Mercado-Blanco & Prieto, 2012; Grierson *et al.,* 2014; Schmidt & Gaudin, 2017). As model system, root hairs provide several advantages not only for the study of cellular processes related to cell polarity (Schiefelbein & Somerville, 1990). Being part of the root epidermis, trichoblasts and therefore also root hairs are easy to access for microscopic visualization as well as experimental treatments. Furthermore, root hairs are present early on during plant development and are not essential rendering corresponding genetic approaches less complicated.

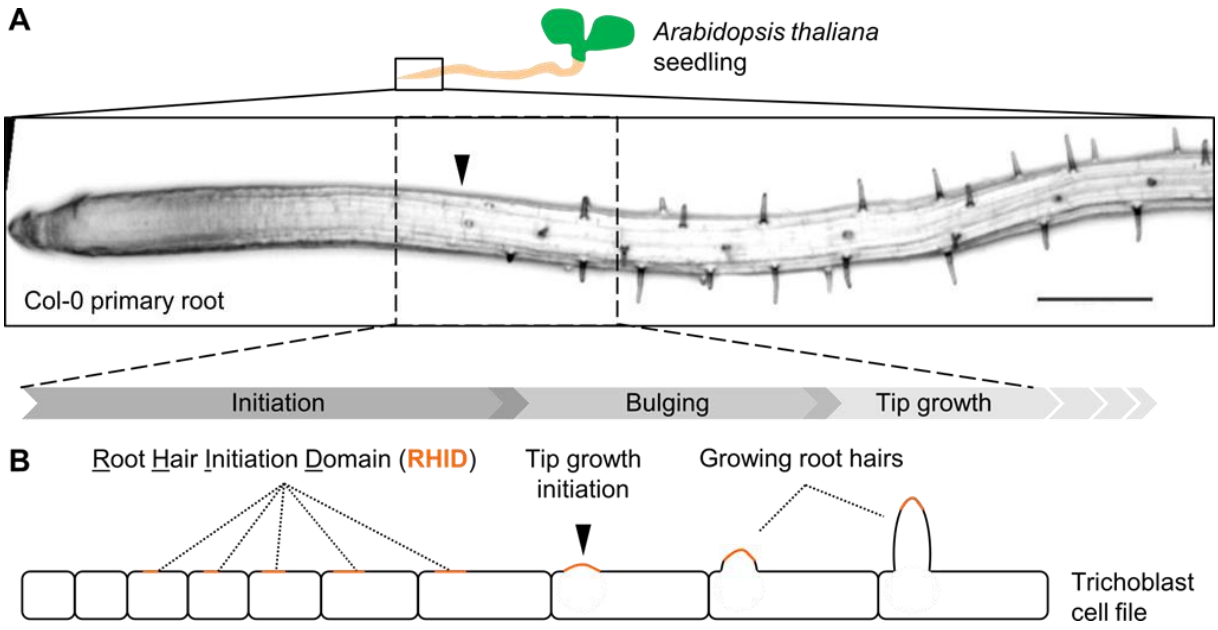

Fig. 2: *Arabidopsis thaliana* as model system to study cell polarity. (A) Scheme of an *Arabidopsis thaliana* seedling with green cotyledons and brownish primary root. Box with black outlines highlights the tip of the primary root. The box below shows a stereoscopic image of *Arabidopsis thaliana* wild type (Colambia 0 ecotype (Col-0)) primary root tip with bulges and root hairs. The arrow head indicates the first macroscopically visible bulge. Box with black, dotted outlines highlights the region of interest, in which root hair development starts. Phases of root hair development are indicated. Scale bar, 250µm, (B) Schematic representation of a hair cell (trichoblast) cell file including young, unelongated trichoblasts (close to primary root tip) and more differentiated trichoblasts with specified RHID, bulges or growing root hairs (towards shoot).

The feature making root hairs a particular attractive model system to study cell polarity is the progressive trichoblast differentiation and, consequently, the progressive development of these structures. Trichoblasts are organized in cell files, which represent a developmental time line including young, unelongated trichoblasts to more differentiated trichoblasts with polarly growing root hairs (Fig. 2B). This feature allows the simultaneous observation of all stages of root hair development in one individual root. In addition, the position of the future root hair in trichoblasts is highly uniform and therefore predictable (Grierson *et al.,* 2014). The site at the plasma membrane, where the future root hair emerges, is called the Root Hair Initiation Domain (RHID) and is marked by the polarization of involved ROPs already in early stages before polar growth becomes macroscopically visible (Fig. 2B; Molendijk *et al.*, 2001; Jones *et al.*, 2002; Stanislas *et al.*, 2015; Denninger & Reichelt *et al.*, 2019). In the following section, an overview over the three phases of root hair development including initiation, bulging and tip growth is provided. The focus of this PhD project was set to early events during root hair development prior to ROP activation, which includes site specification, RHID establishment and maintenance – processes, for which the underlying molecular mechanisms remain to be clarified.

1.1.3 Root hair development: A brief outline

In *Arabidopsis thaliana*, the cell fate specification of root epidermal cells is dependent on the position of these cells relative to the underlying cortex cells. If root epidermal cells contact two underlying cortex cells (H position; (root) Hair cell), the intrinsic root hair developmental program is activated and these cells will become trichoblasts. If root epidermal cells interact with a single cortex cell (N position; Non-hair cell), root hair genes cannot be expressed due to transitional repression, which determines the atrichoblast cell fate (Schiefelbein, 2000; Grierson *et al.,* 2014; Cui *et al.,* 2017).

After cell fate commitment, trichoblasts start differentiating and root hair development begins. The stages of root hair development include the initiation phase, the bulging phase and the final tip growth phase (Fig. 2B). During root hair initiation, trichoblasts elongate by diffuse growth and the site of the future outgrowth is defined by local accumulation of ROP2 and ROP4 as well as ROP6, which are considered key regulators of root hair development. The RHID specification by ROPs happens several cell stages before bulge formation and was the earliest molecular indication of root hair initiation for several years (Molendijk *et al.*, 2001; Jones *et al.*, 2002; Stanislas *et al.*, 2015). Recent work from the Grossmann laboratory revealed that ROP-regulating RopGEFs precede ROP polarization at the RHID and showed that one of the early polarizing RopGEFs, RopGEF3, is involved in ROP2 recruitment to the RHID (Denninger & Reichelt *et al.*, 2019). The finding that RopGEF3 acts as positional cue for ROP2 polarization during root hair initiation challenges the model proposing that ROPs polarize spontaneously in trichoblasts under certain conditions including a cellular auxin gradient (Payne & Grierson, 2009). Furthermore, this finding is particularly striking as it implicates additional functions for RopGEFs in cell polarity establishment – besides their well-established role as ROP-activating proteins –, which are required earlier during root hair development as anticipated before. GEF-mediated GTPase recruitment was also reported in other organisms such as *Saccharomyces cerevisiae*, in which the site of the future bud is defined by the transmembrane landmark protein AXIAL BUDDING (Axl) 2 (Roemer *et al.,* 1996). Interaction of the land mark protein with the RhoGEF BUD SITE SELECTION PROTEIN 5 (Bud5) locally activates the GTPase RAS-RELATED PROTEIN 1 (Rsr1). Activated Rsr1 in turn recruits CELL DIVISION CONTROL PROTEIN 24 (Cdc24p), the RhoGEF for the yeast key polarity regulator Cdc42p (Bender & Pringle, 1989; Adams *et al.,* 1990; Park *et al.,* 1993; Kang *et al.,* 2001; Chiou *et al.,* 2017)

Bulge formation is preceded by an increase of the pH of the cell wall at the future root hair site resulting in local acidification, which is thought to promote expansin activation and therefore cell wall relaxation (Bibikova *et al.,* 1998). During root hair initiation and bulge formation, the growth machinery needs to be assembled at the site of the future root hair to

allow subsequent transition to the phase of polar growth. The regulatory molecular network required for directed growth of root hairs is complex and involves the association of further ROP regulators and ROP effectors with the RHID (Denninger & Reichelt *et al.*, 2019). The type of growth resulting in the elongation of root hairs is called tip growth and can also be observed in pollen tubes and fungal hyphae. Tip growth is a rapid form of cell expansion, which is characterized by the polarization of the cytoplasm containing all cellular constituents of the growth machinery to the apex of the growing structure. The regulatory network of tip growth involves cytoskeleton dynamics, delivery of new material to the apex of the growing structure via targeted vesicle transport, a tip-focused calcium (Ca^{2+}) gradient, production of reactive oxygen species (ROS) and regulation of extracellular pH (Grierson *et al.,* 2014). Together, these pathways enable local membrane and cell wall expansion, which is required to ensure cell integrity during the rapid growth process.

1.2 Regulating the master regulators – RopGEFs activate ROPs

Rho guanine nucleotide exchange factors (RhoGEFs) promote activation of Rho-type GTPases by facilitating the switch from the inactive, GDP-bound to the active, GTP-bound state of the GTPase (Fig 1). GEFs bind inactivated GTPases forming a trimeric complex of GEF-GTPase-GDP. This interaction decreases nucleotide affinity and therefore facilitates nucleotide dissociation, which would otherwise be a slow process. The result is a binary GEF-GTPase complex, which is more stable than the trimeric complex. Subsequent GTP binding to the GTPase induces a conformational switch, which releases the GEF and allows effector protein binding (Vetter & Wittinghofer, 2001). Considering the outstanding role of Rho GTPases in various crucial cellular processes including signal transduction, regulation of cytoskeletal rearrangements and vesicle transport as well as cell polarity, GEF function and regulation is consequently of particular importance to ensure the spatiotemporal control of Rho GTPase activation.

1.2.1 Plant RopGEFs vs. animal RhoGEFs: A comparison of protein features and regulatory mechanisms

In animals, two major families of RhoGEFs are present including the Diffuse B-cell lymphoma (Dbl)-related RhoGEFs and the DEDICATOR OF CYTOKINESIS (DOCK) family RhoGEFs (Rossman *et al.,* 2005; Bos *et al.,* 2007). In the following, the Dbl-related RhoGEFs will be briefly introduced, because they constitute the largest group of RhoGEFs (70 family members in human and numerous conserved orthologs in other species (Cook *et al.,* 2014) including Cdc24p, which serves as GEF for the yeast key polarity regulator Cdc42p (Miller *et al.,* 2020)), in order to allow the comparison between predominant animal RhoGEFs and plant RopGEFs. Dbl-related RhoGEFs are characterized by the presence of Dbl Homology (DH) domains, which mediate GDP-GTP exchange activity. The DH domain comprises

~200 amino acids. C-terminal from the DH domain, ~100 amino acid Pleckstrin Homology (PH) domains are found, which were initially thought to contribute to RhoGEF membrane targeting (Cerione & Zheng, 1996). However, phosphoinositide interactions of PH domains of Dbl-related RhoGEFs alone were shown to be insufficient for membrane targeting (Snyder *et al.,* 2001). Instead, the PH domains are proposed to assist DH domains to regulate GEF function and to provide interaction sites. Regions outside the conserved DH-PH array of Dbl-related RhoGEFs are more variable and often contain additional protein domains required for specific cellular functions (Rossman *et al.,* 2005).

In plants, no homologs of animal Dbl-related RhoGEFs are present (Vernoud *et al.,* 2003). Instead, a unique and plant-specific RhoGEF protein family was identified in two independent studies each using a yeast-two-hybrid approach with mutant ROP4 and ROP1 as baits, respectively (Berken *et al.,* 2005; Gu *et al.,* 2005). These plant RhoGEFs were referred to as RopGEFs and constitute a protein family of 14 members in *Arabidopsis thaliana*. The shared feature of RopGEFs is the large and highly conserved central domain, the so-called Plant-specific Rop Nucleotide Exchanger (PRONE) domain, which is necessary and sufficient for the nucleotide exchange activity. With a length of ~380 amino acid residues, the active domain of RopGEFs is almost twice as long as the classical DH domains in animal RhoGEFs. Based on sequence conservation, the PRONE domain can be divided into three subdomains with highest conservation (S1-3). These subdomains are connected via more variable stretches of ~20 amino acid residues (Berken *et al.,* 2005; Gu *et al.,* 2005). Crystal structure analyses of the PRONE domain of RopGEF8 in complex with ROP4-GDP revealed that the overall structure is largely α-helical (13 α-helices in total, which are divided into structural subunits 1 and 2), except for one β-arm, which stood out from the remaining structure. In addition, the analyses revealed that PRONE8 is a constitutive dimer, which was found to be essential for the nucleotide exchange activity as mutation of a conserved leucine at the dimerization interface largely abolished GEF activity (Thomas *et al.,* 2006; Thomas *et al.,* 2007). A study in rice provided evidence that RopGEFs can also heterodimerize, which might provide another regulatory layer of ROP signaling (Akamatsu *et al.,* 2015). Interestingly, homo- and hetero-oligomerization of GEF domains was also reported for RhoGEFs in animals and is proposed to be a fundamental feature of GEF function (Thomas *et al.,* 2007). For example, the first identified mammalian Dbl-related RhoGEF Dbl (Hart *et al.,* 1991) was shown to oligomerize via its GEF activity-mediating DH domain preferentially in a homotypic manner (Zhu *et al.,* 2001). Similarly, the yeast RhoGEF Cdc24p was reported to homo-oligomerize; interestingly, in this case oligomerization was reported not to directly affect GEF activity *in vitro*, but to be implicated in the subcellular localization of Cdc24p, which effectively reduced GTPase activation *in vivo* (Mionnet *et al.,* 2008).

N- and C-terminal regions flanking the central PRONE domain in RopGEFs are highly variable and lack any known functional domains, motifs or homologous sequences found in other species (Berken *et al.,* 2005; Gu *et al.,* 2006). However, there is evidence that these regions might have regulatory functions. By assessing the GEF activity of N- and C-terminal truncations of RopGEF1 *in vitro*, Gu and colleagues (2006) revealed a GEF activity inhibitory mechanism, which is primarily mediated by the C-terminus. In this study the C-terminus was proposed to inhibit GEF activity by intramolecular binding to the PRONE subdomain S3; a mechanism, which was further supported by independent studies. For instance, similar observations were made *in vivo* showing that C-terminal truncation of RopGEF12 induced ROP overexpression-like phenotypes in pollen in contrast to the full-length version (Zhang & McCormick, 2007). Furthermore, RopGEF7, which is expressed in cells of the quiescent center, was shown to induce seedling phenotypes only upon C-terminal truncation (Chen *et al.,* 2011). Unlike the previous examples, Huang *et al.* (2013) found that root hair phenotypes induced by overexpression of RopGEF10 were reduced upon C-terminal truncation. Also for the N-terminus GEF activity-modulating roles have been proposed. RopGEF1 N-terminus was reported to assist in the autoinhibitory mechanism mediated by the C-terminus as N-terminus removal partly activated RopGEF1 (Gu *et al.,* 2006). However, for the N-terminus of RopGEF12 a GEF activity-promoting function was proposed as PRONE12 alone caused a milder phenotype than the C-terminal truncation of RopGEF12 containing both the N-terminal region as well as the PRONE domain of RopGEF12 (Zhang & McCormick, 2007). Deletion of the N-terminus of *Medicago truncatula* (*Mt*) RopGEF2 caused shorter and thicker root hairs similar to constitutively active *Mt*ROPs. Additionally, increased ROP binding affinities were determined for N-terminally deleted *Mt*RopGEF2 indicating a negative impact of *Mt*RopGEF2 N-terminus on ROP binding and therefore GEF activity (Riley *et al.,* 2011). Taken together, there is substantial evidence for a GEF activity-modulating role of the N- and C-terminal regions, which seem to be distinct for different RopGEFs. However, besides their impact on GEF activity, possible additional roles, such as involvement in RopGEF protein regulation and subcellular localization, are not well understood.

A similar mode of regulation involving intramolecular inhibitory interactions between regions outside the conserved GEF domain and these active domains was also reported for animal RhoGEFs. Both, N- and C-terminal truncations were reported to render many RhoGEFs constitutively active (Schmidt & Hall, 2002). Well known is the autoinhibition mechanism of the RhoGEF Vav as both the autoinhibited as well as the active DH domain was structurally analyzed (Aghazadeh *et al.,* 2000). This study showed that the N-terminus of Vav, which includes a conserved tyrosine, interacts with the DH domain. Tyrosine phosphorylation disturbs this intramolecular interaction resulting in a release of the N-terminus from the DH domain rendering the GTPase interaction site in the DH domain accessible and therefore

Vav active. Dbl activity is regulated via an autoinhibitory mechanism as well. It was reported that the N-terminal region directly binds to the PH domain adjacent to the DH domain and thereby sterically hinders interaction of Rho GTPases with the GEF domain of Dbl (Bi *et al.,* 2001). Similar to Vav, phosphorylation might be involved in the relief of the autoinhibition of Dbl (Kato *et al.,* 2000). In plants there is evidence for a phosphorylation release of GEF activity, too. As mentioned above, RopGEF12 C-terminus was shown to inhibit GEF activity. The phosphomimicking point mutation of a conserved serine residue in the C-terminus caused pollen tube tip swelling indicative of increased ROP activation and therefore abolished inhibition of RopGEF12 activity (Zhang & McCormick, 2007).

1.2.2 Receptor-like kinases as upstream regulators of RopGEF-ROP signaling

Despite being soluble proteins, RopGEFs are observed at the plasma membrane indicating that the interaction with other components in or attached to the plasma membrane are required for RopGEF subcellular localization. Early on, RopGEFs have been handled as putative link between transmembrane receptor-like kinases (RLKs) and ROP signaling based on the initial observation that the tomato RopGEF KINASE PARTNER PROTEIN (KPP) interacts with tomato receptor-like kinases (Kaothien *et al.,* 2005). Therefore, RopGEF plasma membrane association, targeting to specific membrane domains as well as RopGEF regulation might involve interaction with RLKs.

Plant RLKs constitute one of the largest protein families in *Arabidopsis thaliana* with more than 610 members (Shiu & Bleecker, 2001). These single-pass transmembrane proteins are known to sense and transmit extracellular signals in various contexts, e.g. including brassinosteroid signaling via BRASSINOSTEROID INSENSITIVE (BRI) 1 (Li & Chory, 1997; Kinoshita *et al.,* 2005), protophloem differentiation via BARELY ANY MERISTEM (BAM) 3 (Depuydt *et al.,* 2013), pollen tube growth via POLLEN-SPECIFIC RECEPTOR-LIKE KINASE (PRK) 6 (Takeuchi & Higashiyama, 2016) as well as root hair development. In animals, signaling at the cell surface is largely mediated by receptor tyrosine kinases (RTKs), which are – as the name suggests – usually tyrosine kinases, while plant RLKs are serine/ threonine kinases (Shiu & Bleecker, 2001). RLKs consist of an extracellular domain, which is highly variable among RLKs allowing perception of a variety of ligands, a transmembrane domain and the intracellular kinase domain, which upon RLK activation mediates interaction with and usually phosphorylation of downstream factors (Shiu & Bleecker, 2001; Wang *et al.,* 2007). The largest group of RLKs is the family of Leucine-Rich Repeat (LRR) RLKs, which are characterized by a structural motif of repeating amino acid stretches containing numerous leucines in the extracellular domain (Wang *et al.,* 2007). Within the LRR-RLK subfamily, the pollen receptor kinases (PRKs) were found to be involved in regulation of pollen tube tip growth. For example, the pollen-expressed RopGEF12 was found to interact

via its C-terminus with PRK2a. Co-expression of RopGEF12 and PRK2a induced constitutively active ROP-like pollen tube phenotypes while expression of either alone did not (Zhang & McCormick, 2007) suggesting that PRK2a relieves RopGEF12 autoinhibition potentially via phosphorylation. These observations were further supported by the finding that PRK2 increased ROP1 activation in pollen tubes, which was mediated most likely by C-terminal phosphorylation and therefore activation of RopGEF1 (Chang *et al.,* 2013). Additionally, PRK6 was identified as receptor for the female-secreted peptide LURE1, which serves as attractant for the pollen tube during plant fertilization. The intracellular signal mechanism realizing redirection of pollen tube growth towards the external LURE1 source involves the interaction of PRK6 with C-termini of RopGEF12 and possibly RopGEF8 (Takeuchi & Higashiyama, 2016; Yu *et al.,* 2018). Another important subfamily of plant RLKs is the *Catharanthus roseus* (*Cr*) RLK1-like subfamily, which consist of 17 members in *Arabidopsis thaliana* including FERONIA, which was initially found to be involved in male-female interaction during plant reproduction (Huck *et al.,* 2003; Escobar-Restrepo *et al.,* 2007) and later shown to be also involved in root hair growth as outlined in more detail in the next section (Duan *et al.*, 2010; Yu *et al.*, 2012; Huang *et al.,* 2013).

1.2.3 RopGEFs in root hair development

The *Cr*RLK1L member FERONIA (FER) was identified in 2010 as upstream regulator of ROP2 signaling in root hair development by Duan and colleagues. In this study, mutation of FER resulted short, burst and collapsed root hairs being insensitive to auxin, which is well established to stimulate root hair elongation (Pitts *et al.,* 1998; Jones *et al.,* 2009). These root hair defects were restored by overexpression of ROP2 or RopGEF1 suggesting that these defects were due to reduced ROP2 signaling and that FER is actually linked to RopGEF-mediated ROP activation (Duan *et al.,* 2010). In a subsequent study, FER was found to be involved in suppression of the abscisic acid (ABA)-mediated cell growth inhibition via interaction with RopGEF1, 4 and 10, which in turn activate ROP11 (Yu *et al.,* 2012). In the context of root hair development, FER was linked to RopGEF4 and RopGEF10 as well (Huang *et al.,* 2013), which were both reported to be highly expressed in trichoblasts (Won *et al.,* 2009). Functional loss as well as overexpression of RopGEF4 and RopGEF10 revealed distinct root hair phenotypes, which indicate that these RopGEFs contribute to different phases of root hair development (Huang *et al.,* 2013). RopGEF4 was found to be primarily involved in root hair elongation, as loss of function revealed a reduction in root hair length, while the number of root hairs was similar to wild type, and overexpression a wavy root hair phenotype. In contrast, *ropgef10* mutant showed a decreased number of root hairs and overexpression resulted in a large number of branched root hairs (Huang *et al.,* 2013). Further RopGEFs have not been investigated for root hair phenotypes at the time, when this

PhD project was conducted. Additionally, the relationship between trichoblast-expressed RopGEFs and the key regulators of root hair development, namely ROP2 and ROP4, remained to be characterized including functional and physical interactions as well as subcellular localizations. When starting this PhD project, previous work in the Grossmann laboratory showed expression of six RopGEFs in *Arabidopsis thaliana* trichoblasts including RopGEF3, 4, 10, 11, 12 and 14 (Denninger & Reichelt *et al.,* 2019). Expression of these RopGEFs in trichoblasts suggests that they were possibly involved in root hair development implying the need for further studies on RopGEFs in this context.

1.3 Aim of this PhD thesis

The plant-specific family of guanine nucleotide exchange factors (RopGEFs) has been identified 15 years ago (Berken *et al.* 2005, Gu *et al.,* 2006). As outlined above, major advances have been made since then in revealing RopGEF 3D structure, mode of nucleotide exchange action, GEF activity regulation as well as interaction partners. However, simultaneously it became evident, that especially in the context of root hair development, the involved RopGEFs, their functions and regulation mechanisms remained largely obscure. Previous findings in the Grossmann laboratory showing that the trichoblast-expressed RopGEF3 functions as land mark protein for ROP2 (section 1.2.3; Denninger & Reichelt *et al.*, 2019) indicated that RopGEF functions during root hair development are not limited to nucleotide exchange and ROP activation. Moreover, it led to the hypothesis that RopGEFs, despite their high sequence similarity, are functionally distinct. Additionally, studies on the variable N- and C-terminal regions of RopGEFs had so far been focused on their impact on GEF activity, thus largely neglecting their potential roles in subcellular localization and protein regulation.

The aim of this PhD thesis was to investigate the mechanisms of cell polarization and to understand the roles of RopGEFs before ROP GTPase activation in the context of *Arabidopsis thaliana* root hair development. Using different combinations of RopGEF mutant, overexpression and marker lines, I characterized selected RopGEFs in a comparative manner with focus on early stages of root hair development and their relation to relevant ROPs (Chapter 2.1). In addition, I analyzed effects of truncated and mutated RopGEFs on root hair development as well as the subcellular appearance of the respective RopGEF variants to assess the roles of the unstructured RopGEF N-termini in RopGEF regulation. Lastly, I used cross-species alignments and *in silico* prediction tools to identify conserved residues in the RopGEF3 N-terminus, which have the potential to be phosphorylated. By introducing point mutations at these sites, I analyzed the effect of these putative phosphorylation sites on RopGEF3 polarization (Chapter 2.2).

II. RESULTS

2.1 Functions of ROPs and RopGEFs during root hair development

ROP GTPases are crucial regulators of various cellular processes including the establishment of cell polarity (Fu & Yang, 2001; Yang, 2002; Feiguelman *et al*., 2017). Immunocytochemistry and fluorophore fusions revealed the presence of several ROPs including ROP2, 4 and 6 in root hairs (Molendijk *et al.*, 2001; Jones *et al.*, 2002; Stanislas *et al.*, 2015; Denninger & Reichelt *et al.*, 2019). These GTPases polarize early in differentiating trichoblasts at the so-called Root Hair Initiation Domain (RHID), which is a uniform plasma membrane domain at the site, where the future root hair will grow out, and remain there throughout root hair development. Due to their subcellular localization and the phenotypes induced by overexpression or expression of constitutively active (CA-*rop*) or dominant negative (DN-*rop*) variants of trichoblast-expressed ROPs, the significance of ROPs for root hair development was proposed early on. While ROP2 overexpression or CA-*rop* resulted in additional root hair initiation sites, branched and swollen hairs, DN-*rop2* decreased root hair density (Molendijk *et al.*, 2001; Jones *et al.*, 2002). These observations provided strong evidence for ROPs being central regulators of root hair development; however, *rop* single mutants are lacking a strong root hair phenotype (Kang *et al.,* 2017; Gendre *et al.,* 2019) hinting towards functional redundancy among ROPs. The lack of *rop* double or triple knock-out mutants made genetic studies with regard to the relation between ROPs and RopGEFs difficult. Furthermore, specific roles of RopGEFs during root hair development were studied only to a small extent. Huang *et al.* (2013) provided first evidence for a functional distinction of RopGEFs showing that RopGEF4 and RopGEF10 differed in their mutant and overexpression root hair phenotypes (see section 1.2.3). However, not much was known about initial stages including the pre-bulging and bulging stages and about the potential involvement of other RopGEFs. Therefore, I started my PhD project with the characterization of available *rop* and *ropgef* single mutants and generated and analyzed *rop* and *ropgef* double mutants, which were subsequently used as genetic tools to investigate the functional relation between ROPs and RopGEFs.

2.1.1 ROP2 and 4 are central for root hair development

Mining of published ROP expression data in tip growing plant cells was performed previously in the Grossmann laboratory and revealed that ROP2 has the highest expression potential in trichoblasts compared to pollen tubes followed by ROP4 (Denninger, 2018). In order to systematically characterize the root hair phenotypes of the relevant *rop* mutants, I analyzed homozygous ROP2 and ROP4 T-DNA insertion lines (*rop2-1* and *rop4-1* single mutants; Table 4.1), the corresponding *rop2-1xrop4-1* double mutant line (hereafter named as *rop2/4*; Tabe 4.1), as well as a rescue line expressing mCitrine (mCit)-tagged ROP2 under its endogenous promoter in the *rop2/4* mutant background in comparison to *Arabidopsis thaliana* wild type ecotype Columbia-0 (Col-0). It is important to mention that the *rop4-1* single mutant has a different ecotype than *rop2-1*, as the latter has a Col-0 background and *rop4-1* is in the Wassilewskija (WS) background. Therefore, the corresponding *rop2/4* double mutant has a mixed genetic background (Col-0/ WS). Hence, using Col-0 as reference is suboptimal, however, the observed phenotype (Fig. 3) could recently be confirmed in the Grossmann laboratory by *rop2/4* double mutant lines generated with the CRISPR (Clustered Regularly Interspaced Short Palindromic Repeats)/ Cas9 technology (Marjorie Guichard, unpublished), which have a clean Col-0 background.

The following parameters were used in order to quantify phenotypes in root hair initiation and growth (Fig. 3B): (1) The distance between the tip of the primary root and the first, macroscopically visible hair initiation site (bulge) was used as a measure for proper hair initiation timing. (2) Root hair density was assessed in order to quantify the frequency of hair initiation events. (3) The length of root hairs was used as indicator for tip growth regulation. All measurements from one growth plate were normalized to the average values of Col-0 on the respective growth plate and then pooled. Therefore, the average of Col-0 measurements for all parameters is 1 or 100 % and the measurements of all other genotypes are represented in relation to Col-0 facilitating comparisons.

The disadvantage of normalization is that the dimensions of the measured parameters are hidden. Therefore, raw values for Col-0 for the above mentioned parameters determined during phenotyping of *rop* single and double mutants are specified in the following: Under the given growth conditions, the *Arabidopsis thaliana* wild type Col-0 has a distance of almost 1 mm between the primary root tip and the first hair initiation site (939.39 µm ± 30.39 (mean ± standard error of the mean (SEM); same for all following numbers in this paragraph)). Per millimeter primary root, approximately 13 root hairs were counted for Col-0 (12.92 hairs/ mm ± 0.51), which showed an average length of 130.15 µm ± 8.52.

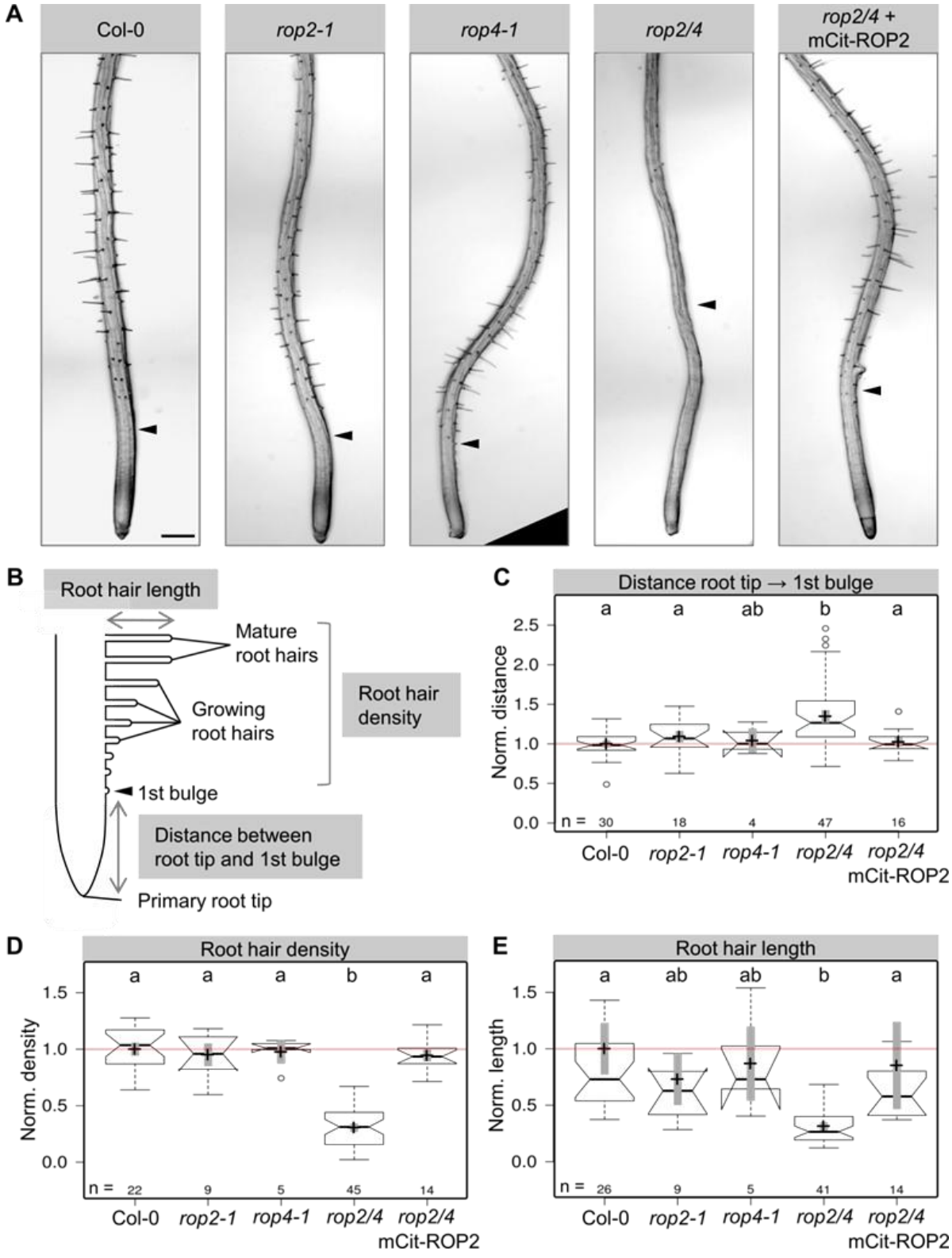

Fig. 3: Loss of ROP2 and ROP4 causes a drastic root hair phenotype. (A) Representative stereoscope images of roots of *A. thaliana* Col-0, *rop2-1* mutant, *rop4-1* mutant, *rop2/4* double mutant as well as a rescue line *rop2/4* + mCitrine (mCit)-ROP2. Arrow heads indicate first bulge. Scale bar, 250 µm. (B) Scheme of primary root showing the first bulge (arrow head), growing and mature root hairs. Parameters for root hair phenotype quantification are indicated (distance, density, length). (C-E) Quantification of root hair phenotypes of above mentioned genotypes. Measured parameters are normalized to the averaged values of Col-0 (= 1.0, marked by light red line). n indicates numbers of analyzed roots; center lines represent medians, crosses represent means; gray bars mark 83% confidence intervals of means; letters show result of a 2-way ANOVA test (significance value, p = 0.05), different letters indicate statistically significant differences.

Previous studies described the *rop* single mutants used in this thesis as knockout mutants due to absence of the corresponding full-length transcripts (Kang *et al.*, 2017; Jeon *et al.*, 2008; Fu *et al.*, 2005). Still, *rop2-1* and *rop4-1* single mutants showed rather none to mild root hair phenotypes indicating that these GTPases act redundantly during root hair development (Fig. 3A, C-E). The only parameter that was slightly affected by loss of ROP2 or ROP4 was root hair length, which was reduced by ~13-27 % in the single mutants compared to Col-0 (Fig. 3A, E; Col-0: 100 % ± 16.02; *rop2-1*: 72.99 % ± 17.02; *rop4-1*: 86.84 % ± 19.50). A reduction of root hair length in a similar range was reported for the *rop2-1* single mutant and a *rop4* RNAi mutant by Gendre and colleages (2019), while Kang *et al*. (2017) found a stronger reduction of root hair length for *rop2-1*. This discrepancy might be attributed to variations in growth conditions.

In contrast to the single mutants, loss of both ROPs (*rop2/4* double mutant) caused a highly significant decrease in root hair density (Fig. 3A, D; Col-0: 100 % ± 3.90; *rop2/4*: 30.54 % ± 3.37) indicating that the initiation rate of root hairs is largely dependent on the action of ROP2 and ROP4. Additionally, the distance between the primary root tip and the first bulge was increased (Fig. 3A, C; Col-0: 100 % ± 2.99; *rop2/4*: 134.62 % ± 5.60). This suggests that ROP2 and ROP4 are also required for timely bulging. The few root hairs being left in the *rop2/4* double mutant were also found to be significantly shorter compared to wild type root hairs (Fig. 3A, E; Col-0: 100 % ± 16.02; *rop2/4*: 31.37 % ± 2.44) indicating that ROPs are not only important for early events during root hair development, but also contribute to tip growth regulation. The introduction of mCit-ROP2 into the *rop2/4* double mutant background was sufficient to fully rescue the delay in bulging (Fig. 3A, C; Col-0: 100 % ± 2.99; *rop2/4* + mCit-ROP2: 102.29 % ± 3.80) as well as the reduction in root hair density (Fig. 3A, D; Col- 0: 100 % ± 3.90; *rop2/4* + mCit-ROP2: 94.39 % ± 3.38). In terms of root hair length, the introduction of mCit-ROP2 into the *rop2/4* double mutant background restored the phenotype as well, however, to a slightly lesser extent (Fig. 3A, E; Col-0: 100 % ± 16.02; *rop2/4* + mCit-ROP2: 85.20 % ± 26.41). The wild type appearance of the rescue line confirms that the root hair phenotypes observed in the *rop2/4* double mutant are indeed a consequence of loss of ROP function. Whether introduction of mCit-ROP4 is also sufficient to rescue the *rop2/4* double mutant phenotype remains to be shown.

2.1.2 RopGEF3 is highly polarized in early stages of root hair development

The subcellular localization of ROP2 was visualized already in 2002 by Jones *et al.*, where they showed that GFP-tagged ROP2 formed uniform polar domains at the site of the future root hair already in young, still elongating trichoblasts well before bulging. This localization pattern was described in more detail in the Grossmann laboratory by Philipp Denninger (Denninger & Reichelt *et al.,* 2019), who numbered the cells in one trichoblast cell file using the bulging cell as reference (cell +1; Fig. 5A). Younger trichoblasts (closer to root tip compared to cell +1) were assigned negative numbers, while older, more mature trichoblasts got positive numbers. By forming the ratio between background-subtracted signal intensities inside the RHID (Int_{RHID}) and outside (Int_{out}), the degree of asymmetric localization of the respective protein of interest into the RHID can be quantified. This value is referred to as polarity index (PI; Fig. 5A). According to this system, Philipp Denninger found the ROP2 GTPase polarizing in cell stage -4 (Denninger & Reichelt *et al.,* 2019); meaning the fluorescent ROP2 marker could be observed polarizing at the RHID four cells before the first bulge becomes macroscopically visible. However, how this early ROP targeting is regulated and which factors might be involved, is still not clear. ROP guanine nucleotide exchange factors (RopGEFs) act as ROP activating proteins by promoting GDP dissociation from inactive ROPs thereby allowing GTP rebinding (Fig. 1). Hence, RopGEFs are promising candidates to be involved in events upstream of ROP activation including growth site specification, ROP targeting and local regulation.

RopGEFs being preferentially expressed in trichoblasts were identified using publicly available expression data (Fig. 4, Genevestigator, expression data sets: Birnbaum *et al.,* 2003; Brady *et al.,* 2007; Wang *et al.,* 2008). From the 14 RopGEFs encoded in the genome of *Arabidopsis thaliana* (Berken *et al.,* 2005; Kaothien *et al.,* 2005; Gu *et al.* 2006), 6 RopGEFs with higher expression potential in trichoblasts compared to atrichoblasts and pollen were identified (RopGEF3, 4, 10, 11, 12 and 14). Fluorescent marker lines based on the genomic sequence of RopGEFs revealed two groups: Early polarizing RopGEFs including RopGEF3 and RopGEF14 precede ROP2 polarization by one cell stage (cell -5). Late polarizing RopGEFs such as RopGEF4 and 12 accumulate at the RHID only upon bulging (Denninger & Reichelt *et al.*, 2019). As the scope of this project was directed to early events during root hair development, I focused on the early polarizing RopGEF3. RopGEF3 stood out, because of its high trichoblast-specificity (Fig. 4) as well as its high degree of polarization at the RHID during root hair development (Denninger & Reichelt *et al.*, 2019; Fig. 5B, C). I followed a comparative approach and therefore included two additional RopGEFs to my analyses: The second early polarizing RopGEF, RopGEF14, was included because the polarization timing is similar to RopGEF3, although the degree of polarization is lower (Denninger & Reichelt *et al.*, 2019; Fig. 5B, C). In addition, RopGEF14 expression potential

was highest in root hairs compared to atrichoblasts and pollen (Fig. 4). RopGEF4 was also included into the comparative RopGEF analyses as it has the highest degree of polarization at the RHID amongst the late polarizing RopGEFs (Denninger & Reichelt *et al.*, 2019). Additionally, on the basis of the primary sequence RopGEF4 is closest related to RopGEF3 amongst the trichoblast-expressed RopGEFs (Berken *et al.*, 2005; Table 2.2; almost 62 % of RopGEF3 and RopGEF4 amino acid sequence is identical). For this triplet of RopGEFs I generated new fluorescent marker lines on the basis of the RopGEF coding sequence (CDS) with an N-terminal mCitrine (mCit) tag similar to the genomic marker lines presented in Denninger & Reichelt *et al.* (2019). However, in contrast to the constructs presented here, these contained both exonic and intronic sequences. These RopGEF full-length (FL) CDS constructs served as templates for the generation of RopGEF truncations and chimeras (see Chapter 2.2). Additionally, RopGEF CDS constructs can be employed in heterologous systems. As the RopGEF CDS constructs are based on the sequence of the primary gene models of the respective RopGEFs (The *Arabidopsis* Information Resource (TAIR) database; RopGEF3: AT4G00460.2; RopGEF4: AT2G45890.1; RopGEF14: AT1G31650.1), these splice variants used in this thesis can be confirmed to be the biological functional and relevant ones.

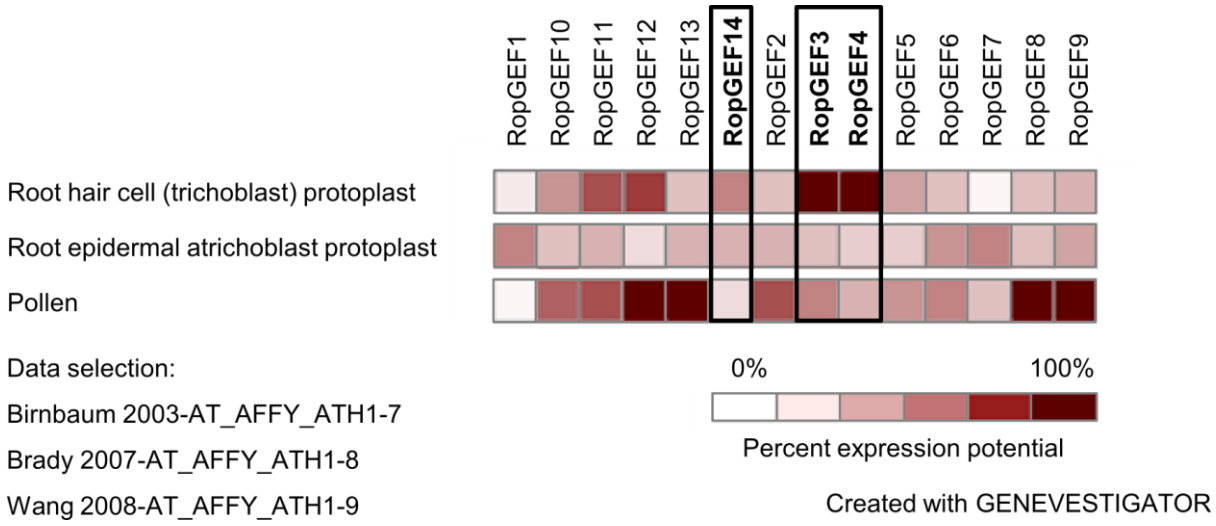

Fig. 4: Percent expression potential of RopGEFs in trichoblasts, atrichoblasts and pollen. Expression profiles of members of the *Arabidopsis thaliana* RopGEF family in hair cells (trichoblasts), non-hair cells (atrichoblasts) and pollen created with Genevestigator using the indicated data sets. Black outlines highlight results for RopGEFs of interest (RopGEF3, 4 and 14).

The mCit-RopGEF CDS markers (hereafter named as RopGEF) were introduced into the corresponding *ropgef* single mutant background to observe subcellular localization and polarization timing from cell stage -5 to +2 (Fig. 5B, C) as well as to confirm their functionality (Fig. 7). In order to quantify the degree of polarization of the respective RopGEFs at the RHID, I determined the PI as described above.

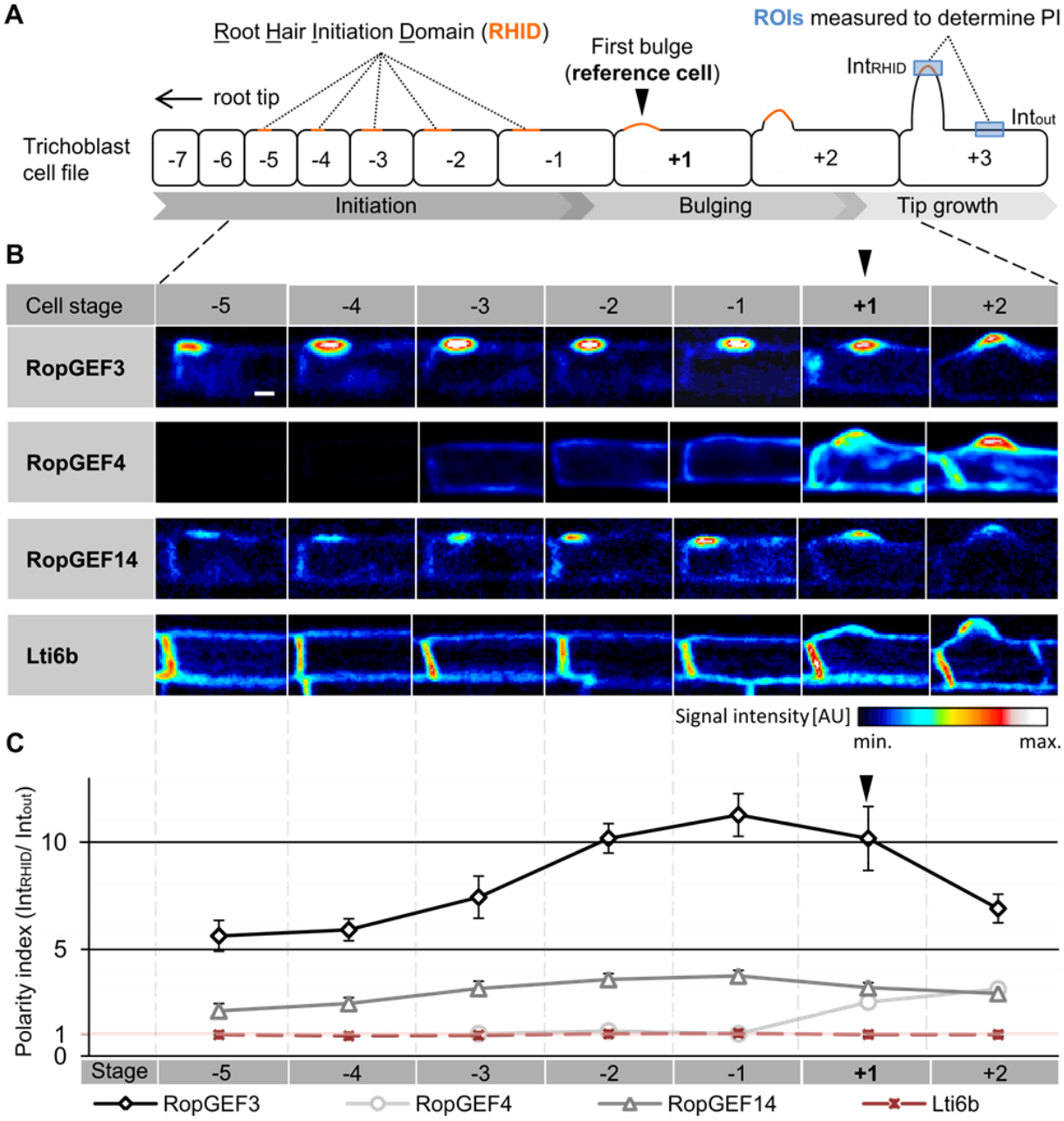

Fig. 5: Fluorescently-labeled RopGEF CDS constructs confirm early polarization of RopGEF3 and RopGEF14 and later polarization of RopGEF4 at the RHID. (A) Scheme of a trichoblast cell file from young trichoblasts (left, negative numbers) to more mature trichoblasts with hairs (right, positive numbers). The first cell with a macroscopically visible bulge serves as reference (cell +1) in the cell numbering system. Regions of interest (ROIs) in which signal intensities were measured to determine the polarity index (PI) are shown exemplarily in cell +3 (blue boxes). The PI is determined by the ratio of the background-subtracted signal intensities inside the RHID (Int_{RHID}) and outside (Int_{out}). (B) Representative z-projections of trichoblasts (cell stage -5 to +2) of *A. thaliana* lines expressing mCit-RopGEF3, mCit-RopGEF4, mCit-RopGEF14 and GFP-Lti6b. RopGEF markers are expressed in the corresponding *ropgef* mutant background. Signals are depicted in the pseudo-color LUT 'royal' of ImageJ. Scale bar, 10 µm. (C) Polarity indices of above mentioned fusion proteins during root hair initiation (cell stage -5 to +2). Mean values and standard errors of the mean (SEM) are plotted for each cell stage. Note that for RopGEF4 the curve starts at cell -3, because no signal could be observed in the cell stages before. Arrow head indicates the reference cell +1; light red line indicates no polarity at the RHID (PI = 1); n = 7-10 trichoblast cell files from 5-10 individual roots.

As a control, GFP-tagged LTI6B (LOW TEMPERATURE INDUCED PROTEIN 6B), a homogenously distributed plasma membrane marker, was used (Cutler *et al.,* 2000). The polarity index of LTI6B in each investigated cell stage was close to 1 (Fig. 5C; PI(LTI6B; cell -5 to +2) = 0.93-1.06 ± 0.03-0.07 (mean ± SEM; same for all following numbers in this paragraph)) indicating that this protein is not polarized at the RHID. Similar to observations in Denninger and Reichelt *et al.* (2019), I found RopGEF3 highly polarized from cell -5 to cell +2 with a peak in polarization degree in cell -1 (Fig. 5C; PI(RopGEF3; cell -1) = 11.26 ± 0.99). For RopGEF4, fluorescent signal of the fusion protein could only be detected from cell stage -3 on (Fig. 5B). Therefore, the polarity index was determined between cell stage -3 and +2 (Fig. 5C). Before bulging, RopGEF4 signal was rather low and evenly distributed at the plasma membrane and in the cytosol (Fig. 5C; PI(RopGEF4; cell -1) = 1.03 ± 0.05). Upon bulging, expression increased and polarization of RopGEF4 at the RHID could be observed. In contrast to RopGEF3, for which most of the signal was found in the RHID only, RopGEF4 signal could still be observed along the plasma membrane outside the RHID leading to a lower polarity index (Fig. 5C; PI(RopGEF4; cell +2) = 3.13 ± 0.29; PI(RopGEF3; cell +2) = 6.9 ± 0.67). RopGEF14 was also found to be polarized already in cell -5, however, to a lower degree than RopGEF3 (Fig. 5B, C; PI(RopGEF14; cell -5) = 2.12 ± 0.36; PI(RopGEF3; cell -5) = 5.62 ± 0.81). Similar to RopGEF3, RopGEF14 polarization was highest in cell stage -1 (Fig. 5C; PI(RopGEF14; cell -1) = 3.74 ± 0.26), but still lower than the lowest PI of RopGEF3 between cell stage -5 and cell +2. The RopGEF CDS marker lines confirmed the polarization behavior observed previously for RopGEF3, 4 and 14 marker lines based on the complete genomic sequence (Denninger and Reichelt *et al.*, 2019).

2.1.3 Loss of early and late polarizing RopGEFs affects different phases of root hair development

This distinct polarization timing of RopGEF3, 4 and 14 suggested that their action is required in different phases of root hair development. In order to identify the phases of root hair development in which RopGEF3, 4 and 14 function, I analyzed homozygous *ropgef* T-DNA insertion lines (*ropgef3-1*, *ropgef3-4*, *ropgef4-2* and *ropgef14-2*) and generated corresponding rescue lines. In addition, I generated and analyzed homozygous double mutant lines (*ropgef3-1xropgef4-2* (hereafter named *ropgef3/4*), *ropgef3-1xropgef14-2* (hereafter named *ropgef3/14*), *ropgef4-2xropgef14-2* (hereafter named *ropgef4/14*) in order to identify genetic interactions of these RopGEFs (Fig. 6, 7).

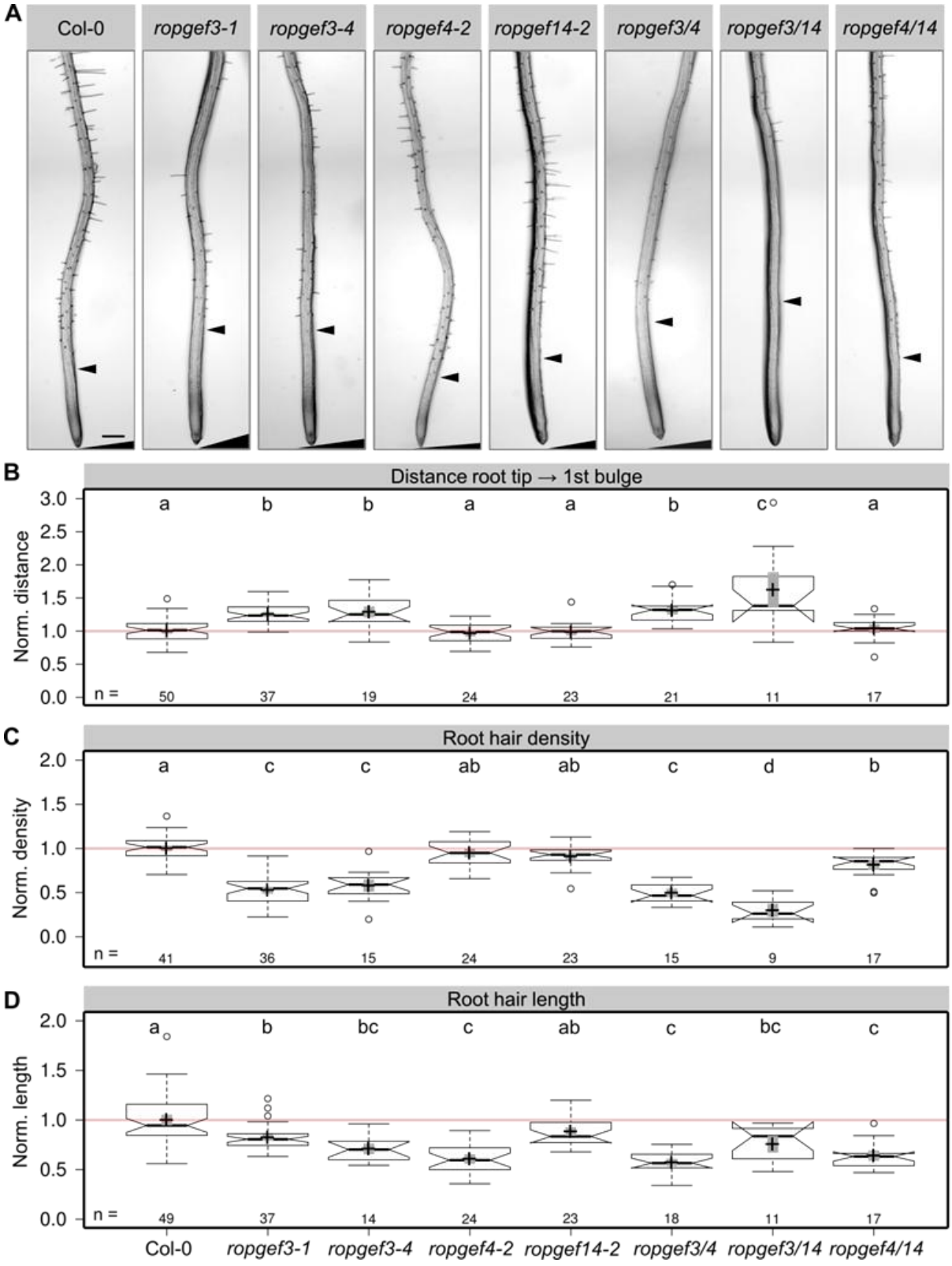

Fig. 6: Loss of the early polarizing RopGEF3 affects root hair initiation timing and frequency while loss of the late polarizing RopGEF4 causes a short root hair phenotype. (A) Representative stereoscope images of roots of *A. thaliana* Col-0, *ropgef3-1*, *ropgef3-4*, *ropgef4-2*, *ropgef14-2* mutants and *ropgef3/4*, *ropgef3/14* and *ropgef4/14* double mutants. Arrow heads indicate the first bulge. Scale bar, 250 µm. (B-D) Quantification of root hair phenotypes of above mentioned genotypes. Measured parameters are normalized to the averaged values of Col-0 (= 1.0, marked by light red line). n indicates numbers of analyzed cell files; center lines represent medians, crosses represent means; gray bars mark 83% confidence intervals of means; letters show result of a 2-way ANOVA test (significance value, p = 0.05), different letters indicate statistically significant differences.

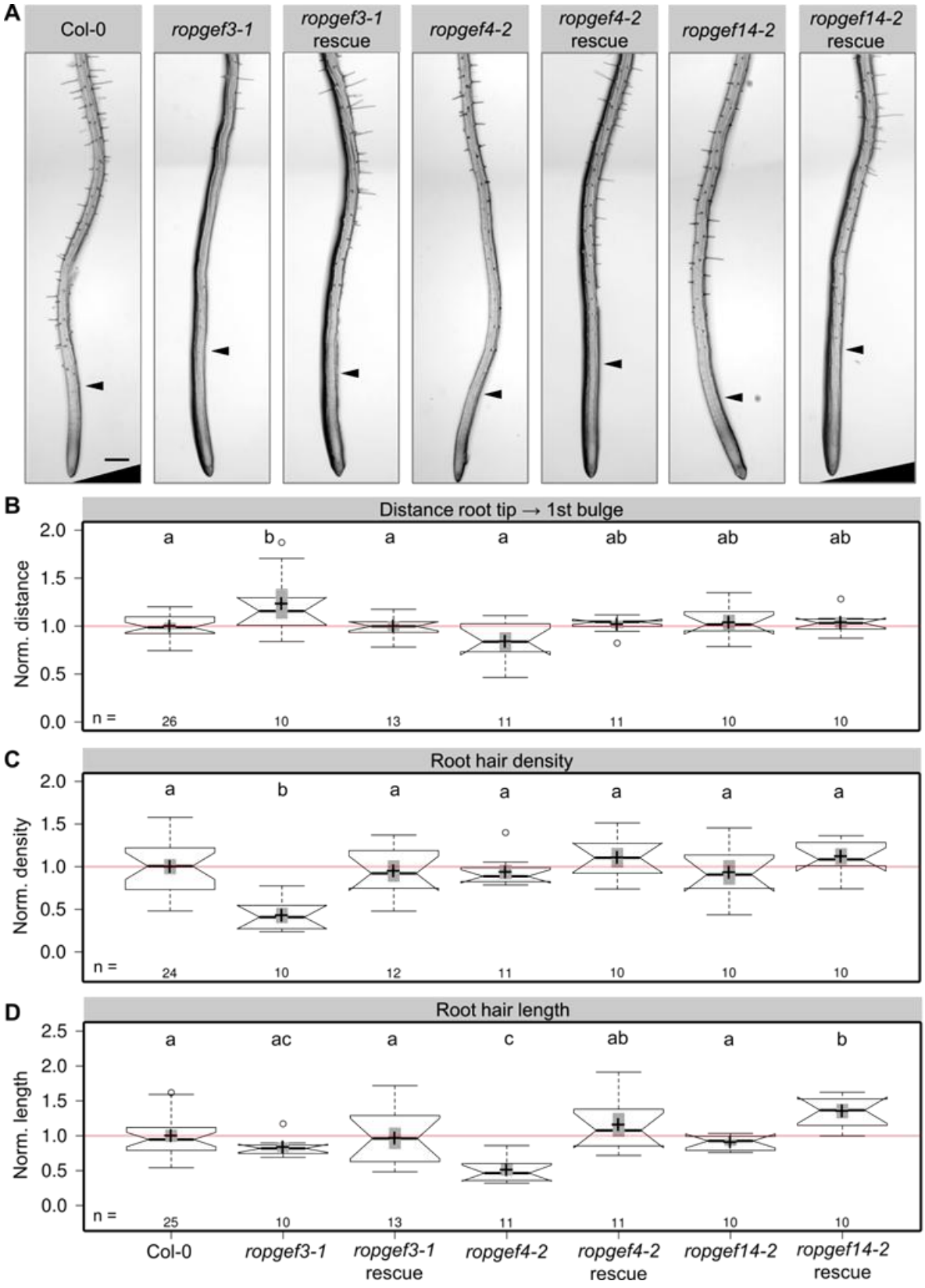

Fig. 7: RopGEF rescue lines confirm specificity of observed *ropgef* mutant phenotypes. (A) Representative stereoscope images of roots of *A. thaliana* Col-0, *ropgef3-1*, *ropgef4-2* and *ropgef14-2* mutants and rescues. Rescue lines express mCit-RopGEF under the respective RopGEF promoter. Arrow heads indicate first bulge. Scale bar, 250 µm. (B-D) Quantification of root hair phenotypes of above mentioned genotypes. Measured parameters are normalized to the averaged values of Col-0 (= 1.0, marked by light red line). n indicates numbers of analyzed cell files; center lines represent medians, crosses represent means; gray bars mark 83% confidence intervals of means; letters show result of a 2-way ANOVA test (significance value, p = 0.05), different letters indicate statistically significant differences.

Root hair phenotypes of *ropgef* single and double mutants were quantified by analyzing the same parameters as described above (Fig. 3B). In *ropgef3-1* single mutant, which was shown to largely lack the full-length transcript (Denninger & Reichelt *et al.,* 2019), bulging was delayed indicated by an increase in the distance between the primary root tip and the first bulge (Fig. 6A, B; Col-0: 100% ± 2.34 (mean ± SEM; same for all following numbers in this paragraph); *ropgef3-1*: 125.41 % ± 2.41). This increase is statistically significant and can also be reproduced in another *ropgef3* mutant allele (Fig. 6A, B; *ropgef3-4*: 128.96 % ± 5.44). This phenotype suggests that RopGEF3 is involved in the regulation of root hair initiation, as it cannot occur timely upon RopGEF3 loss and fits to the early polarization of RopGEF3 at the RHID. In addition, root hair density was reduced by half in *ropgef3-1* compared to wild type (Fig. 6A, C; Col-0: 100% ± 2.05; *ropgef3-1*: 52.73 % ± 2.60). These effects of RopGEF3 loss are reminiscent of the *rop2/4* double mutant phenotype, albeit to a lesser extent (Fig. 3A, C, D; *rop2/4* distance: 134.62 % ± 5.60; density: 30.54 % ± 3.37). In terms of root hair length, *ropgef3-1* single mutant showed a reduction of ~20 % compared to wild type (Fig. 6A, D; Col-0: 100 % ± 3.65; *ropgef3-1*: 82.26 % ± 2.07). As the root hair length was measured in a region in similar distance to the primary root tip for all genotypes, the reduction in length might be a consequence of the delayed root hair initiation in *ropgef3-1*. When initiation is delayed, root hairs in the same region of the primary root might be developmentally younger and therefore shorter in *ropgef3-1* compared to Col-0, in which initiation occurs earlier. This assumes, however, that root hair growth rates are similar in these two genotypes. Introduction of a mCit-RopGEF3 CDS construct under the control of the endogenous RopGEF3 promoter into the *ropgef3-1* mutant background rescued all observed defects in root hair development to wild type level (Fig. 7; *ropgef3-1* + mCit-RopGEF3 distance: 99.81 % ± 3.07; density: 94.98 % ± 8.42; length: 96.46 % ± 10.22). Therefore, the observed root hair phenotypes in *ropgef3-1* single mutant can be considered specific for RopGEF3 loss and the mCit-RopGEF3 CDS construct is proven to be functional and sufficient to rescue loss of endogenous RopGEF3.

Due to its early polarization, *ropgef14-2* was suspected to potentially also affect bulging timing. However, in contrast to *ropgef3-1*, the distance between root tip and the first bulge was found to be unaffected in the *ropgef14-2* mutant *(*Fig. 6A, B). For both, root hair density as well as root hair length a minor phenotype could be observed upon loss of RopGEF14. Root hair density was reduced by ~10 % (Fig. 6A, C; Col-0: 100 % ± 2.05; *ropgef14-2*: 90.87 ± 2.54) and root hair length was reduced by ~12 % (Fig. 6A, D; Col-0: 100 % ± 3.65; *ropgef14-2*: 88.32 % ± 2.81). In the corresponding rescue line expressing mCit-RopGEF14 under its endogenous promoter in *ropgef14-2* distance to the first bulge, root hair density and root hair length were similar to Col-0 or slightly elevated (Fig. 7; *ropgef14-2* + mCit-RopGEF14 distance: 103.67 % ± 3.42; density: 112.02 % ± 6.22; length: 135.33 % ± 6.69).

The absence of a strong phenotype in this mutant can be due to residual expression of RopGEF14 in this T-DNA insertion line, however, as the T-DNA is located in the first exon, the corresponding gene is likely to be efficiently disrupted and expression or a functional gene product is not expected. Experimental evidence for that is not provided in this thesis, though. Therefore, analysis of potential residual RopGEF14 transcripts in this mutant remains to be done. Another possibility is redundancy in RopGEF functions. Potentially, RopGEF14 action is less crucial in the initial stages of root hair development, as long as the other early polarizing and prominent RopGEF3 is present. In order to define the genetic interaction between these similarly polarizing RopGEFs, I generated the corresponding double mutant by crossing of the homozygous single mutants and analyzed the phenotype. I found that *ropgef3/14* double mutant has a further increased distance between the first bulge and the primary root tip compared to *ropgef3-1* (Fig. 6A, B; *ropgef3-1*: 125.41 % ± 2.41; *ropgef3/14*: 162.30 % ± 17.72). Also root hair density was significantly reduced in the *ropgef3/14* double mutant compared to *ropgef3-1* single mutant (Fig. 6A, C; *ropgef3-1*: 52.72 % ± 2.60; *ropgef3/14*: 29.76 % ± 4.71). Root hair length was slightly decreased in *ropgef3/14* double mutant compared to the corresponding single mutants, however, not in a statistically relevant manner (Fig. 64A, D; *ropgef3-1*: 82.23 % ± 2.07; *ropgef14-2*: 88.32 % ± 2.81; *ropgef3/14*: 75.58 % ± 5.52). In conclusion, the phenotype of the *ropgef3/14* double mutant is more extreme than the single mutants indicated pointing towards a synergistic interaction between the corresponding mutations. This indicates that RopGEF3 and RopGEF14 are both involved in the process of root hair initiation.

In contrast, RopGEFs polarizing later at the RHID might not be needed in the early events of root hair initiation, but likely later, during bulging, when they accumulate at the RHID. Indeed, for the late polarizing RopGEF4, the mutant phenotype was different from those observed in the single mutants of early polarizing RopGEFs. In *ropgef4-2* mutant bulging timing as well as hair initiation frequency were similar to wild type (Fig. 6A-C). Only for root hair length, a significant effect could be observed upon RopGEF4 loss. Root hair length was reduced by ~40 % compared to wild type (Fig. 6A, D; Col-0: 100 % ± 3.65; *ropgef4-2*: 60.77 % ± 3.16). This was the strongest effect on root hair length observed for the investigated *ropgef* single mutants indicating that RopGEF4 might function predominantly in later stages of root hair development, e.g. upon onset of and during tip growth. These observations are in line with previous reports using the same T-DNA insertion line as presented in this thesis (Won *et al.*, 2009) or another mutant allele for RopGEF4 (Huang *et al.,* 2013), which reported a reduction in hair length by ~20-30% compared to wild type. These reports further strengthen the conclusion that RopGEF4 is required for root hair elongation. By expressing RopGEF4 under its own promoter in the *ropgef4-2* mutant background, the short root hair phenotype could be abolished further confirming the specificity of the phenotype to RopGEF4 loss as well as the

functionality of the mCit-RopGEF4 CDS construct (Fig. 7; *ropgef4-2* + mCit-RopGEF4 root hair length: 115.7 % ± 11.27). The combination of *ropgef3-1* and *ropgef4-2* (*ropgef3/4*) resulted in the following phenotype: The distance between root tip and the first bulge as well as root hair density of *ropgef3/4* double mutant, which were both unaffected in the *ropgef4-2* single mutant, resembled *ropgef3-1* (Fig. 6A-C; distance *ropgef3-1*: 125.41 % ± 2.41; *ropgef3/4*: 131.11 % ± 4.05; density *ropgef3-1*: 52.73 % ± 2.60; *ropgef3/4*: 49.64 % ± 3.10). Root hair length of the *ropgef3/4* double mutant, however, was closer to the phenotype observed in *ropgef4-2* single mutant (Fig. 6A, D; *ropgef3-1*: 82.26 % ± 2.07; *ropgef4-2*: 60.77 % ± 3.16; *ropgef3/4*: 57.20 ± 2.45). These results indicate that root hair initiation and subsequent root hair elongation by tip growth are separate pathways involving predominantly RopGEF3 or RopGEF4, respectively.

Finally, I analyzed the combination of *ropgef4-2* and *ropgef14-2* (*ropgef4/14*). I found that the distance between the primary root tip and the first hair initiation site in the *ropgef4/14* double mutant remained unaffected as in the corresponding single mutants (Fig. 6A, B). Root hair density of the *ropgef4/14* double mutant was decreased by almost 20 % compared to wild type and thus slightly lower than in both single mutants (Fig. 6A, B; *ropgef4-2*: 94.70 % ± 3.14; *ropgef14-2*: 90.87 % ± 2.54; *ropgef4/14*: 81.33 % ± 3.45). In terms of root hair length, *ropgef4/14* showed a similar short hair phenotype as *ropgef4-2* (Fig. 6A, D; *ropgef4-2*: 57.20 % ± 2.45*; ropgef4/14*: 63.99 % ± 3.38). Again, this shows that the early and late polarizing RopGEFs are predominantly involved in different phases of root hair development.

Taken together, the *ropgef* mutant analysis revealed that the investigated RopGEFs have distinct priority tasks, yet partially overlap in their functions. RopGEF3 seems to be the predominant factor involved in the regulation of root hair initiation timing and frequency, which fits to its early polarization to the RHID. RopGEF14, which is also present early at the RHID, appears to be functionally related to RopGEF3. RopGEF4 is not polarized at the RHID before bulging and in line with that its action is required in later stages of root hair development especially in the phase of polar root hair growth.

2.1.4 RopGEF3 is sufficient to ectopically polarize ROP2

Previous work in the Grossmann laboratory showed that mCit-RopGEF3 overexpression induced ectopic, RHID-like RopGEF3 domains in both atrichoblasts and trichoblasts. Additionally, multiple bulges and branched hairs could be observed in individual trichoblasts, which usually only grow a single, unbranched root hair at a defined position (Denninger and Reichelt *et al.*, 2019). Together with the early polarization of RopGEF3 at the RHID (Denninger and Reichelt *et al.*, 2019; Fig. 5) and the pronounced root hair phenotype (Denninger and Reichelt *et al.*, 2019; Fig. 6) this strongly suggests that RopGEF3 is central for initial events in root hair development. To test whether RopGEF3 is actually involved in

ROP2 recruitment to the RHID, Philipp Denninger expressed a fluorescently-labeled ROP2 marker under its endogenous promoter in the *ropgef3-1* mutant background and revealed a significant reduction in ROP2 polarization at the RHID (Denninger and Reichelt *et al.*, 2019). Additionally, a direct physical interaction between RopGEF3 and ROP2 was demonstrated using a ratiometric bimolecular fluorescence complementation assay in *Nicotiana benthamiana* and a split-ubiquitin assay in yeast (Denninger and Reichelt *et al.*, 2019; Grefen laboratory). Taken together, these observations provide convincing evidence that RopGEF3 is necessary for the polar recruitment of ROP2 to the RHID during root hair initiation.

Building on these findings, I further investigated the relationship between RopGEF3 and ROP2 and investigated whether RopGEF3 is also sufficient to ectopically recruit ROP2 into above-mentioned additional, RHID-like RopGEF3 domains. To this end, I analyzed the mCit-RopGEF3 overexpression line, which additionally expressed mTurquoise (mTurq)-ROP2 under the endogenous ROP2 promoter (Fig. 8).

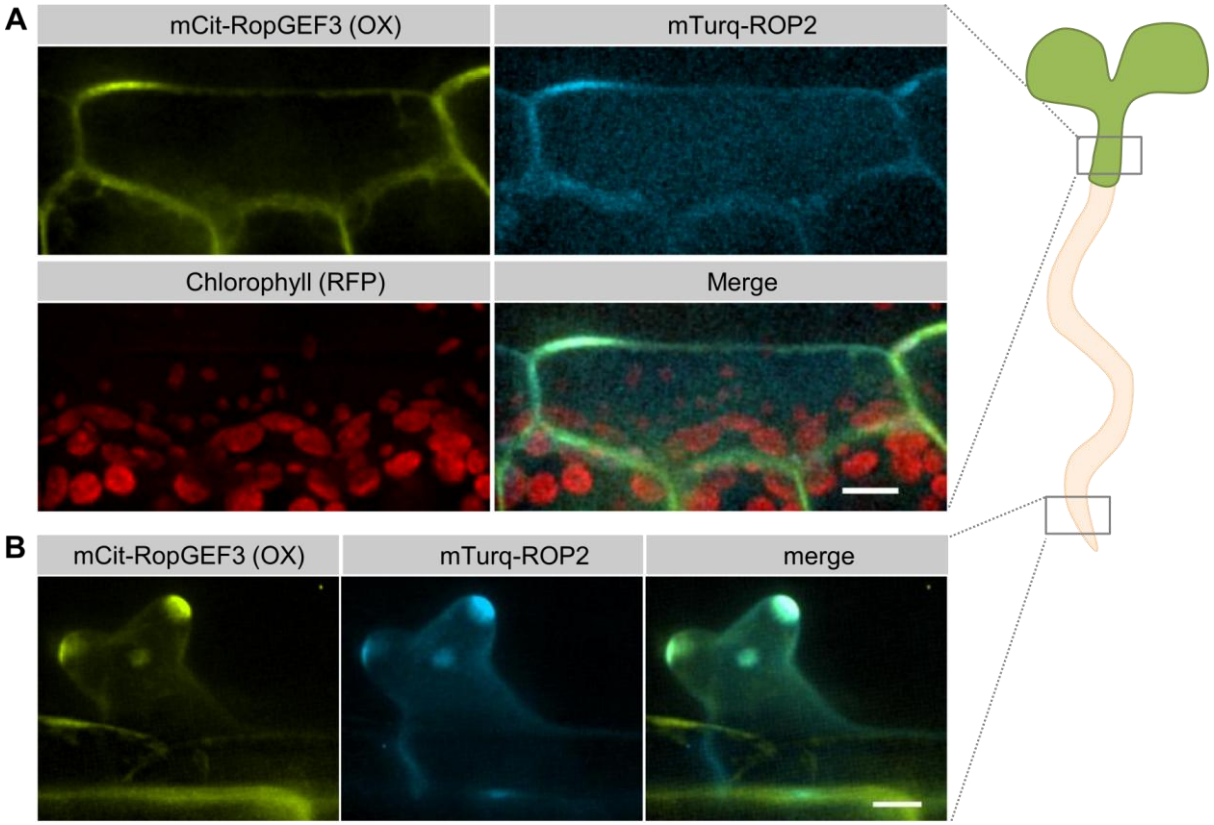

Fig. 8: RopGEF3 overexpression results in additional, RHID-like domains and induces ectopic ROP2 polarization in trichoblasts and other cell types. (A) Example of an epidermal cell of the hypocotyl of an *A. thaliana* double marker cell line expressing mCitrine (mCit)-RopGEF3 (yellow) inducibly and mTurquoise (mTurq)-ROP2 (cyan) under its endogenous promoter. RopGEF3 overexpression was induced for 24 h with 20 µM estradiol. RFP signal (red) was acquired in order to visualize chloroplasts. Scale bar, 10 µm. (B) Example of a branched root hair induced upon RopGEF3 overexpression in the *A. thaliana* double marker line used in (A). Polar accumulation of RopGEF3 and ROP2 can be observed in the tips of the branched hair. Scale bar, 10 µm.

I found that ROP2 was indeed accumulated into ectopic RopGEF3 domains in trichoblasts, e.g. into the tips of branched hairs (Fig. 8B). This suggests that RopGEF3 is sufficient to recruit ROP2 into ectopic domains and also to ectopically trigger tip growth in trichoblasts. Additionally, ectopic RopGEF3 and ROP2 polarization was found in atrichoblasts (Denninger and Reichelt *et al.*, 2019), however, ectopic tip growth initiation at these sites visualized by a macroscopic bulge formation, was not observed. Interestingly, RopGEF3 overexpression occasionally also induced ectopic, polar RopGEF3 domain formation in epidermal cells of the hypocotyls (Fig. 8A). Also in this different tissue, these RopGEF3 domains ectopically polarized ROP2. Again, despite ectopic polarization of ROP2, an actual and macroscopic visible initiation of polar growth at these sites could not be observed in epidermal cells of the hypocotyls. This indicates that ectopic polarization of RopGEF3 and ROP2 are not sufficient to efficiently trigger polar growth in other cell types than trichoblasts. This further suggests that one or several additional trichoblast-specific factor(s) is/ are needed to allow tip growth initiation. However, also in trichoblasts, induced early RopGEF3 overexpression did not push RopGEF3 polarization or bulging to an earlier time point (Denninger and Reichelt *et al.*, 2019) indicating that the formation of polar RopGEF3 domains and tip growth initiation is dependent on specific conditions, which are not given in very young trichoblasts.

2.1.5 Initial RopGEF3 polarization is independent of ROP2 and ROP4

The establishment and regulation of cell polarity underlie numerous regulatory mechanisms, which enhance or restrict involved molecular factors at the site of symmetry breaking through positive or negative feedback loops (e.g. Kost, 2008; Yang & Lavagi, 2012; Craddock *et al.,* 2012). These feedback mechanisms enhance robustness as well as controllability of cell polarity. For example, in pollen tubes, the tip-localized ROP1 domain is established and laterally propagated by apical actin microfilaments (F-actin) assembly, which promotes ROP activator recruitment via F-actin-mediated exocytosis. These actin dynamics are promoted by RIC4 (ROP-interactive CRIB motif-containing protein 4), an effector of ROP1. Restriction of the ROP1 domain is mediated by the RopGAP REN1, which is in turn dependent on ROP1-regulated F-actin assembly and cytosolic calcium oscillations (Gu *et al.*, 2005; Hwang *et al.*, 2005; Yan *et al.*, 2009; Hwang *et al.*, 2010).

After showing that RopGEF3 is necessary and sufficient for ROP2 polarization at the RHID (Denninger and Reichelt *et al.*, 2019; Fig. 8), I investigated the effect of ROP2 and ROP4 loss on RopGEF polarization in order to uncover potential feedback mechanisms between RopGEFs and ROPs during root hair development. Therefore, mCit-RopGEF markers under the respective endogenous RopGEF promoters were introduced into the *rop2/4* double mutant background and RopGEF polarization along a cell file was observed (Fig. 9). As the *rop2/4* double mutant has barely any root hairs left (Fig. 3), the reliable identification of the

reference cell with the first bulge was difficult. To ensure that RopGEF polarization in Col-0 and *rop2/4* was compared at similar developmental stages, the average distance between the root tip and the reference cell +1 was determined for the RopGEF markers in the wild type background. Based on this information, the cell stages along a cell file in the *rop2/4* double mutant were identified.

For the early polarizing RopGEF3 and RopGEF14, an early cell stage (corresponding to cell -4) as well as later cell stages (corresponding to cell -1 and +1), in which the polarization degrees of these RopGEFs peaked and bulging started, were investigated (Fig. 9A, C, D). Early polarization of RopGEF3 and RopGEF14 was not affected by loss of both ROP GTPases (PI(RopGEF3; cell -4) = 4.46 ± 0.59 (Col-0)/ 4.76 ± 0.32 (*rop2/4*; mean ± SEM; same for all following numbers in this paragraph); PI(RopGEF14; cell -4) = 2.09 ± 0.12 (Col-0)/ 2.10 ± 0.32 (*rop2/4*)). As RopGEF3 and RopGEF14 were found to be polarized one cell stage before ROP2 (Denninger and Reichelt *et al.,* 2019), it was likely that initial polarization of these RopGEFs is ROP-independent. However, feedback mechanisms might be present, which upon successful ROP2 polarization stabilize the growth machinery including RopGEFs at the RHID. Indeed, while in wild type background, the PI of RopGEF3 and RopGEF14 respectively increased with progressing trichoblast differentiation (Fig. 5B, C; Fig. 9A, C, D), polarization decreased continuously in later stages in the *rop2/4* mutant background (Fig. 9A, C, D; PI(RopGEF3; cell +1) = 6.52 ± 0.59 (Col-0)/ 2.92 ± 0.34 (*rop2/4*); PI(RopGEF14; cell +1) = 5.00 ± 0.14 (Col-0)/ 1.70 ± 0.37 (*rop2/4*)).

For the late polarizing RopGEF4, polarization in cell stages -1, +1 and +2 in Col-0 and *rop2/4* were compared as its endogenous polarization only starts in these cells (Fig. 5B, C). In wild type as well as *rop2/4*, RopGEF4 was evenly distributed in cell -1. Upon bulging, RopGEF4 polarized at the RHID in Col-0 and the PI increased further in cell +2. In contrast, RopGEF4 remained non-polar in *rop2/4* mutant background (Fig. 9B, C; PI(RopGEF4; cell +2) = 2.77 ± 0.16 (Col-0)/ 1.14 ± 0.07 (*rop2/4*)), while the general expression pattern along the primary root was similar to the wild type situation (Fig. 9B). These data suggest that the presence of ROP GTPases is crucial for the stabilization of RopGEF domains in later stages of root hair development, when polar growth is about to start. Thus, the initial hypothesis of a ROP-RopGEF feedback mechanism is supported. While the initial polarization cue for RopGEF3 and RopGEF14 is apparently still present in the *rop2/4* mutant and therefore, initial polarization of these proteins can still occur at the RHID, the maintenance mechanisms ensuring RopGEF3 and RopGEF14 polarity in later stages are ROP2/4-dependent. This leads to the dissolution of RopGEF domains (and potentially also to dissociation of other present factors of the growth machinery) reflected in the decreasing PI values of RopGEF3 and RopGEF14 in later stages. In contrast, RopGEF4 polarization appears to be ROP-dependent, which fits the observation that RopGEF4 polarizes after ROP2.

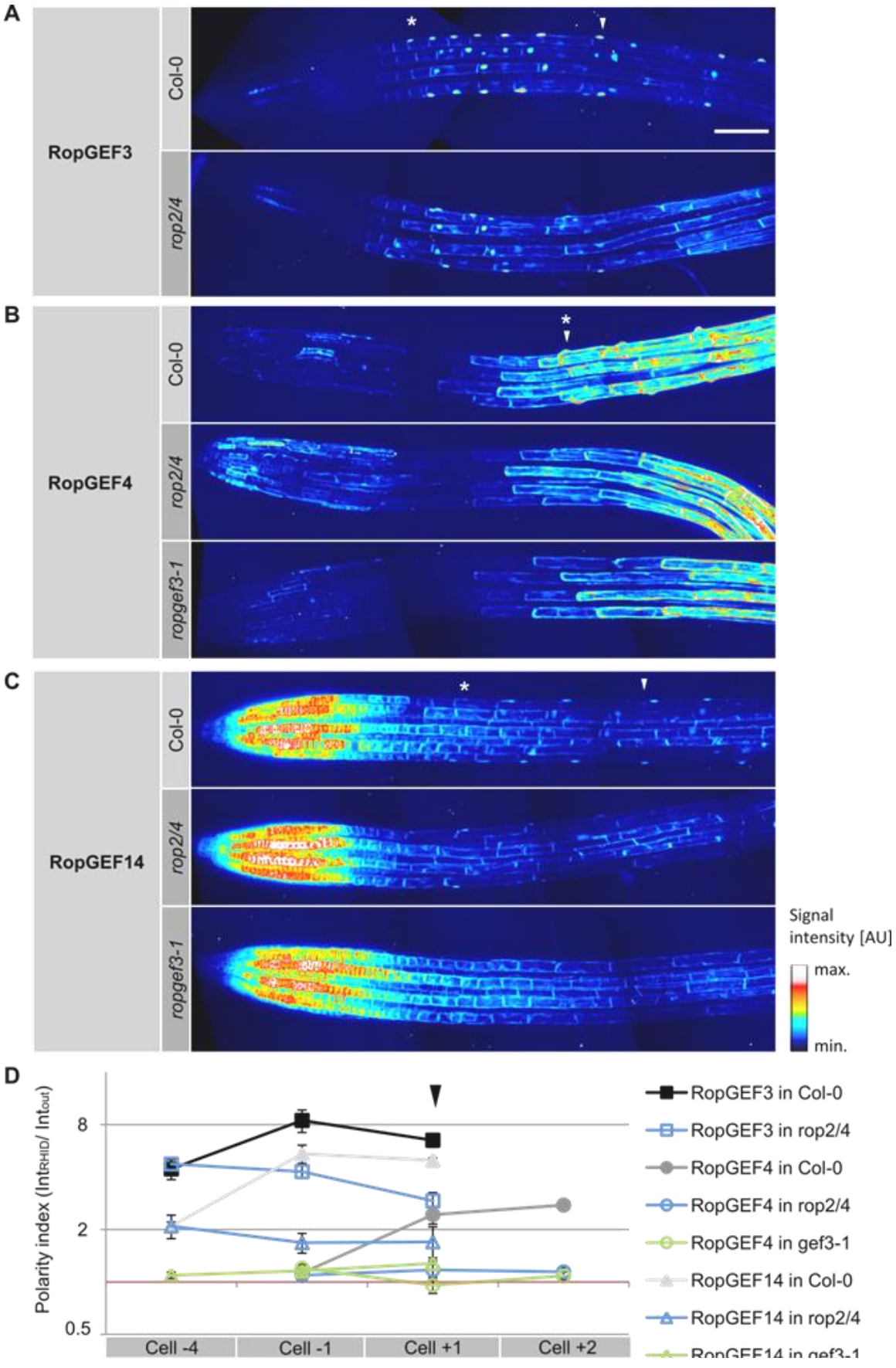

Fig. 9: Loss of ROP2 and ROP4 reduces polarization of RopGEFs in later stages of root hair development. Complete figure legend on next page.

Fig. 9 (previous page)**: Loss of ROP2 and ROP4 reduces polarization of RopGEFs in later stages of root hair development.** (A-C) Representative z-projections from primary roots of *A. thaliana* lines expressing mCit-RopGEF3 (A), mCit-RopGEF4 (B) and mCit-RopGEF14 (C) in Col-0 (first panel in A-C), *rop2/4* double mutant background (second panel in A-C) and *ropgef3-1* mutant background (third panel in B, C). RopGEF markers are expressed under the respective endogenous promoter. Signals are depicted in the pseudo-color LUT 'royal' of ImageJ. Asterisks mark first polarization of RopGEFs in Col-0; arrow heads indicate bulging stage. Scale bar, 100 µm. (C) Polarity indices of above mentioned fusion proteins in the different genetic backgrounds in initial stages (cell -4) and later stages of root hair development (cell -1 to cell +2). Mean values and standard errors of the mean (SEM) are plotted for each cell stage (note that base 2 log scale is used for y-axis). Note that for RopGEF4 only later stages are measured (cell -1, cell +1, cell +2) as RopGEF4 expression starts later than RopGEF3 and RopGEF14. Arrow head indicates the reference cell +1; light red line indicates no polarity at the RHID (PI = 1); n = 6-8 trichoblast cell files from 5-8 individual roots.

Above presented results demonstrating that RopGEF polarization depends on ROP2/4 in later stages of root hair development and the fact, that ROP2 polarization is largely dependent on RopGEF3 (Denninger and Reichelt *et al.,* 2019) raised the question about the effect of RopGEF3 on the polarization of the other RopGEFs. When ROP2 polarization is reduced upon loss of RopGEF3, other RopGEFs, whose polarizations are affected by ROPs, may be affected as well. To address this question, I generated and analyzed stable *Arabidopsis thaliana* lines endogenously expressing mCit-RopGEF14 and mCit-RopGEF4 in the *ropgef3-1* mutant background (Fig. 9B-D). RopGEF14, which was also found to be polarized at the RHID in cell stage -5 in Col-0 similar to RopGEF3, was not polarized in the *ropgef3-1* single mutant in cell -4 anymore (Fig. 9C, D; PI(RopGEF14; cell -4) = 1.09 ± 0.05) suggesting that the initial polarization of RopGEF14 is dependent on RopGEF3 or on a RopGEF3-dependent factor, but specifically not on ROP2 and ROP4. RopGEF4 polarization at the RHID in cell stages -1, +1 and +2 was completely lost in the *ropgef3-1* single mutant background (PI(RopGEF4; cell -1,+1,+2) = 0.96-1.20 ± 0.05-0.1) similar to what was observed in the *rop2/4* double mutant background indicating that RopGEF4 polarization is RopGEF3-dependent. These data underline again the critical role of RopGEF3 for the establishment of the RHID by promoting polarization of not only ROP2 but also additional involved RopGEFs.

2.2 Regulation of RopGEF protein localization, polarization timing and protein abundance during root hair development

In the first chapter of this thesis (see section 2.1), I could show that RopGEFs, which polarize at the RHID early (RopGEF3 and RopGEF14) or late (RopGEF4) during root hair development also act in distinct phases of root hair growth. It is likely that RopGEFs share some cellular tasks in this process due to their close relation. However, analyses of *ropgef* single and double mutants showed that early and late polarizing RopGEFs differ in their priority functions. While RopGEF3 was shown to be directly involved in RHID setup by ROP2 recruitment, RopGEF4 might be more efficient in ROP2 activation as RopGEF4 polarization at the RHID occurs upon start of polar growth. Considering the high conservation among RopGEF proteins (Berken *et al.*, 2005; Gu *et al.*, 2005), it is an interesting question how the differential recruitment timing of RopGEF3, 4 and 14 is implemented on a molecular level. To address this question, one can focus on extrinsic factors, such as RopGEF-specific interaction partners, which might differ for early and late polarizing RopGEFs, or on intrinsic protein features, which could mediate such selective interactions. The RopGEF3-specific interactome is being investigated by in the Grossmann laboratory using a Biotin identification (BioID) proximity labeling approach. I dedicated the second part of my PhD thesis to the characterization of RopGEF protein domains and their involvement in RopGEF protein localization and regulation. I analyzed the contributions of the conserved PRONE domain as well as the N-termini of RopGEF3, 4 and 14 by generation of *Arabidopsis thaliana* marker lines expressing RopGEF3 truncations and RopGEF chimeric proteins. I analyzed the polarization and general subcellular appearance of the marker proteins during root hair development as well as the macroscopic root hair phenotypes of these marker lines. Additionally, I identified conserved, phosphorylatable amino acid residues in the RopGEF3 N-terminus and putative phosphorlyation sites *in silico*, which might contribute to the regulation of the early polarizing RopGEF3 during root hair initiation.

2.2.1 The late polarizing RopGEF4 protein shares higher sequence identity with RopGEF3 than RopGEF14

The RopGEF protein family is plant-specific and members share a central, highly conserved Plant-specific ROP Nucleotide Exchanger (PRONE) domain (Berken *et al.*, 2005; Gu *et al.*, 2005; Fig. 10). In *Arabidopsis thaliana*, this active domain spans ~380 amino acid residues and makes up more than two thirds of RopGEF proteins. When aligning the protein sequences of the PRONE domains of trichoblast-expressed RopGEFs including RopGEF3, 4, 10, 11, 12 and 14 (Fig. 4) using the multiple sequence alignment program Clustal Omega 1.2.4 (https://www.ebi.ac.uk/Tools/msa/clustalo/; default setting), the obtained sequence

identity percentages range from 38.15 to 75.69 % (Table 2.1). This is a considerable degree of identity especially considering that similar residues are not taken into account.

Table 1: Sequence identity [%] of PRONE protein sequences of trichoblast-expressed RopGEFs. This percent identify matrix was created with Clustal Omega 1.2.4 using corresponding protein sequences obtained from UniProt (https://www.uniprot.org/).

Protein	**Uniprot ID**	**Percent identity PRONE domains only**					
		RopGEF 14	RopGEF 3	RopGEF 4	RopGEF 10	RopGEF 11	RopGEF 12
RopGEF14	Q56WM6	100.00	40.22	38.15	42.08	40.44	40.22
RopGEF3	A4IJ27	40.22	100.00	67.47	44.44	48.73	48.74
RopGEF4	Q0WNP7	38.15	67.47	100.00	44.85	48.31	47.75
RopGEF10	Q1KS66	42.08	44.44	44.85	100.00	64.09	62.36
RopGEF11	Q9M811	40.44	48.73	48.31	64.09	100.00	75.69
RopGEF12	Q9CA89	40.22	48.74	47.75	62.36	75.69	100.00

The PRONE domain is divided into three subdomains, which share highest conservation and are connected by more variable linker sequences of approximately 20 amino acids (Berken *et al.*, 2005; Gu *et al.*, 2005). This is shown exemplarily for RopGEF3 in Fig. 10 (cartoon in Fig. 10A; labels S1-3 in Fig. 10B). RopGEF3 is a protein of 473 amino acids. The PRONE domain spans from amino acid 95 to 473. The largest PRONE subdomain S1 includes 133 amino acids (amino acids 104 to 236), followed by S2, which is 117 amino acids long (amino acids 257 to 373). PRONE subdomain S3 includes 74 amino acids (amino acids 397 to 470). The highly conserved PRONE domain of RopGEFs is flanked by variable N- and C-terminal sequences, which do not contain any known functional domains or sequence motifs (Berken *et al.*, 2005; Gu *et al.*, 2005). For RopGEF3 and 4, the N-terminus is almost 100 amino acids long (RopGEF3: 94 amino acids; RopGEF4: 83 amino acids). For both, the end of the PRONE domain is the end of the protein meaning that the PRONE domain is not followed by additional variable sequences at the C-termini (Fig. 10A). Interestingly, a cross-species phylogenetic analysis revealed that RopGEF3 and RopGEF4 are in the same phylogenetic subgroup, in which all other members are also lacking a C-terminal, noncatalytical domain (Riely *et al.,* 2011). RopGEF14 is the largest of the investigated RopGEFs (576 amino acids). The N-terminal sequence includes the first 126 amino acids. In contrast to RopGEF3 and RopGEF4, RopGEF14 PRONE domain is also flanked C-terminally by a stretch of variable amino acids (Fig. 10A; 76 amino acids). Simply in terms of RopGEF protein domain structure and overall protein size, the early polarizing RopGEF3 and RopGEF14 are less similar than RopGEF3 and the late polarizing RopGEF4.

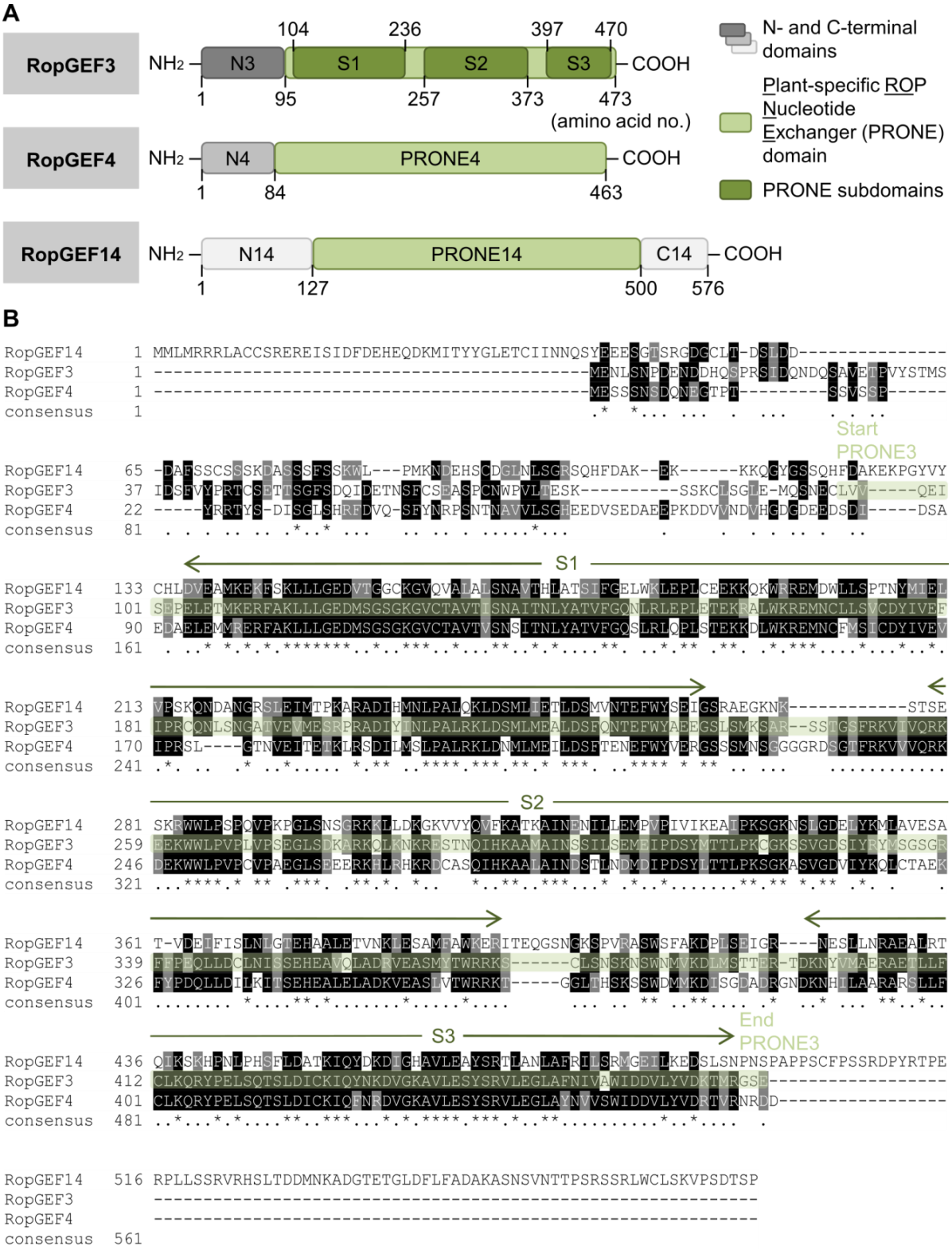

Fig. 10: Alignment of full-length protein sequences of early and late polarizing RopGEFs. (A) True to scale cartoon of RopGEF3, 4 and 14 protein domain structures. N- and C-terminal sequences are in grey shades. The catalytic Plant-specific ROP Nucleotide Exchanger (PRONE) domain is depicted in light green. For RopGEF3, the highly conserved PRONE subdomains S1-3 are indicated in dark green. Amino acid numbers at the start and end of the respective domains are indicated. (B) Multiple sequence alignment of protein sequences of RopGEF3, 4 and 14 created by Clustal Omega 1.2.4 (protein sequences obtained from Uniprot; see Table 2.1) and printed and shaded using BoxShade 3.21. Identical residues are highlighted in black, similar residues in grey. Consensus line: Asterisks mark totally identical residues in all protein sequences; dots similar residues at a position. The sequence of the PRONE domain of RopGEF3 (PRONE3) is highlighted in light green. PRONE3 subdomains S1-3 are indicated by dark green arrows.

Multiple sequence alignment of the complete protein sequences of RopGEF3, 4 and 14 using Clustal Omega 1.2.4 depicts the close relation of RopGEF3 and RopGEF4 protein sequences, while RopGEF14 protein sequence is more different in both the N-terminal part as well as the active RopGEF domain (Fig. 10B). While RopGEF3 and RopGEF4 PRONE domains share 67.47 % sequence identity, RopGEF3 and RopGEF14 PRONE domains share only 40.22 % sequence identity (Table 2.1). Noticeable are the linker sequences between PRONE subdomains S1-S2 and S2-S3, which differ substantially between the early polarizing RopGEFs, while they share more similarities in sequence as well as in length in RopGEF3 and RopGEF4 (Fig. 10B). The N-terminal sequences vary more between RopGEF3, 4 and 14 (Table 2.2). Again, RopGEF3 N-terminal sequence is more similar to the one in RopGEF4 (sequence identity: 34.92 %) than RopGEF14 (sequence identity: 21.43 %). This is in line with the phylogenetic analysis done on the complete *Arabidopsis thaliana* RopGEF protein family by Berken and colleagues in 2005 showing that the closest relative of RopGEF3 is RopGEF2, followed by RopGEF4.

Table 2: Sequence identity [%] of full-length protein sequences (or *N-terminal sequences only*) of RopGEF3, RopGEF4 and RopGEF14. This percent identify matrix was created with Clustal Omega 1.2.4 using corresponding protein sequences obtained from UniProt (https://www.uniprot.org/).

Protein	**UniProt ID**	**Percent identity full-length proteins *(N-termini only)***		
		RopGEF14	RopGEF3	RopGEF4
RopGEF14	Q56WM6	100.00 *(100.00)*	38.34 *(21.43)*	36.28 *(20.59)*
RopGEF3	A4IJ27	38.34 *(21.43)*	100.00 *(100.00)*	61.97 *(34.92)*
RopGEF4	Q0WNP7	36.28 *(20.59)*	61.97 *(34.92)*	100.00 *(100.00)*

Three-dimensional information about the PRONE domain is available based on the crystal structure resolved for RopGEF8 PRONE domain and shows a mostly α-helical structure (Thomas *et al.,* 2006; Thomas *et al.,* 2007; see section 1.2.1). For the N- and C-termini of RopGEFs, however, there is no structural information available. The variable sequence of these terminal regions of RopGEFs potentially indicates also a structural diversity. To test whether the non-catalytical regions of RopGEF3, 4 and 14 have a fixed or ordered three-dimensional structure at all, RopGEF protein sequences were subjected to the Cspritz web server 1.2 (http://old.protein.bio.unipd.it/cspritz/; prediction type: X-ray short; Walsh *et al.,* 2011). The Cspritz web server identifies regions within protein sequences lacking structural content and provides a probability of disorder for each residue. The tool identified one disordered region (> 50 amino acids) in RopGEF3 and RopGEF4 and two in RopGEF14. These regions basically contain the N- and C-terminal sequences of RopGEFs (Fig. 11). Additional, but shorter disordered segments were identified within the PRONE domain for all three RopGEFs (10-22 amino acids long). These disordered segments largely correspond to the linker sequences between the individual PRONE subdomains (Fig. 11A). Taken together,

the *in silico* prediction revealed that the less conserved regions of RopGEF proteins are structurally dynamic in contrast to the conserved and mostly α-helical PRONE subdomains S1-3. Linker sequences or loops between defined domains are often regions of disorder within a protein providing conformational flexibility to arrange functional domains as required and therefore allow binding diversity. Structural disorder is also often found in factors involved in cell signaling providing variable interaction surfaces, which often mediate binding with high specificity and low affinity rendering interactions reversible (Dunker *et al.,* 2005). The structural disorder of RopGEF N-termini suggests their involvement in dynamic binding processes such as protein-protein interactions and/ or intramolecular interactions with the active PRONE domain as it was suggested by Gu *et al.* (2006) for the RopGEF1 C-terminus (see section 1.2.1).

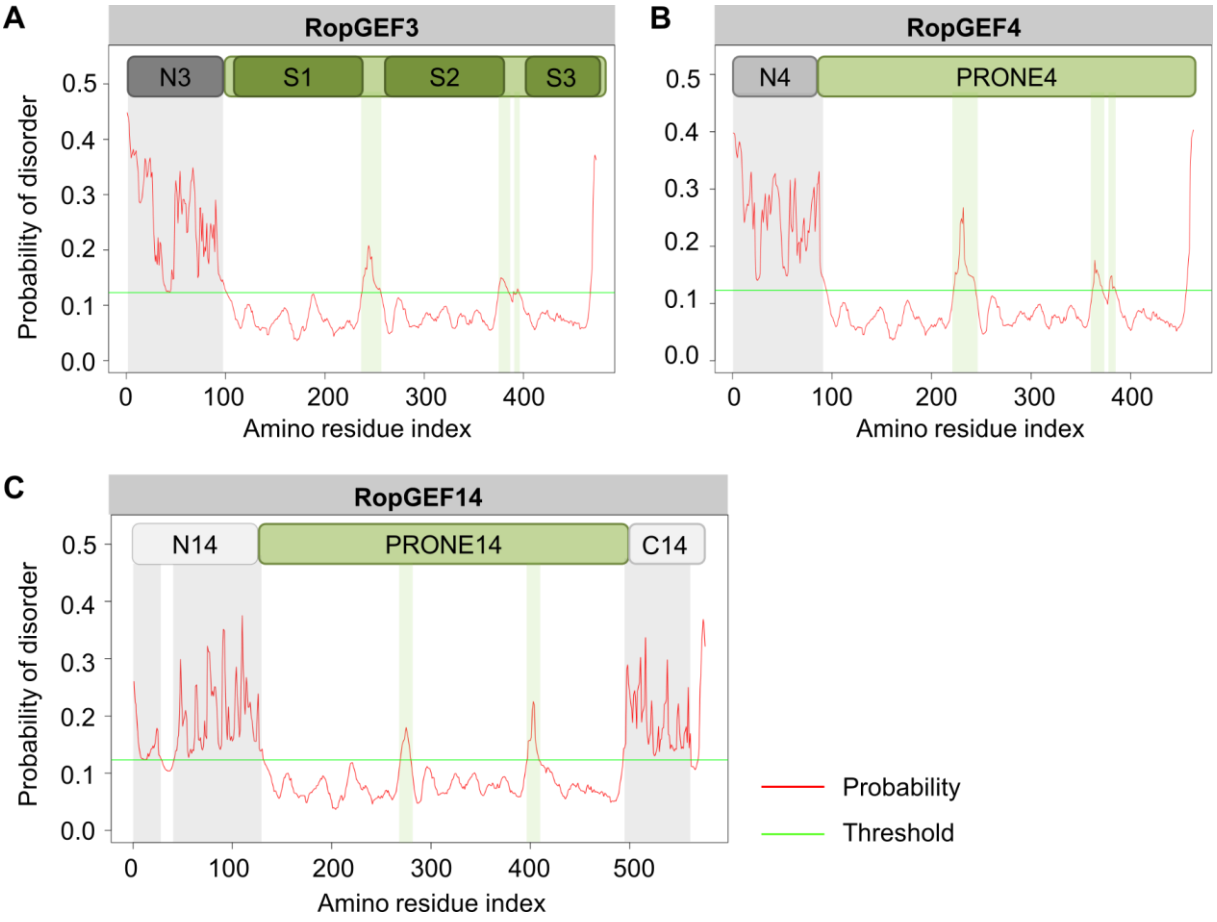

Fig. 11: RopGEF N- and C-termini are intrinsically disordered. (A-C) Disorder plots for RopGEF3 (A), RopGEF4 (B) and RopGEF14 (C) showing the probability of disorder (red line) with a cut-off threshold (green line) for each amino acid residue. Plots were created using the Cspritz web server 1.2 (prediction type: X-ray (short)). True to scale schemes of RopGEF proteins show the variable termini in grey shades and the active PRONE domain in green. For RopGEF3 (A), PRONE subdomains are indicated in dark green. Light grey/ green backgrounds highlight regions with a probability of disorder exceeding the internal probability threshold defined by the software.

However, based on the primary sequence and structural characteristics of the different RopGEF domains, no obvious pattern, sequence motifs or other features distinguishing the early polarizing RopGEF3 and RopGEF14 from the late polarizing RopGEF4 could be identified. Since RopGEFs mostly vary in their terminal sequences and RopGEF3 and RopGEF4 are lacking the variable C-terminal sequences, the N-termini might still hold clues regarding differential RopGEF localization and regulation during root hair development. To investigate the influence of the individual RopGEF domains including the N-terminus, the PRONE domain as well as the single PRONE subdomains on the subcellular appearance of the protein as well as on root hair development, corresponding RopGEF3 truncations were characterized in the following.

2.2.2 RopGEF3 N-terminus does not mediate early polarization timing, but contributes to RopGEF3 regulation at the RHID

Previous *in silico* analyses of RopGEF N-termini (Fig. 10, 11) did not reveal obvious features, which could account for the differential polarization timing of RopGEF3 and RopGEF14 compared to RopGEF4, or any hints regarding the function of these domains. Still, the variable N-terminal regions are promising to differentiate RopGEFs in some way. Therefore, the potential impact of RopGEF N-termini on subcellular localization and polarization timing of RopGEFs was investigated *in vivo*. To this end, I generated fluorescently-labeled RopGEF3 truncations and expressed these fusion proteins under the endogenous RopGEF3 promoter in the *ropgef3-1* mutant background. This way, the fusion proteins could also be tested for their capability to compensate for the loss of endogenous RopGEF3 protein by assessing the macroscopic root hair phenotypes. These constructs included the RopGEF3 N-terminus (N3), RopGEF3 PRONE domain (PRONE3) as well as the individual PRONE3 domain subunits S1-3. Phenotypes of the truncations were compared to the corresponding rescue line expressing fluorescently-labeled RopGEF3 full-length CDS (RopGEF3 FL) under the endogenous promoter in the *ropgef3-1* mutant background presented in Fig. 5.

When expressing RopGEF3 N-terminus only (N3; Fig. 12A), no polarization at the RHID could be observed from cell stage -5 to cell stage +2 (Fig. 12B, C). Most signal was found in the cytosol and the nucleus, suggesting that N3 alone might not be able to efficiently associate with the plasma membrane anymore.

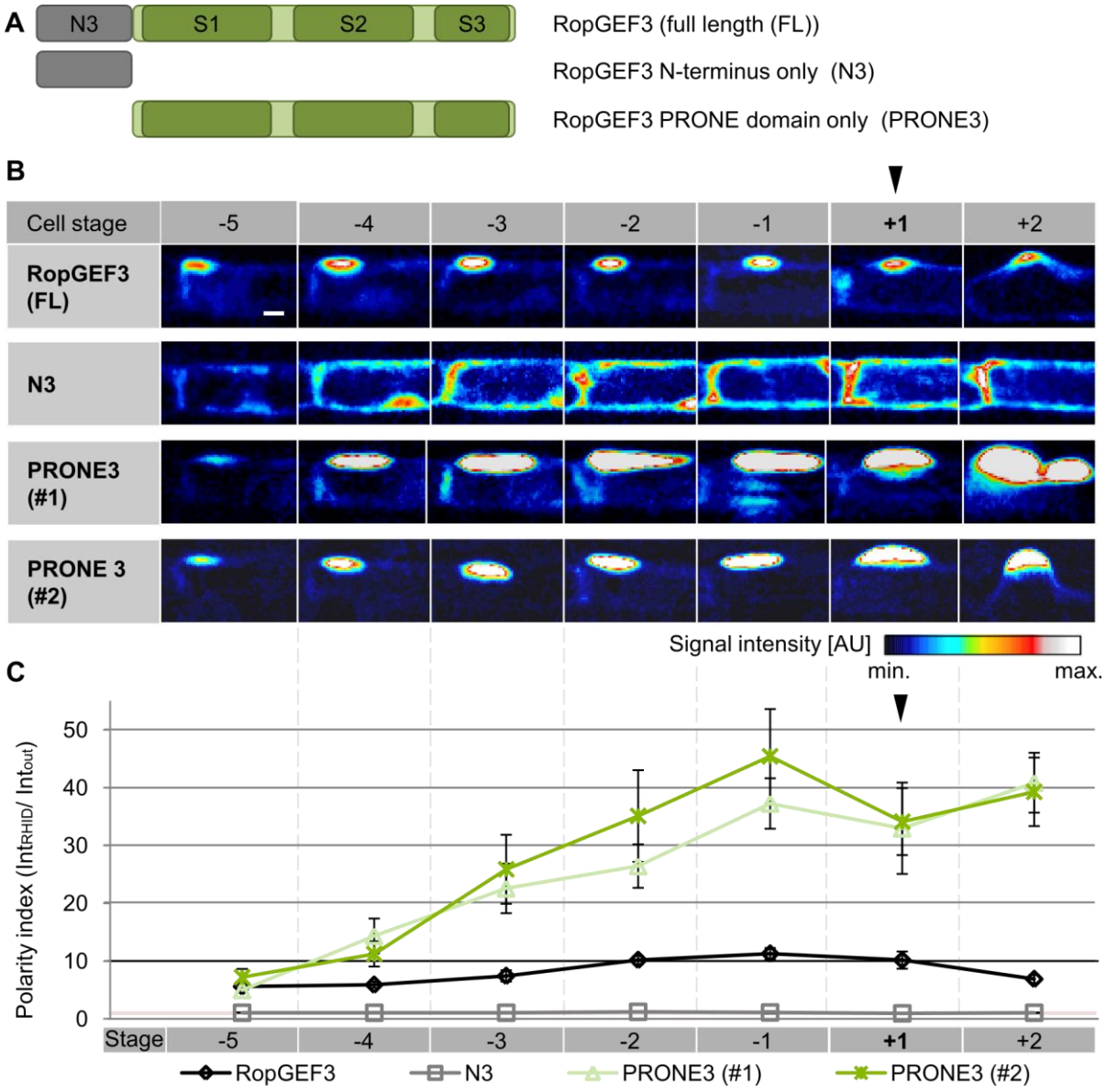

Fig. 12: N-terminal truncation does not affect RopGEF3 polarization timing. (A) True to scale scheme of RopGEF3 truncations. RopGEF3 N-terminus (N3) is depicted in grey. The highly conserved active RopGEF domain (PRONE3) is depicted in green with subunits S1-3 in dark green. (B) Representative z-projections of trichoblasts (cell stage -5 to +2) of *A. thaliana* lines expressing mCit-RopGEF3, mCit-N3 and mCit-PRONE3 (two independent lines: PRONE3 #1/ 2) in the *ropgef3-1* mutant background. Images of PRONE3 are not overexposed, but scaled the same way as RopGEF3 FL to emphasize the difference in signal intensity at the RHID. Note that images (B) as well as polarity indices of mCit-RopGEF3 (C) are reused from Fig. 5B, C. Signals are depicted in the pseudo-color LUT 'royal' of ImageJ. Scale bar, 10 µm. (C) Polarity indices of above mentioned fusion proteins during root hair initiation (cell stage -5 to +2). Mean values and standard errors of the mean (SEM) are plotted for each cell stage. Arrow head indicates the reference cell +1; light red line indicates no polarity at the RHID (PI = 1); n = 7-10 trichoblast cell files from 6-10 individual roots.

In contrast, expressing the complete active RopGEF domain alone (PRONE3 (#1/2 are independent lines)) revealed a polarization timing indistinguishable from the full-length (FL) RopGEF3 (Fig. 12B, C). Polarization of PRONE3 started as soon as its expression could be detected in cell stage -5 as it could be observed for RopGEF3 FL. In this early stage, the polarity indices (PIs) of PRONE3 and RopGEF3 FL were in a similar range (Fig. 12B, C; PI(RopGEF3 FL; cell -5) = 5.6 ± 0.81 (mean ± SEM; same for all following numbers in this

paragraph); PI(PRONE3 (#1); cell -5) = 4.96 ± 0.01; PI(PRONE3 (#2); cell -5) = 7.22 ± 1.42). However, soon after this initial cell stage, RHIDs in PRONE3 differed substantially from RopGEF3 FL domains. Signal intensities in PRONE3 domains increased rapidly leading to very high polarity indices, which peaked in cell stage -1 similar to RopGEF3 FL. In this cell stage, polarity indices for PRONE3 were increased by a factor of 3.3 or 4.0 respectively compared to polarity indices of RopGEF3 FL (Fig. 12B, C; PI(RopGEF3 FL; cell -1) = 11.27 ± 0.99; PI(PRONE3 (#1); cell -1) = 37.27 ± 4.36; PI(PRONE3 (#2); cell -1) = 45.45 ± 8.17). To ensure that this is not an overexpression artifact specific to one transgenic line, I quantified two independent lines (PRONE3 #1 and #2).

Additionally, domain diameters of PRONE3 increased more rapidly over the course of root hair development compared to RopGEF3 FL (Fig. 12B; Fig. 13A, B). To precisely compare RHID sizes, intensity profiles along the outer plasma membrane of trichoblasts starting at the rootward cell edge over the RHID were plotted and Full Width at Half Maximum (FWHM) values in cell stages -4, -1 and +1 were determined (Fig. 13B). In early stages (cell stage -4), the domain sizes (DS) between PRONE3 and RopGEF3 FL did not differ significantly (DS(RopGEF3 FL; cell -4) = 12.94 µm ± 1.07; DS(PRONE3 (#1); cell -4) = 15.07 µm ± 1.56; DS(PRONE3 (#2); cell -4) = 15.15 µm ± 1.23). While RopGEF3 FL domain sizes increased to a FWHM value of 15.19 µm ± 0.96 in the bulging stage, PRONE3 domains reached up to almost double FWHM values (DS(PRONE 3 (#1); cell +1) = 27.41 µm ± 2.03; DS(PRONE 3 (#2); cell +1) = 23.92 µm ± 3.37). Furthermore, ectopic domains of irregular sizes located at various positions along the outer plasma membrane of trichoblasts could frequently be observed in the PRONE3 lines (Fig. 13A, arrow heads). Such additional domains showing aberrant positioning are usually not observed in the RopGEF3 FL marker lines. Interestingly, PRONE3 domains (at the endogenous position of the RHID) in later stages (starting from cell -1) often showed two peaks in signal intensity at the edges of the domain, while the signal in the middle of the domain was decreased (Fig. 13C, middle panel; Fig. 12B) as if the domain was about to separate into two parts. In other cases, irregularly sized domains could be observed directly next to each other (Fig. 13C, upper and lower panel) sometimes resulting in two more or less merged bulges (Fig. 13C, upper panel).

Taken together, these data show that N3 is not required for the proper polarization timing and potentially also membrane association of RopGEF3. A study in *Medicago truncatula* (*Mt*) on *Mt*RopGEF2 also reported that the N-terminus is not required to localize the marker protein to the tips of root hairs (Riely *et al.,* 2011).

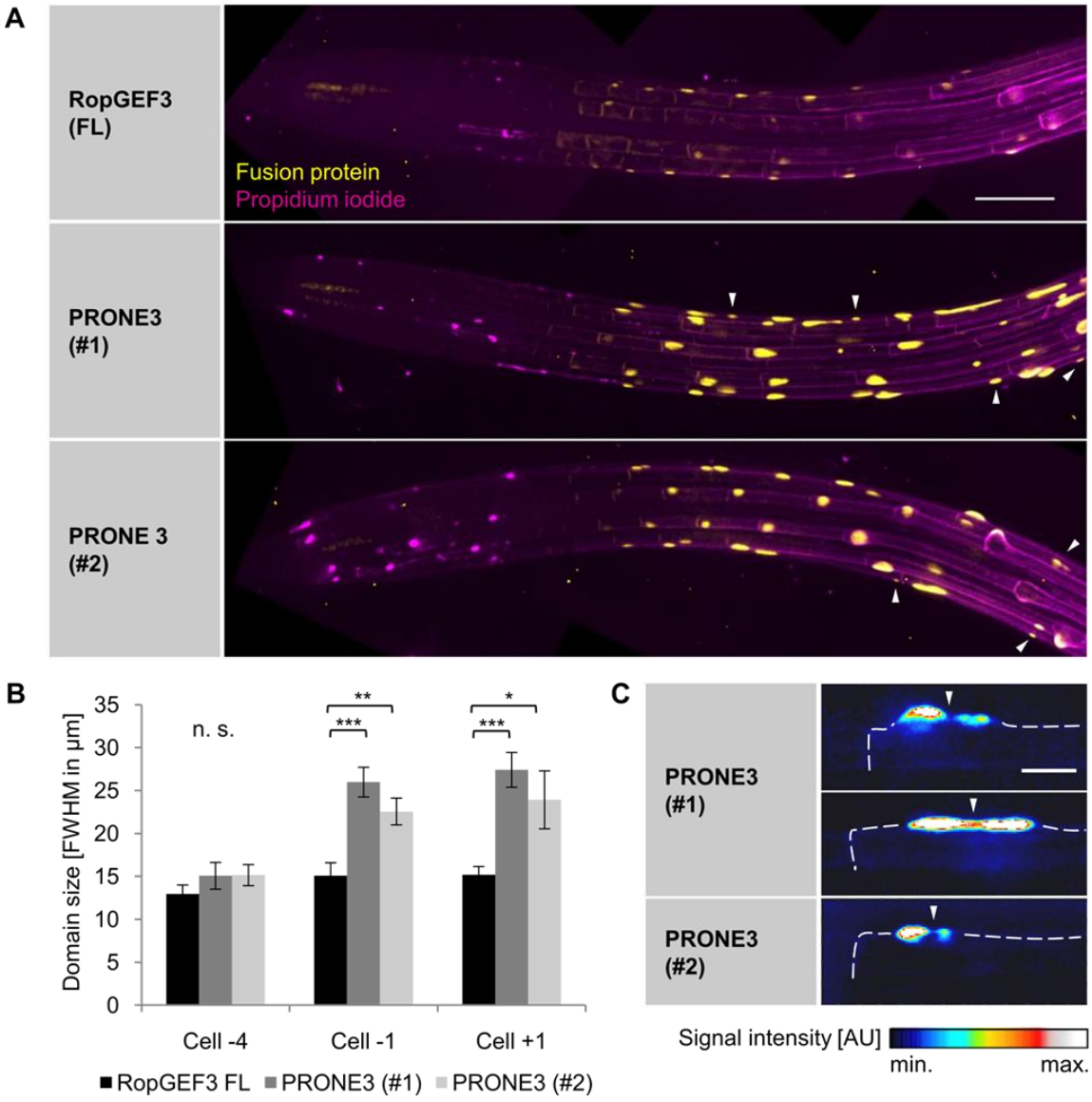

Fig. 13: Removal of RopGEF3 N-terminus creates enlarged RHIDs in later stages and ectopic domains. (A) Representative z-projections of primary roots of *A. thaliana* lines expressing mCit-RopGEF3 and mCit-PRONE3 (two independent lines: PRONE3 #1/ 2). Fusion proteins are depicted in yellow. Cell outlines were visualized using propidium iodide staining (magenta). Arrow heads highlight ectopic signal outside the RHID. Scale bar, 100 µm. (B) Quantification of RHID sizes in cell stages -4, -1 and the bulging stage +1 in above mentioned marker lines. Means of Full Width at Half Maximum (FWHM) values and standard errors of the mean are shown for each cell stage. Statistical differences to RopGEF3 FL were determined by a two-sided, unpaired Student's t-test assuming unequal variances: Not significant (n.s.) $p > 0.05$; * $p \leq 0.05$; ** $p \leq 0.01$; *** $p \leq 0.001$. n = 7-10 trichoblasts from 5-10 individual roots. (C) Example z-projections from trichoblasts in the bulging state or older from *A. thaliana* lines expressing PRONE3. Signals are depicted in the pseudo-color LUT 'royal' of ImageJ. Arrow heads highlights signal minimum within the domain/ signal gap. Scale bar, 25 µm.

Instead, it is the active RopGEF domain that is required to efficiently bring the protein to the membrane and to timely polarize it at the RHID. This is in line with observations made for RopGEF1 truncations in pollen tubes showing that PRONE1 was necessary and sufficient for membrane targeting (Gu *et al.*, 2006). In contrast, PRONE12 was shown not to be sufficient for membrane targeting (Zhang & McCormick, 2007). Intriguingly, removal of the N-terminus resulted in more signal at the RHID and created larger domains compared to the full-length

RopGEF3. The occurrence of additional, ectopically localized RopGEF domains is an observation, which was also made when RopGEF3 was overexpressed (Denninger and Reichelt *et al.,* 2019; Fig .8). These ectopic domains were more uniform in size and localization (Denninger and Reichelt *et al.,* 2019; often close to the shoot-ward cell pole) than ectopic PRONE3 domains. However, ectopic PRONE3 domains were also capable to create additional hair initiation sites similar to RopGEF3 overexpression.

To further investigate RopGEF3 truncations with regard to their functionality, the macroscopic root hair phenotypes of these lines were assessed. Expressing N3 alone did not rescue the *ropgef3-1* mutant phenotype. The distance between root tip and the first bulge remained increased and root hair density and length were still decreased to a similar extent in N3 compared to *ropgef3-1* (Fig. 14A, C-E). These observations are in line with the expectations as N3 is lacking the active RopGEF domain and therefore cannot fulfill the RopGEF function. Additionally, N3 is not polarized at the RHID (Fig. 12B, C), where the RopGEF function would be required. In contrast, expression of PRONE3 did rescue the delayed bulging as well as the decrease root hair initiation frequency (Fig. 14A, C-E; distance Col-0: 100 % ± 1.54; distance PRONE3 (#1): 115.62 % ± 4.29; PRONE3 (#2): 95.20 % ± 4.28; density Col-0: 100 % ± 1.93; density PRONE3 (#1): 103.59 % ± 3.84; density PRONE3 (#2): 104.39 % ± 5.80). This observation matches the localization data presented before showing that PRONE3 polarization timing at the RHID is similar to RopGEF3 FL (Fig. 12B, C). However, PRONE3 expressing lines were not capable of growing regular long root hairs. Instead, root hair length in PRONE3 was further decreased compared to *ropgef3-1* mutant (Fig. 14A, E; length Col-0: 100 % ± 5.91; length *ropgef3-1*: 77.17 % ± 2.32; length PRONE3 (#1): 49.67 % ± 2.78; length PRONE3 (#2): 58.89 % ± 6.56). Furthermore, additional hair initiation sites in single trichoblasts as well as branched root hairs could be observed regularly in PRONE3 (Fig. 14B, asterisks/ arrow heads), while Col-0 usually grows only one, unbranched root hair per trichoblast. This phenotype remarkably resembles the phenotype observed for RopGEF3 overexpression, which can also initiate additional bulges, however, fails in efficiently triggering polar growth (Denninger and Reichelt *et al.,* 2019). In addition, root hairs in PRONE3 appear thicker compared to wild type root hairs; especially the diameter of the root hair base seemed to be increased (Fig. 14B), which would fit the increased domain sizes in PRONE3 (Fig. 13B). In summary, expression of PRONE3 is largely reminiscent of RopGEF3 overexpression observed on both the subcellular as well as on the macroscopic level. The observation that lack of the N-terminus leads to RopGEF3 overexpression-like effects, even though expression is controlled by the endogenous RopGEF3 promoter, might hint towards a function of N3 in the regulation of protein abundance on a post-transcriptional level.

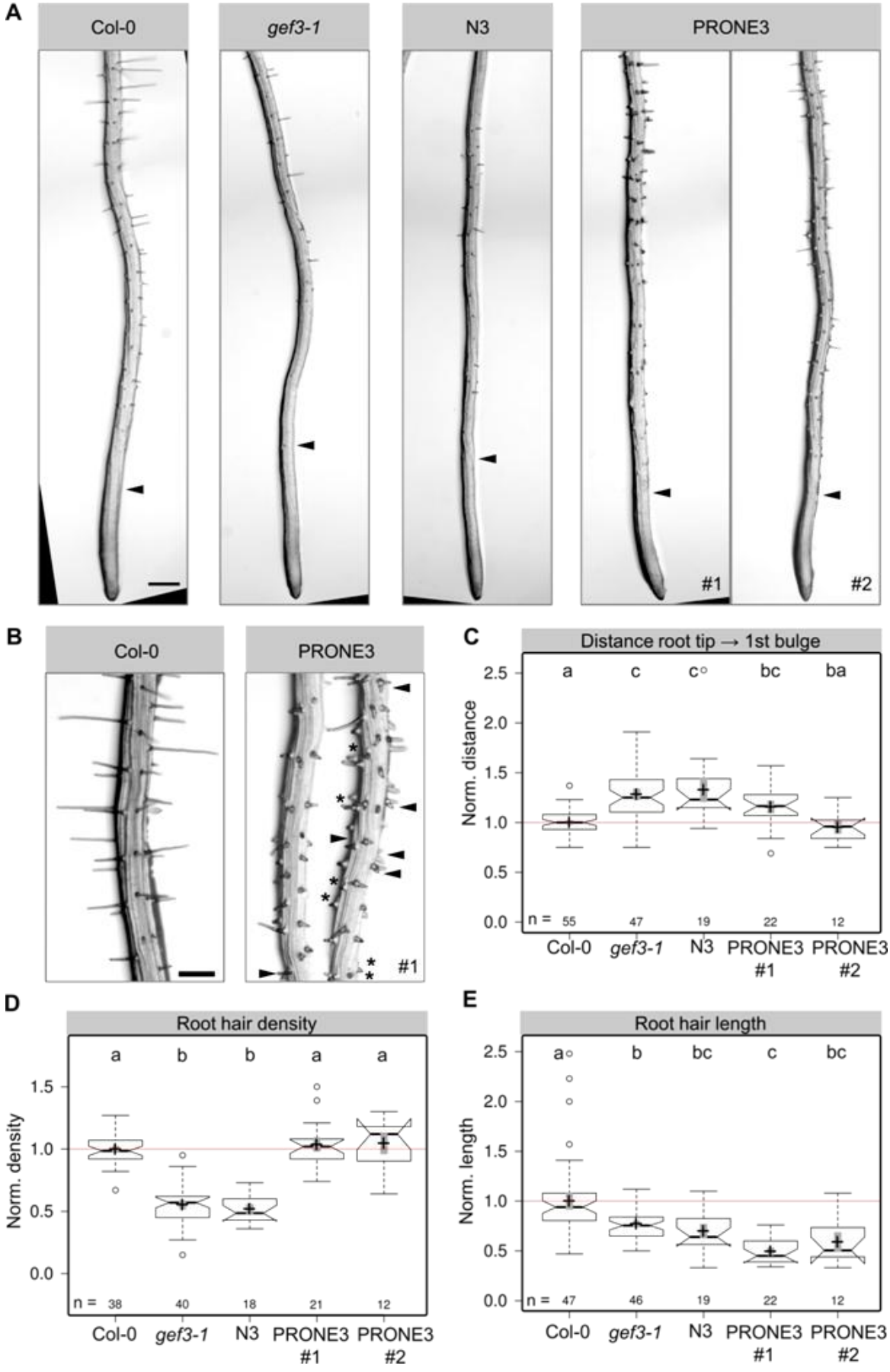

Fig. 14: Expression of PRONE3 largely rescues the *ropgef3-1* mutant phenotype, but generates short, additional and partially branches root hairs. Complete figure legend on next page.

Fig. 14 (previous page)**: Expression of PRONE3 largely rescues the *ropgef3-1* mutant phenotype, but generates short, additional and partially branches root hairs.** (A) Representative stereoscope images of roots of *A. thaliana* Col-0, *ropgef3-1* mutant and marker lines expressing RopGEF3 N-terminus (N3) and RopGEF3 PRONE domain (PRONE3; two independent lines #1/ 2) in the *ropgef3-1* single mutant background. Arrow heads indicate first bulge. Scale bar, 250 µm. (B) Representative close-ups of primary roots of Col-0 and PRONE3. Asterisks indicate additional hair initiation sites in single trichoblasts. Arrow heads highlight branched root hairs. Scale bar, 150 µm. (C-E) Quantification of root hair phenotypes of above mentioned genotypes. Measured parameters are normalized to the averaged values of Col-0 (= 1.0, marked by light red line). n indicates numbers of analyzed cell files; center lines represent medians, crosses represent means; gray bars mark 83% confidence intervals of means; letters show result of a 2-way ANOVA test (significance value, p = 0.05), different letters indicate statistically significant differences.

2.2.3 The complete PRONE3 domain is required for efficient membrane association and polarization at the RHID

Previous studies showed that the complete PRONE domain including all three subdomains is required for the nucleotide exchange activity of RopGEFs as any truncation of this active domain resulted in complete inactivation of RopGEF proteins (Berken *et al.,* 2005; Gu *et al.,* 2006). However, individual PRONE subdomains might be differentially relevant for membrane association and polarization at the RHID. For example, individual PRONE subdomains might contain posttranslational modifications required for the association of the protein with the membrane such as protein S-acylation. Attached lipids can intercalate into the membrane and therefore increase the membrane affinity of the respective protein (Li & Qi, 2017). An initial analysis using the online prediction tool for lipid modification sites *GPS-Lipid* revealed indeed two putative S-palmitoylation sites in the RopGEF3 protein (http://lipid.biocuckoo.org/webserver.php; low threshold; Ren *et al.,* 2008; Xie *et al.,* 2016). The first site reported by the prediction tool was at position 94 in the RopGEF3 protein (Cysteine 94 (C94); score: 2.03). This residue is part of the N-terminus, which was shown not to be required for efficient membrane targeting and polarization (Fig. 12). The second putative S-palmitoylation site was C320, which is part of the PRONE3 subdomain S2 (score: 1.031; Fig. 15A) and therefore could be involved in membrane targeting of RopGEF3. Moreover, the individual PRONE subdomains might harbor distinct interaction sites, which possibly mediate the interaction with a RopGEF-specific recruitment factor. To test whether one individual PRONE subdomain is sufficient for RopGEF3 membrane association and polarization at the RHID, I generated *A. thaliana* lines expressing fluorescently-labeled PRONE3 subdomains S1-3 in the *ropgef3-1* mutant background and observed the subcellular localization of these fusion proteins as well as the macroscopic root hair phenotypes.

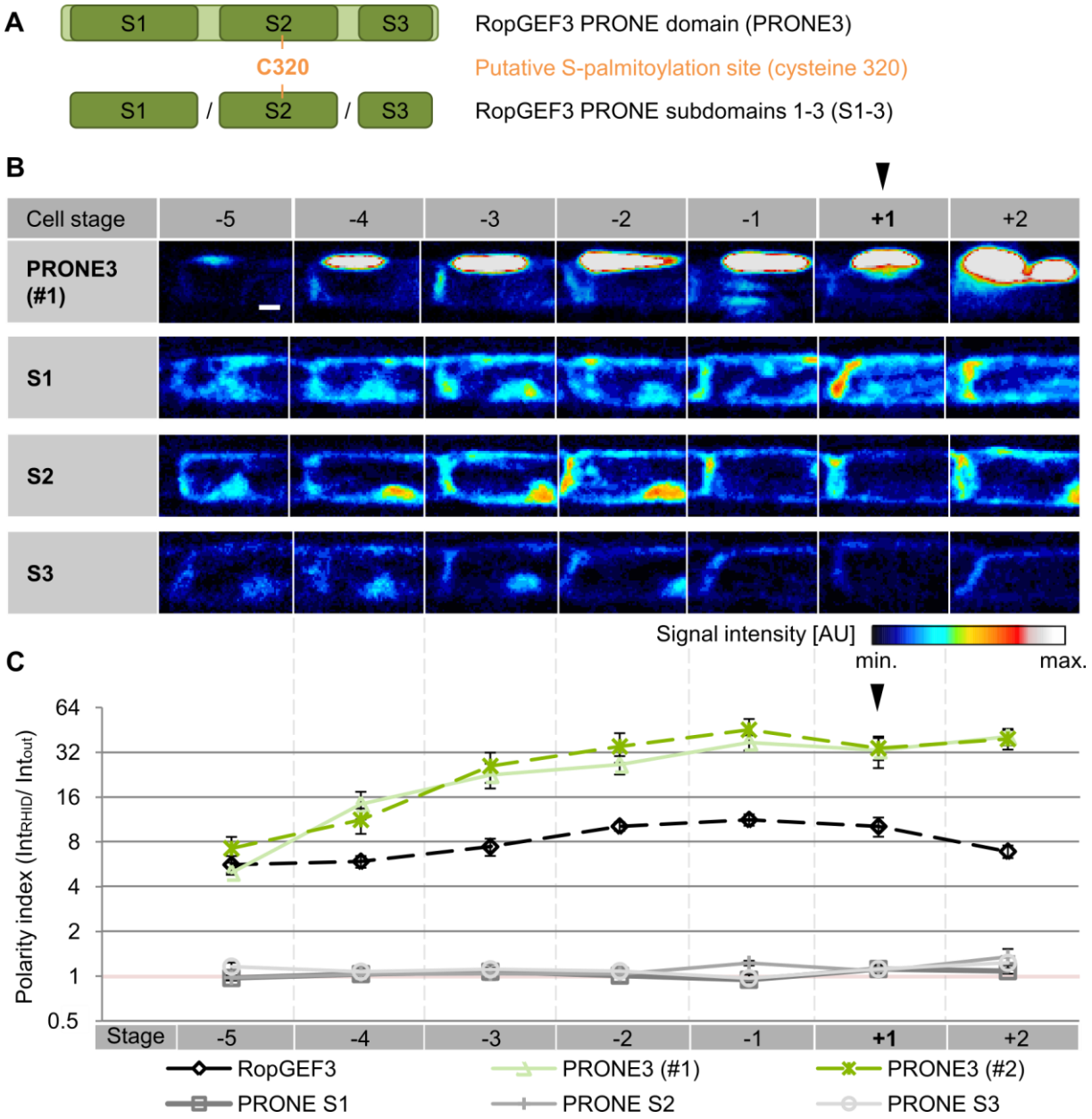

Fig. 15: Individual PRONE3 subdomains S1-3 mainly localize to the cytosol. (A) True to scale scheme of PRONE3 and PRONE3 subdomains S1-3. The highly conserved active RopGEF domain (PRONE3) is depicted in green with subunits S1-3 in dark green. Cysteine 320 (C320) in PRONE3 subdomain S2 (orange) is the only S-acylation site in the active domain predicted by the online prediction tool GPS-Lipid. (B) Representative z-projections of trichoblasts (cell stage -5 to +2) of *A. thaliana* lines expressing mCit-PRONE3, mCit-S1, mCit-S2 and mCit-S3 in the *ropgef3-1* mutant background. Note that images of mCit-PRONE3 (#1) are reused from Fig. 5B, C. Signals are depicted in the pseudo-color LUT 'royal' of ImageJ. Scale bar, 10 µm. (C) Polarity indices of above mentioned fusion proteins during root hair initiation (cell stage -5 to +2). Note that polarity indices of PRONE3 (#1/2) as well as RopGEF3 FL are reused from Fig. 5C. Note that images of PRONE3 are not overexposed, but scaled the same way as RopGEF3 FL (see Fig. 12) to emphasize the difference in signal intensity at the RHID. Polarity indices from genotypes not represented in (B) are plotted as dashed lines. Note that base-2 log scale is used for the y-axis to better resolve PIs of S1-3. Mean values and standard errors of the mean (SEM) are plotted for each cell stage. Arrow head indicates the reference cell +1; light red line indicates no polarity at the RHID (PI = 1); n = 7-11 trichoblast cell files from 5-11 individual roots.

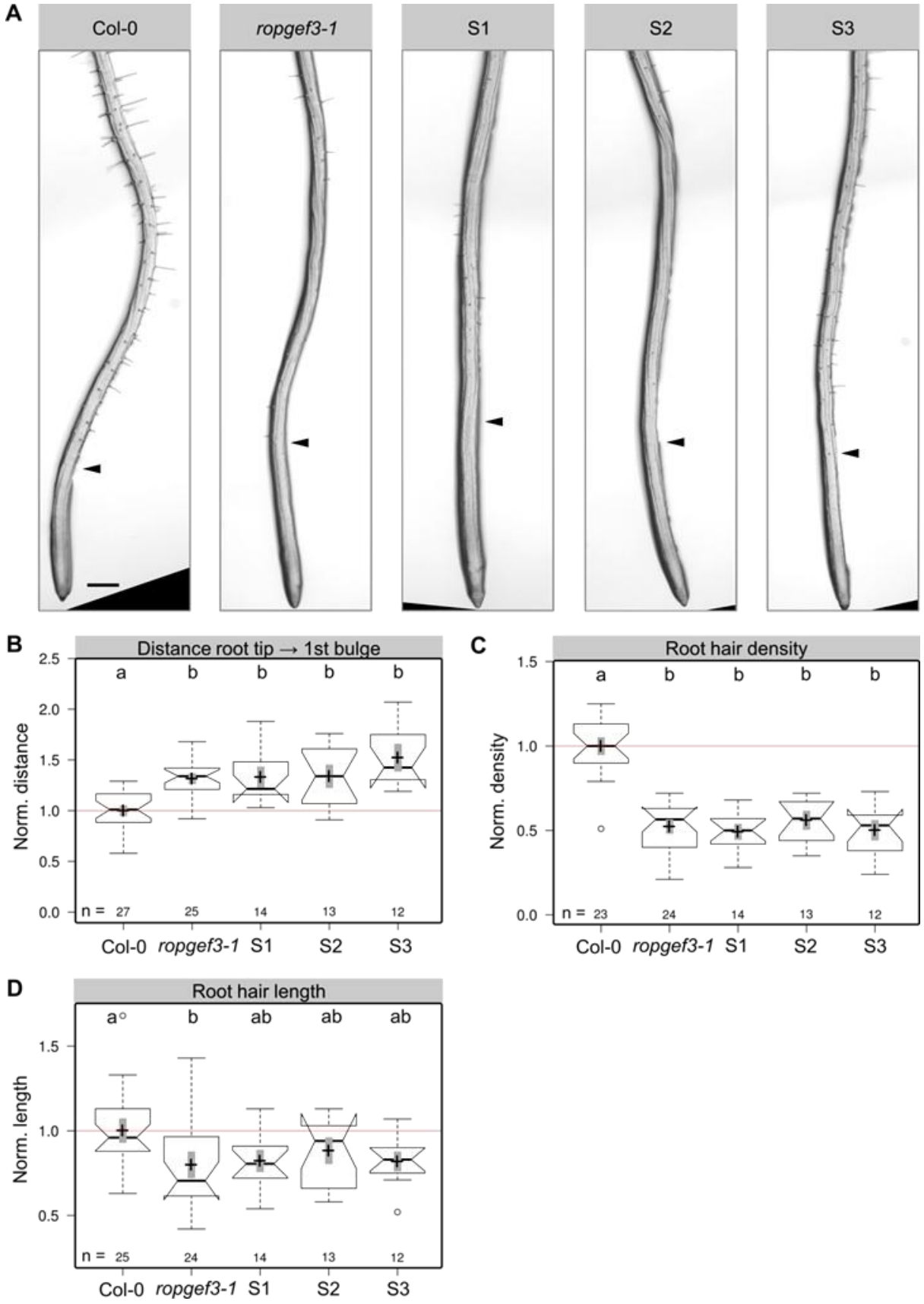

Fig. 16: Single PRONE3 subdomains S1-3 cannot rescue *ropgef3-1* single mutant phenotype. Complete figure legend on next page.

Fig. 16 (previous page)**: Single PRONE3 subdomains S1-3 cannot rescue *ropgef3-1* mutant phenotype.** (A) Representative stereoscope images of roots of *A. thaliana* Col-0, *ropgef3-1* mutant and marker lines expressing PRONE3 subdomains S1-3 in the *ropgef3-1* mutant background. Arrow heads indicate first bulge. Scale bar, 250 µm. (B-D) Quantification of root hair phenotypes of above mentioned genotypes. Measured parameters are normalized to the averaged values of Col-0 (= 1.0, marked by light red line). n indicates numbers of analyzed cell files; center lines represent medians, crosses represent means; gray bars mark 83% confidence intervals of means; letters show result of a 2-way ANOVA test (significance value, p = 0.05), different letters indicate statistically significant differences.

I found that all three PRONE3 subdomains mainly localized to the cytosol and the nucleus (Fig. 15B) similar to the localization of the noncatalytic N3 (Fig. 12B). The polarity indices determined for S1-3 between cell stages -5 and +2 ranged from 0.95 to 1.35 (Fig. 15B) and show that none of these fusion proteins polarized at the RHID. These results indicate that the PRONE domain as a whole is required to efficiently associate RopGEF3 to the membrane and polarize it. Possibly, the interaction site mediating RopGEF3 recruitment to the RHID involves parts of all or a combination of PRONE3 subdomains S1-3. The fact that also PRONE3 subdomain S2 is mostly found in the cytosol, also reduces the potential impact of the putative S-palmitoylation site C320 on RopGEF3 membrane association. In line with these observations and above-mentioned studies on PRONE truncations and RopGEF nucleotide exchange activity, expression of single PRONE3 subdomains could not rescue the *ropgef3-1* mutant root hair phenotype (Fig. 16). For all parameters investigated, lines expressing S1-3 were indistinguishable from *ropgef3-1* mutant indicating that these RopGEF3 truncations are not functional.

2.2.4 N-termini of early polarizing RopGEFs are functionally related

Previously, I have shown that RopGEF3 N-terminus (N3), which is the part of the protein that exhibits least sequence conservation RopGEFs (Fig. 10B), is not involved in the differential polarization timing (Fig. 12B). However, based on the observations that RHIDs are enlarged and root hair phenotypes are reminiscent of RopGEF3 overexpression in PRONE3 expressing lines (Fig. 12-14), I concluded that N3 might be involved in local protein abundance regulation at the RHID. This led to the hypothesis that the N-termini of early polarizing RopGEFs – despite little sequence similarity – might share functional features, which differ from functions mediated by N-terminal sequences of late polarizing RopGEFs. To test this hypothesis, I generated stable *A. thaliana lines* expressing fluorescently-labeled RopGEF chimeric proteins under the endogenous RopGEF3 promoter in the *ropgef3-1* mutant background. RopGEF chimeras shared the active PRONE3 domain and differed in the N-termini (Fig. 17A): In the first RopGEF chimera, the N-terminus of RopGEF4 was fused to PRONE3 (termed N4-PRONE3) and in the second chimera the N-terminus of RopGEF14 was fused to PRONE3 (termed N14-PRONE3).

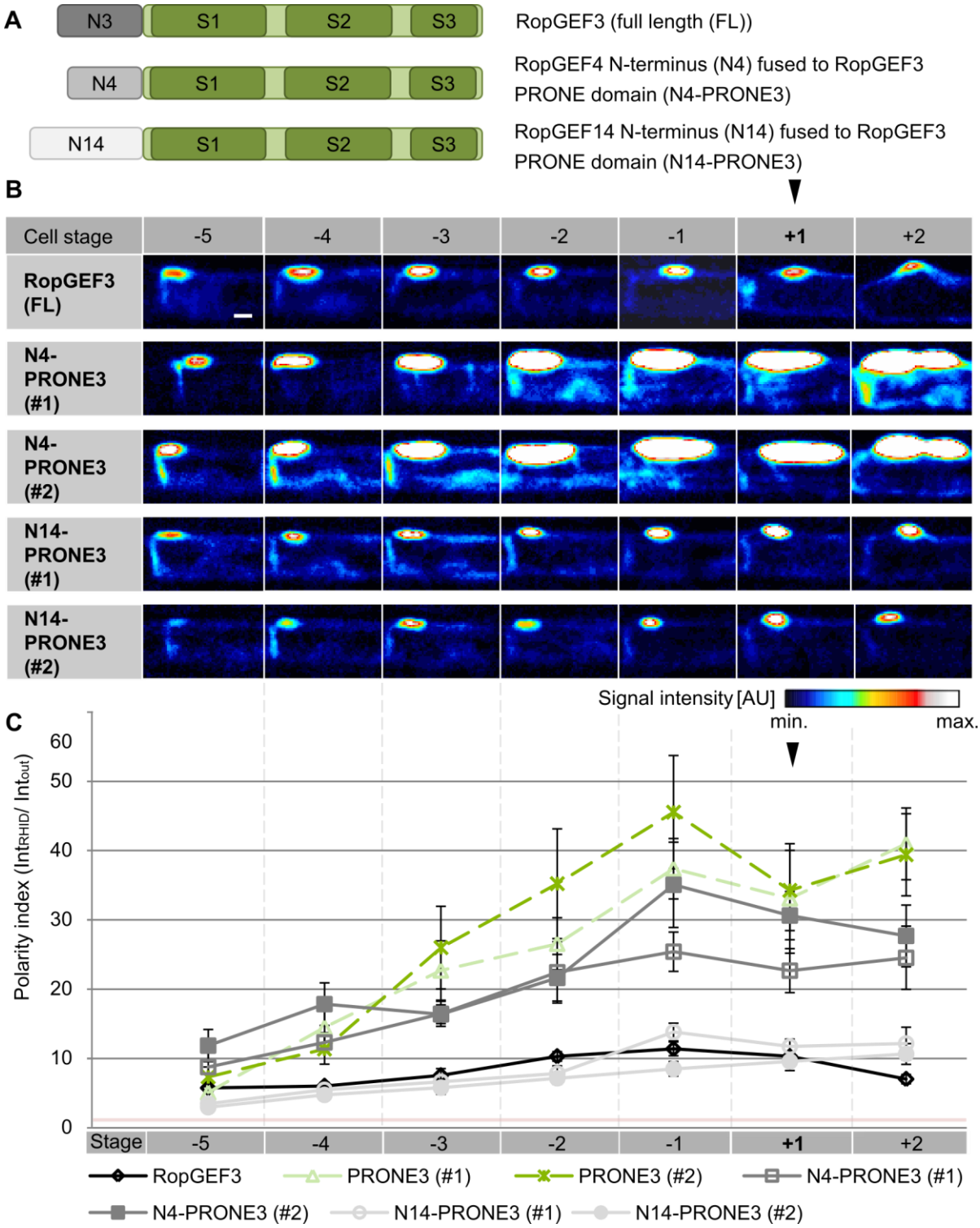

Fig. 17: Exchanging RopGEF3 N-terminus by RopGEF14 N-terminus results in a similar degree of polarization at the RHID. (A) True to scale scheme of RopGEF3 full-length (FL) and RopGEF chimeric proteins (N4-PRONE3 and N14-PRONE3). RopGEF3 N-terminus (N3) is depicted in dark grey, RopGEF4 N-terminus (N4) in grey and RopGEF14 N-terminus (N14) in light grey. The highly conserved active RopGEF domain (PRONE3) is depicted in green with subunits S1-3 in dark green. (B) Representative z-projections of trichoblasts (cell stage -5 to +2) of *A. thaliana* lines expressing mCit-RopGEF3, mCit-N4-PRONE3 and mCit-N14-PRONE3 (two independent lines each (#1/ 2)) in the *ropgef3-1* mutant background. Images of N4-PRONE3 are not overexposed, but scaled the same way as RopGEF3 FL to emphasize the difference in signal intensity at the RHID. Note that images (B) as well as polarity indices of mCit-RopGEF3 FL (C) are reused from Fig. 5B, C. Signals are depicted in the pseudo-color LUT 'royal' of ImageJ. Scale bar, 10 µm. (C) Polarity indices of above mentioned fusion proteins during root hair initiation (cell stage -5 to +2). Mean values and standard errors of the mean (SEM) are plotted for each cell stage. Arrow head indicates the reference cell +1; light red line indicates no polarity at the RHID (PI = 1); n = 7-10 trichoblast cell files from 6-10 individual roots.

Subcellular localization and polarization timing of these RopGEF chimeras using two independent lines each (#1/ 2) were analyzed during root hair development (cell stage -5 to +2) as described above (Fig. 17B, C). For both RopGEF chimeras, the polarization timing was indistinguishable from RopGEF3 FL. In cell stage -5, all fusion proteins were found to be polarized at the RHID, even though, the degree of polarization was slightly higher for N4-PRONE3 and slightly lower for N14-PRONE3 compared to RopGEF3 FL (Fig. 17C; PI(RopGEF3 FL; cell -5) = 5.62 ± 0.81 (mean ± SEM; same for all following numbers in this paragraph); PI(N4-PRONE3 (#1); cell -5) = 8.65 ± 2.28; PI(N4-PRONE3 (#2); cell -5) = 11.74 ± 2.33; PI(N14-PRONE3 (#1); cell -5) = 3.43 ± 0.36; PI(N14-PRONE3 (#2); cell -5) = 2.88 ± 0.28). During the course of root hair development, the PIs determined for N4-PRONE3 increased rapidly and peaked in cell -1 (Fig. 17C; PI(N4-PRONE3 (#1); cell -1) = 25.28 ± 2.83; PI(N4-PRONE3 (#2); cell -1) = 34.95 ± 6.15), similar to the PIs determined for PRONE3 (Fig. 12C; PI(PRONE3 (#1); cell -1) = 37.27 ± 4.36; PI(PRONE3 (#2); cell -1) = 45.45 ± 8.17). In contrast, PIs of N14-PRONE3 increased slower with progressing root hair development and stayed more in the range of PIs determined for RopGEF3 FL (Fig. 5C: PI(RopGEF3 FL; cell -1) = 11.27 ± 0.99; Fig. 17C: PI(N14-PRONE3 (#1); cell -1) = 13.69 ± 1.28; PI(N14-PRONE3 (#2); cell -1) = 8.38 ± 1.04).

Additionally, domain sizes (DS; given as FWHM values) differed between the different RopGEF chimeras (Fig. 18): N4-PRONE3 expression led to large RHIDs, which even exceeded the diameter of PRONE3 domains especially in later stages (Fig. 13B: DS(PRONE3 (#1); cell +1) = 27.41 µm ± 2.03; DS(PRONE3 (#2); cell +1) = 23.92 µm ± 3.37; Fig. 18B: DS(N4-PRONE3 (#1); cell +1) = 35.73 µm ± 2.82; DS(N4-PRONE3 (#2); cell +1) = 43.33 µm ± 6.99). Additional domains of various diameters showing aberrant positioning within the cells could frequently be observed in N4-PRONE3 expressing lines (Fig. 18A, arrow heads) similar to the observations made for PRONE3 (Fig. 13A). In contrast, N14-PRONE3 domain sizes in early stages were similar to RopGEF3 FL domains (Fig. 13B: DS(RopGEF3 FL; cell -4) = 12.94 µm ± 1.07); Fig. 18B: DS(N14-PRONE3 (#1); cell -4) = 10.50 µm ± 0.86; DS(N14-PRONE3 (#2); cell -4) = 12.21 µm ± 0.93). However, N14-PRONE3 domains did not increase in diameter over the course of root hair development. Instead, the domains shrank slightly (DS(N14-PRONE3 (#1); cell +1) = 7.7 µm ± 0.81; DS(N14-PRONE3 (#2); cell +1) = 10.06 µm ± 1.17) and did often not even cover the emerging bulge entirely (Fig. 18A).

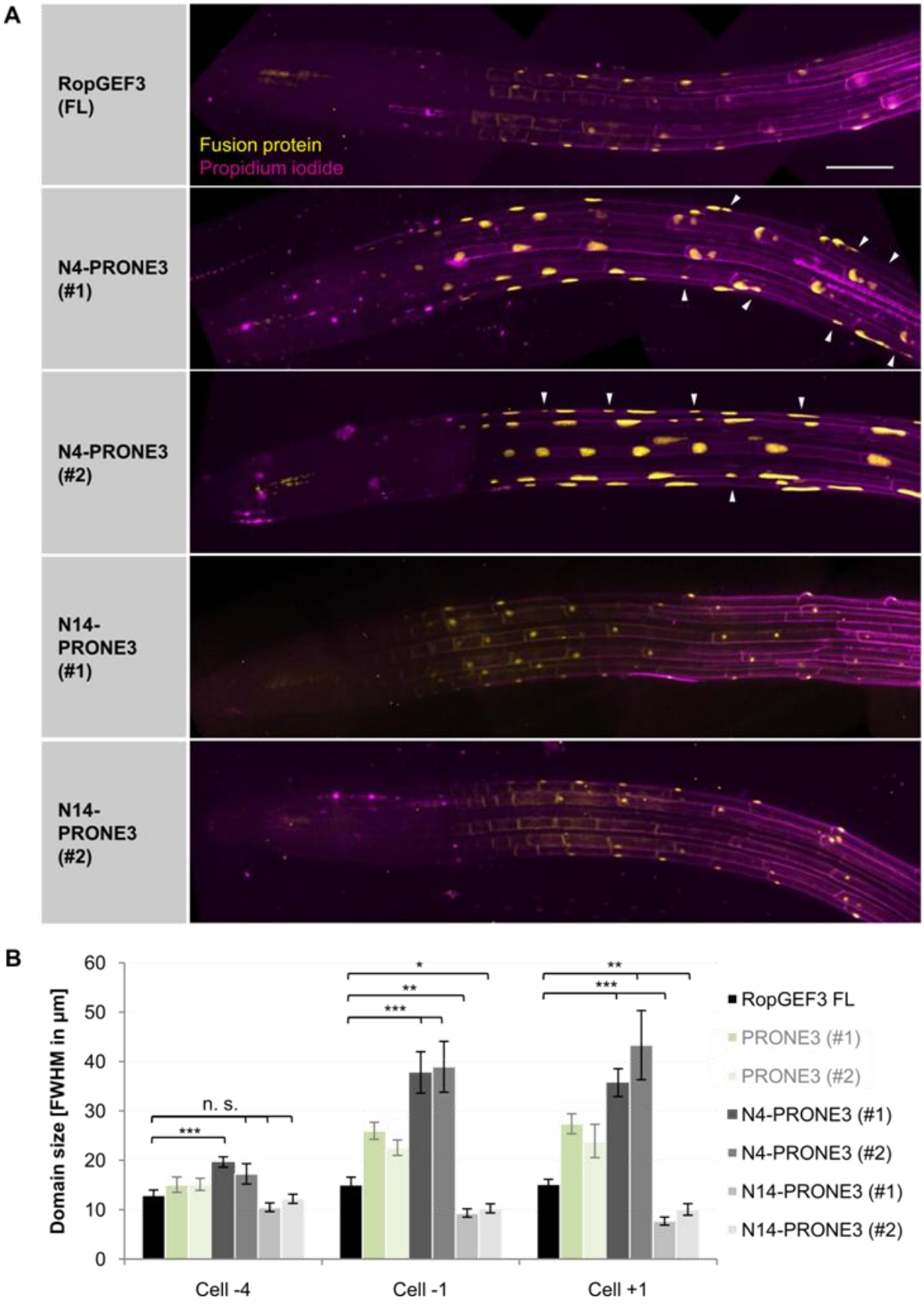

Fig. 18: N-termini of early and late RopGEFs have opposite effects on RHID size. Complete figure legend on next page.

Fig. 18 (previous page)**: N-termini of early and late RopGEFs have opposite effects on RHID size.** (A) Representative z-projections of primary roots of *A. thaliana* lines expressing mCit-RopGEF3 FL and mCit-N4-PRONE3 and mCit-PRONE14 (two independent lines each (#1/ 2)). Fusion proteins are depicted in yellow. Cell outlines were visualized using propidium iodide staining (magenta). Arrow heads highlight ectopic signal outside the RHID. Scale bar, 100 µm. (B) Quantification of RHID sizes in cell stages -4, -1 and the bulging stage +1 in above mentioned marker lines. Means of Full Width at Half Maximum (FWHM) values and standard errors of the mean are shown for each cell stage. Note that RHID sizes for RopGEF3 FL and PRONE3 #1/ 2 (faded green shades) from Fig. 13 are included to facilitate comparison between RopGEF3 truncation and RopGEF chimeras. Statistical differences to RopGEF3 FL were determined by a two-sided, unpaired Student's t-test assuming unequal variances: Not significant (n.s.) $p > 0.05$; * $p \leq 0.05$; ** $p \leq 0.01$; *** $p \leq 0.001$. n = 7-10 trichoblasts from 5-10 individual roots.

The similarities observed for PRONE3 and N4-PRONE3 on the subcellular level are also reflected in the resulting root hair phenotypes (Fig. 19): Expression of N4-PRONE3 could rescue the delayed bulging as well as the reduced root hair initiation frequency of the *ropgef3-1* mutant (Fig. 19A, C, D; distance Col-0: 100 % ± 2.18; distance N4-PRONE3 (#1): 112.46 % ± 8.34; distance N4-PRONE3 (#2): 103.85 % ± 2.61; density Col-0: 100 % ± 1.87; density N4-PRONE3 (#1): 94.23 % ± 9.29; density N4-PRONE3 (#2): 123.35 % ± 11.81). Again, similar to PRONE3 (Fig. 14A, E), root hair length was significantly reduced by almost up to 70 % compared to wild type and *ropgef3-1* mutant (length Col-0: 100 % ± 3.27; length *ropgef3-1*: 81.89 % ± 3.62; length N4-PRONE3 (#1): 33.38 % ± 1.66; length N4-PRONE3 (#2): 31.60 % ± 3.79). Furthermore, additional hair initiation sites in trichoblasts and branched hairs were observed frequently in N4-PRONE3 expressing lines (Fig. 19B asterisks/ arrow heads). These phenotypes are reminiscent of the RopGEF3 overexpression (Denninger and Reichelt et al., 2019) as is the phenotype of PRONE3 described above (Fig. 14). The picture changes when the N-terminus of the early polarizing RopGEF14 is fused to PRONE3 instead of N4. The N14-PRONE3 chimera is not capable of rescuing the delayed bulging despite being polarized at the right time at the RHID (Fig. 19A, C; distance N14-PRONE3 (#1): 128.66 % ± 3.83; distance N14-PRONE3 (#2): 121.92 % ± 4.18). This might be linked to the small N14-PRONE3 domain sizes observed around the bulging stage (Fig. 18A, B). Root hair density in N14-PRONE3 is not entirely restored to wild type level (Fig. 18A, D; density N14-PRONE3 (#1): 88.93 % ± 4.87; density N14-PRONE3 (#2): 88.71 % ± 4.26), however, to a large extent. In terms of root hair length, N14-PRONE3 were in a range between Col-0 and *ropgef3-1* (Fig. 18A, E; length N14-PRONE3 (#1): 86.93 % ± 2.71; length N14-PRONE3 (#2): 94.89 ± 4.91). Taken together, N14-PRONE3 cannot take over the function of RopGEF3 FL to induce bulging with the proper timing, but generally has the ability to initiate and grow root hairs clearly more successfully than *ropgef3-1* mutant, even though not completely to wild type level.

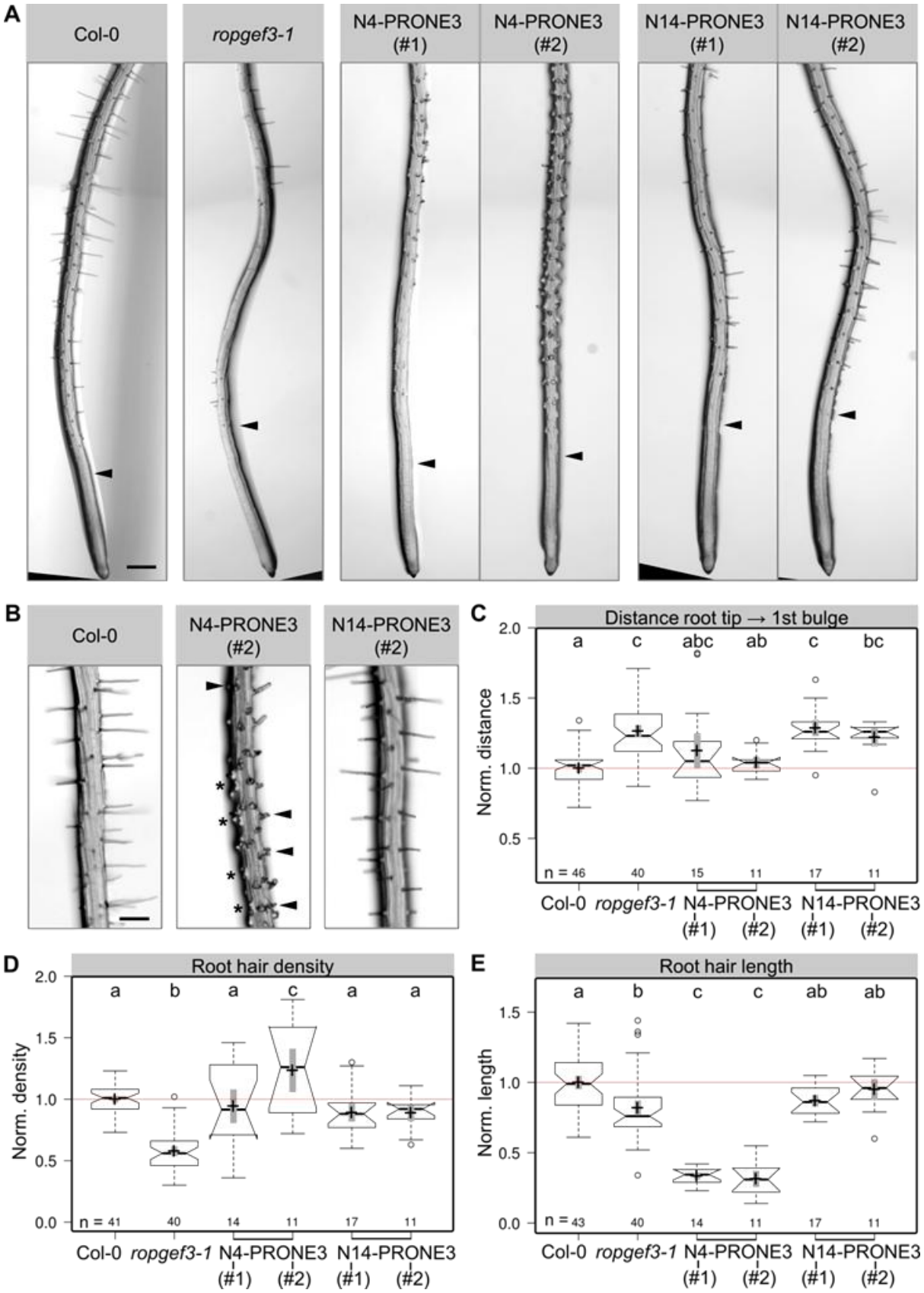

Fig. 19 : Expression of N4-PRONE3 in *ropgef3-1* results in short root hairs with additional initiation sites and branched tips while N14-PRONE3 root hairs are more wild type-like. Complete figure legend on next page.

Fig. 19 (previous page): **Expression of N4-PRONE3 in *ropgef3-1* results in short root hairs with additional initiation sites and branched tips while N14-PRONE3 root hairs are more RopGEF3 FL-like.** Representative stereoscope images of roots of *A. thaliana* Col-0, *ropgef3-1* mutant and marker lines expressing N4-PRONE3 and N14-PRONE3 chimeras (two independent lines each (#1/ 2)) in the *ropgef3-1* mutant background. Arrow heads indicate first bulge. Scale bar, 250 µm. (B) Representative close-ups of primary roots of Col-0, N4-PRONE3 and N14-PRONE3. Asterisks indicate additional hair initiation sites in single trichoblasts. Arrow heads highlight branched root hairs. Scale bar, 150 µm. (C-E) Quantification of root hair phenotypes of above mentioned genotypes. Measured parameters are normalized to the averaged values of Col-0 (= 1.0, marked by light red line). n indicates numbers of analyzed cell files; center lines represent medians, crosses represent means; gray bars mark 83% confidence intervals of means; letters show result of a 2-way ANOVA test (significance value, p = 0.05), different letters indicate statistically significant differences.

2.2.5 RopGEF N-termini differentially impact protein stabilization at the RHID

Previous observations showed that the absence of N3 or the exchange by N4 in RopGEF3 protein resulted in RopGEF3 overexpression-like effects (Fig. 12-14, Fig. 17-19), while the exchange of N3 by N14 results in more wild type-like root hairs and RHIDs (Fig. 17-19). This raised the hypothesis that RopGEF N-termini might differentially contribute to the regulation of RopGEF proteins in trichoblasts. More precisely, N-termini of early polarizing RopGEFs (N3 and N14) seem to carry signals leading to protein destabilization at the RHID, while the absence of these N-termini or presence of N4 seem to promote protein stabilization leading to overrepresentation of these RopGEF3 variants at the RHID.

In order to test this hypothesis and compare the protein stability of these RopGEF3 variants, I made use of the translational inhibitor cycloheximide (CHX). Upon cycloheximide treatment, *de novo* protein biosynthesis is blocked and the degradation kinetics of a protein of interest can be determined. Usually, CHX is used in a biochemical approach involving CHX treatment of cells or tissue for different time periods and subsequent quantitative Western Blot analysis. This classical approach requires sufficient amounts of the protein of interest to reliably quantify protein levels in each sample and therefore the degradation rate. RopGEF3 expression is restricted to a small subset of cells in the root epidermis and therefore detection of endogenous RopGEF3 protein levels by Western Blot is difficult. This is why I decided to analyze the effect of CHX on RopGEF3 FL, PRONE3 and RopGEF chimeras live in a microscopic approach using the corresponding fluorescent marker lines. The advantage of this live setup is that additional information, e.g. on the subcellular distribution of the proteins before and after treatment, can be extracted. A disadvantage is that the precise quantification of total cellular signals is difficult due to the absence of a marker for cell outlines making conclusions on general protein half lives in this setup impossible. Therefore, the focus was set on the protein stabilization of the different RopGEF3 variants specifically at the RHID. Marker lines expressing RopGEF3 FL and corresponding variants (mCit-RopGEF3 FL, mCit-PRONE3, mCit-N4-PRONE3 and mCit-N14-PRONE3) under the endogenous RopGEF3 promoter were grown directly on microscopic slides in small chambers.

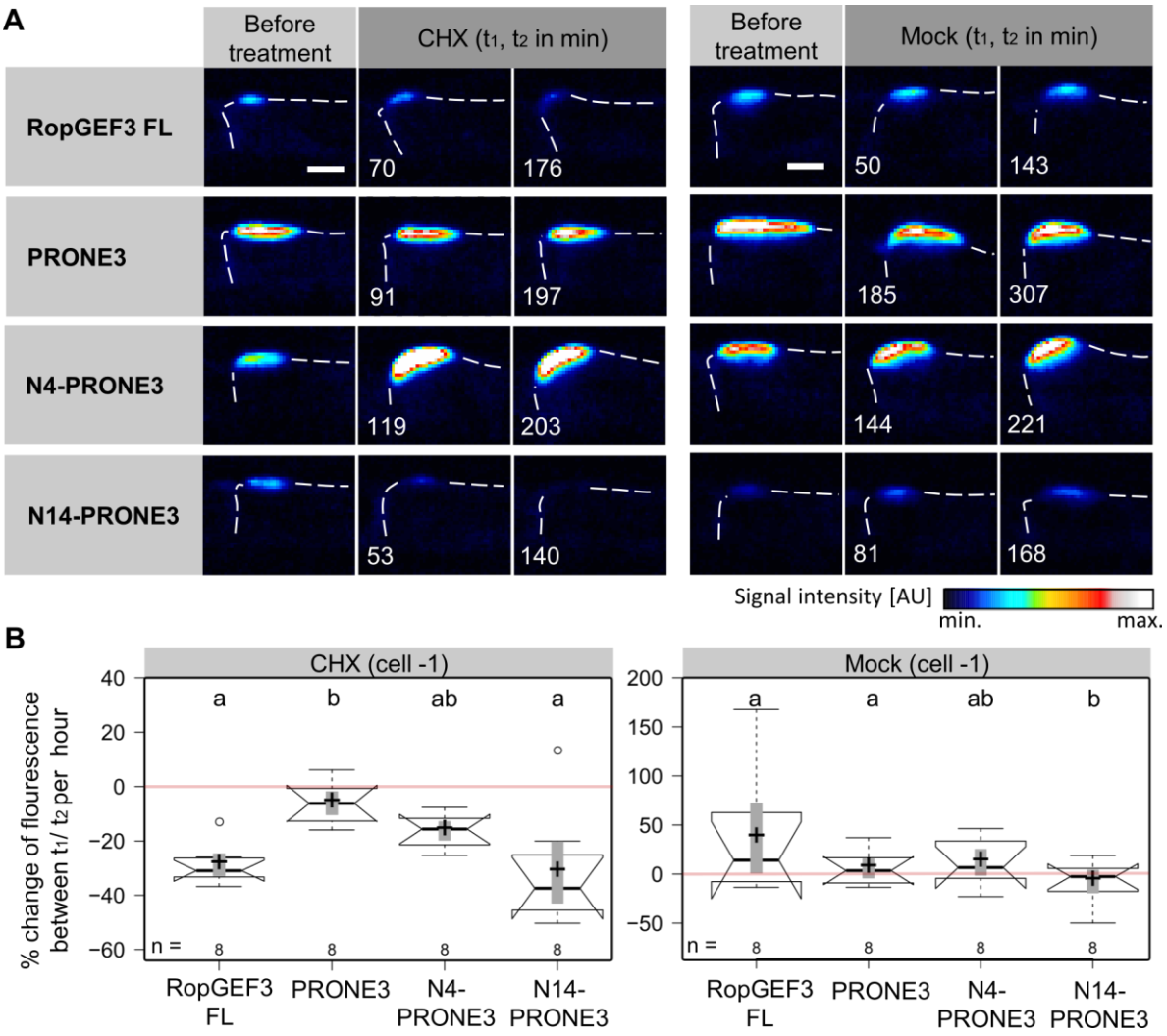

Fig. 20: Translational inhibition reveals differential stabilization of RopGEF3 FL, PRONE3 and RopGEF chimeras at the RHID. (A) Representative z-projections of RHIDs in cell stage -1 (before bulging) of CHX (left) or mock (right) treated marker lines (RopGEF3 full length (FL), PRONE3, N4-PRONE3, N14-PRONE3) before and at two time points after treatment (t_1, t_2) are shown in the pseudo-color LUT 'royal' of ImageJ. All images were acquired with the same microscope settings and are scaled equally. Scale bar, 10 µm. (B) Quantification of percentage changes of fluorescence per hour between t_1 and t_2 of the different genotypes. n indicates numbers of analyzed cell files; center lines represent medians, crosses represent means; gray bars mark 83% confidence intervals of means; letters show result of a 2-way ANOVA test (significance value, p = 0.05), different letters indicate statistically significant differences; light red line marks 0% and serves as visual aid.

CHX and corresponding mock treatments were performed 7 DAG by adding liquid ½ MS medium with or without 400 µg/ ml CHX into the growth chambers. Confocal z-stacks from cell stages -1 and +1 were acquired before treatments and at two time points after addition of CHX and mock solutions (t_1, t_2; average time difference: 95 min ± 14 min; Fig. 20, 21). As roots were imaged successively, the time points before treatment are not identical for all roots. Additionally, the speed of diffusion of the treatment solutions through the agar and therefore the time from which on roots are actually in contact with the solutions could only be estimated. Trials to quantify the time period required for a compound to diffuse through the agar in the growth chambers and actually affect roots growing on the microscopic slide with fluorescein revealed that the signal was stably present in root hair tips after approx. 30 min,

while this was longer for regions at the root hair base (preliminary data from Marjorie Guichard and Aylona Minina, unpublished). In order to ensure that all roots are measured upon exposure to the treatment, the percentage changes of fluorescent signal per hour at the RHID between t_1 and t_2 was determined and compared between the different genotypes (Fig. 20B, 21B). In line with the previously stated hypothesis, RopGEF3 FL (-28.82% per h ± 2.63) and N14-PRONE3 (-31.59% per h ± 7.37) signals at the RHID in cell stage -1 decreased significantly faster upon CHX treatment compared to PRONE3 (-6.11% per h ± 2.75) and N4-PRONE3 (-16.31% per h ± 2.23). This indicates that PRONE3 and N4-PRONE3 are more stably localized at the RHID, while RopGEF3 FL and N14-PRONE3 are removed with a higher rate. These differences could not be observed during mock treatment (Fig. 20B).

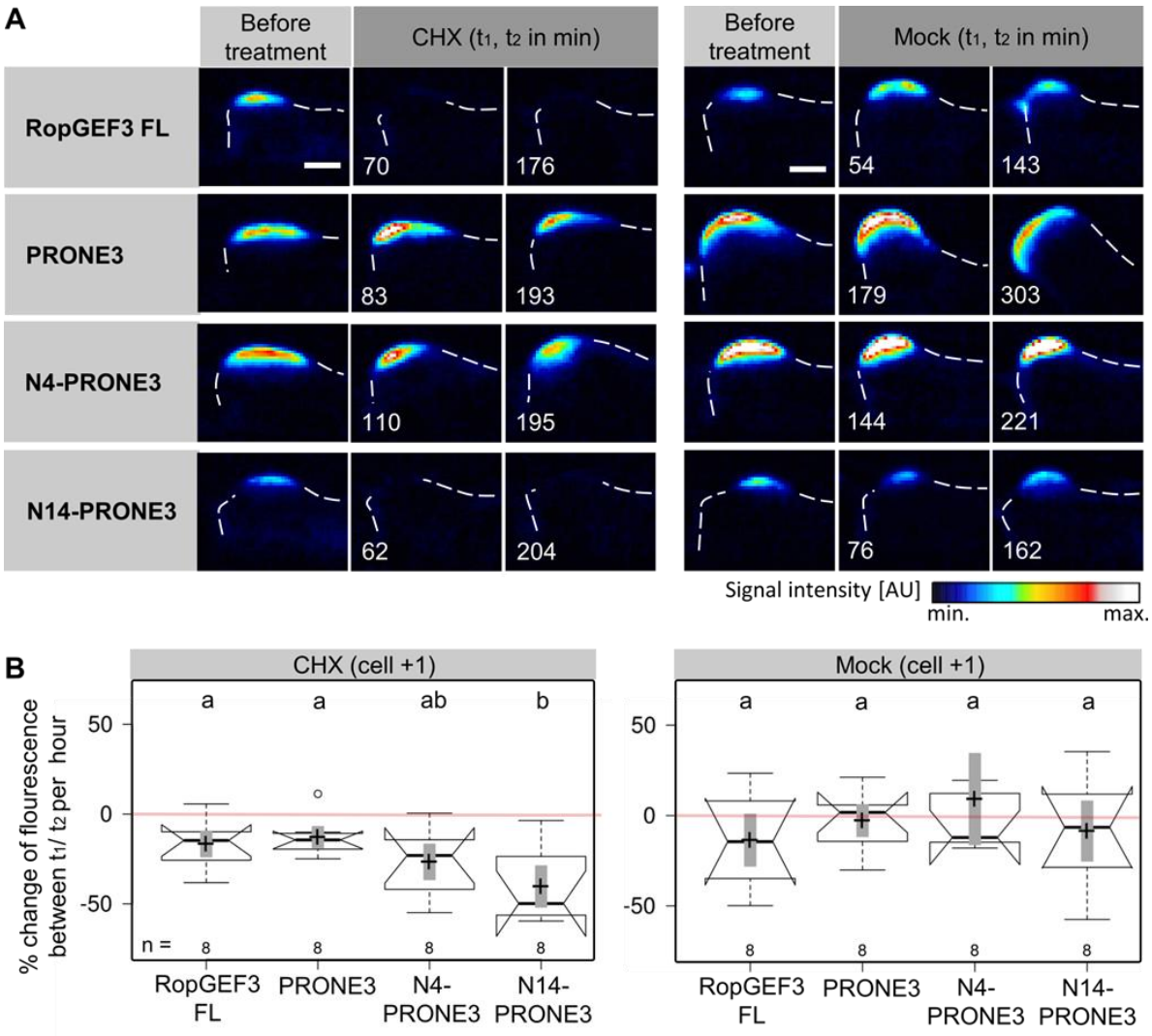

Fig. 21: Upon tip growth onset, differential stabilization of RopGEF3 FL, RopGEF3 truncation and RopGEF chimeras becomes more pronounced. (A) Representative z-projections of RHIDs in cell stage +1 of CHX (left) or mock (right) treated marker lines (RopGEF3 full length (FL), PRONE3, N4-PRONE3, N14-PRONE3) before and at two time points after treatment (t_1, t_2) are shown in the pseudo-color LUT 'royal' of ImageJ. All images were acquired with the same microscope settings and are scaled equally. Scale bar, 10 µm. (B) Quantification of percentage changes of fluorescence per hour between t_1 and t_2 of the different genotypes. n indicates numbers of analyzed cell files; center lines represent medians, crosses represent means; gray bars mark 83% confidence intervals of means; letters show result of a 2-way ANOVA test (significance value, p = 0.05), different letters indicate statistically significant differences; light red line marks 0% and serves as visual aid.

In the bulging stage (cell +1), a similar and even more pronounced trend could be observed as representative images of the corresponding genotypes upon CHX treatment show (Fig. 21A). While the signals for PRONE3 and N4-PRONE3 only decrease slightly, RopGEF3 FL and N14-PRONE3 signals are close to background already at the first treatment time point t_1. Therefore, the percentage changes in fluorescence between t_1 and t_2 needs to be interpreted with caution in this case. For RopGEF3 FL and N14-PRONE3, most of the signal has vanished already at t_1 resulting in misleading minor changes between t_1 and t_2, which are statistically not different from PRONE3 and N4-PRONE3 (Fig. 21B).

Taken together, translational inhibition by CHX revealed a significantly faster removal of RopGEF3 variants harboring the N-termini of early polarizing RopGEF (N3, 14) from the RHID compared to RopGEF3 variants without these N-termini or with N4. This indicates that the absence of N3 and N14 or the presence of N4 promotes RopGEF stabilization at the RHID. Interestingly, the difference between protein stabilization at the RHID between cell stages -1 and +1 indicates that RopGEF3 removal at the RHID is differentially regulated before and upon onset of tip growth. Potentially, RopGEF3 changes to a more dynamic behavior when the growth process starts.

2.2.6 RopGEF3 is phosphorylated *in vivo*

The molecular mechanisms underlying RopGEF regulation including targeting to the RHID and turnover are still largely unclear. Several studies showed that RopGEFs interact with membrane-bound receptor-like kinases (RLKs) pointing towards the involvement of RLK-mediated phosphorylation in RopGEF function and regulation. For example, in root hairs, the *Cr*RLK1L (*Catharanthus roseus* RLK1-like) member FERONIA (FER) was shown to regulate ROP activity via interaction with RopGEF1, 4 and 10 (Duan *et al.*, 2010; Yu *et al.*, 2012; Huang *et al.,* 2013). Another example is $[Ca^{2+}]_{cyt}$-associated protein kinase 1/ ERULUS (CAP1/ ERU), which was shown to be involved in root hair growth and to interact with RopGEF1 (Huang *et al.*, 2019). In pollen tubes, the involvement of RLKs in regulation of polar growth via RopGEFs has been shown as well. The pollen RLK PRK2 was reported to interact with RopGEF12 through its C-terminus, which was shown to mediate RopGEF12 autoinhibition (Zhang and McCormick, 2007). Additionally, PRK2 was shown to stimulate RopGEF1 activity towards ROP1 by phosphorylation of the C-terminal domain (Chang *et al.,* 2013). These studies, among others, show that regulation of the nucleotide exchange activity of RopGEFs involves RLKs and phosphorylation in the nonactive terminal RopGEF domains. However, how phosphorylation might affect RopGEF subcellular localization and regulation of cellular protein abundance is not investigated well. Two studies from the Schroeder lab reported the translocation and degradation of RopGEF1 in response to abscisic acid (ABA) via the action of calcium-dependent protein kinase 4 (CPK4), while PP2C-type protein

phosphatases have a stabilizing effect on RopGEF1 ((Li *et al.,* 2016; Li *et al.*, 2018b). RopGEF1 truncations revealed that the N-terminal region promoted the interaction with CPK4 and that N-terminal phosphorylated serines detected by tandem mass spectrometry were phosphorylated by CPK4 *in vitro*. This hints towards a possible mechanism of RopGEF translocation and degradation mediated by regulatory phosphorylations in RopGEF N-terminal regions. These studies prompted the hypothesis that early and late polarizing RopGEFs might be differentially turned over at the RHID through distinct phosphorylation sites in the respective N-termini. In the following section I focused on the early polarizing RopGEF3 and analyzed its phosphorylation status, investigated RopGEF3 N-terminus (N3) for conserved, phoshorylatable residues *in silico* and compared the RopGEF N-termini with regard to their putative phosphorylation sites. Based on this, I identified four promising candidate residues in N3 potentially being involved in RopGEF3 regulation at the RHID.

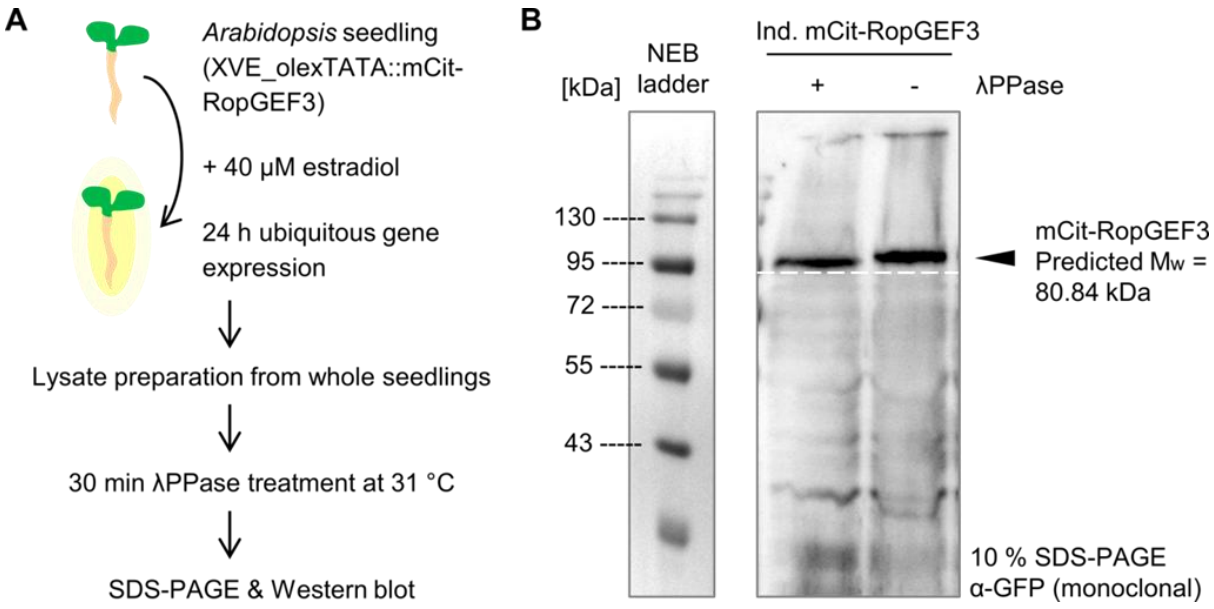

Fig. 22: Phosphatase treatment induces electromobility shift of mCit-RopGEF3 in SDS-PAGE indicating that RopGEF3 is phosphorylated *in vivo*. (A) Workflow overview: Transgenic *A. thaliana* seedlings stably expressing mCit-RopGEF3 (genomic) under an estradiol-inducible promoter (XVE_olexTATA::mCit-RopGEF3) were grown until 7 DAG. Gene expression was induced ubiquitously with ½ MS containing 40 µM estradiol supplemented with 0.01% Silwet Gold for 24 h. Plant lysate was prepared from whole seedlings. Lysate was separated in two fractions and treated with NEB λPPase (+) or water (-) in the corresponding buffer for 30 min at 31 °C. After denaturation samples were subjected to SDS-PAGE and subsequent Western Blot. (B) Representative Western Blot analysis of phosphatase (+) and control reactions (-). mCit-RopGEF3 was detected using a monoclonal α-GFP antibody (n =4). White, dotted line aids recognition of migration shift of mCit-RopGEF3 band upon λPPase treatment.

Firstly, I performed a phosphatase experiment to investigate whether RopGEF3 protein is phosphorylated *in vivo* at all. As previously mentioned, RopGEF3 expression is restricted to a small number of root epidermal cells complicating detection of RopGEF3 in Western Blot. Therefore, I made use of an estradiol-inducible mCit-RopGEF3 marker line generated by Philipp Denninger to increase RopGEF3 expression. Upon estradiol treatment, RopGEF3 expression was induced ubiquitously in the complete *Arabidopsis* seedling (Fig. 22A).

Proteins were extracted from whole seedlings and the prepared lysate was subjected to lambda protein phosphatase (+ λPPase) treatment or water as a control (- λPPase). mCit-RopGEF3 was visualized on the Western Blot using a monoclonal α-GFP antibody. The mCit-RopGEF3 band was found to run at a height of approximately 95 kDa, which is slightly higher than the predicted molecular weight for this fusion protein (80.84 kDa; Fig. 22B). Upon λPPase treatment, mCit-RopGEF3 electromobility increased resulting in a small shift of the corresponding band towards the lower molecular weight range compared to mCit-RopGEF3 in the control reaction. This indicates that RopGEF3 protein is phosphorylated *in vivo*.

2.2.7 N3 and N14, but not N4, share putative phospho sites at the beginning and at the end of the termini

Conservation of phosphorylation sites within protein families, but also across species is being observed with increasing frequency (Maathuis, 2008). Therefore, I next analyzed RopGEF3 protein sequence for conserved residues specifically in the N-terminus. To identify potential RopGEF3 orthologs in the plant kingdom, I made use of the “Reciprocal Best Hits (RBH)” approach. This method involves an initial Basic Local Alignment Search Tool (BLAST) search with a query sequence of a protein of interest and a second BLAST search with the sequence of the best scoring match of the initial BLAST search. A RBH is found when the best hit of the second BLAST search revealed the query sequence and therefore the protein of interest from the initial BLAST search. As the PRONE domain is highly conserved across plant species (Berken *et al.,* 2005) a BLAST search with the full-length RopGEF3 protein sequences would score the hits mainly according to similarities in this domain instead of N3. Therefore, the N3 sequence only (of *Arabidopsis thaliana* RopGEF3 (*At*RopGEF3); amino acid 1-94) was used as query for the BLAST search. I restricted the BLAST search to plant species, which typically serve as plant models for different plant families amongst both eudicots and the more distantly-related monocots (Chang *et al.,* 2018; Table 2.3).

Table 3: Plant species used as targets for N3 BLAST search. Plant species and corresponding plant families are listed with decreasing relation to *Arabidopsis thaliana*.

Class	Family	Species name	
Eudicot	Fabaceae	*Glycine max*	(soy bean)
		Medicago truncatula	(barrel medic)
	Solanaceae	*Solanum tuberosum*	(potato)
		Solanum lycopersicum	(tomato)
Monocot	Poaceae	*Brachypodium distachyon*	(purple false brome)
		Oryza sativa	(rice)
		Zea mays	(maize)
Others	Funariaceae	*Physcomitrella patens*	
	Marchantiaceae	*Marchantia polymorpha*	
	Chlamydomonadaceae	*Chlamydomonas reinhardtii*	

For the ortholog search, I used two databases specific for plants: Phytozome12 BLAST software (https://phytozome.jgi.doe.gov/pz/portal.html#!search?show=BLAST; tBLASTn, default settings; Goodstein *et al.,* 2012) and EnsemblPlants BLAST software (https://plants.ensembl.org/Multi/Tools/Blast; BLASTP, default settings; Yates *et al.,* 2020). Both tools did find N3 orthologous sequences, however, only among eudicots. The Phytozome12 BLAST search revealed four hits, three of which were also identified by EnsemblPlants BLAST (Table 2.4). The sequences of all four hits were retrieved from Phytozome12 and used as queries for BLAST searches in Phytozome12 and EnsemblPlants. *At*RopGEF3 was found as the best or among the best hits for all queries with both tools. If *At*RopGEF3 was not the best scoring match, it was most often *At*RopGEF2, the closest relative of *At*RopGEF3 among all *At*RopGEFs (Berken *et al.,* 2005). In two cases, also *At*RopGEF4, the second closest relative of *At*RopGEF3, and *At*RopGEF7, which is much less related to *At*RopGEF3 (Berken *et al.,* 2005), were listed before *At*RopGEF3. Based on this, the hits obtained from two independent N3 BLAST searches (see Table 2.4) are considered being orthologous to *At*RopGEF3 and will be used in the following as

Table 4: BLAST results from Phytozome12 and EnsemblPlants using N3 sequence as query. N3 BLAST search was performed with both tools in selected plant species (see Table 2.3). As there were no hits for monocots, only results for soy bean, barrel medic, potato and tomato are listed here.

Species	Phytozome12	EnsemblPlants
Glyine max	Glyma.07G073200.1 (Uniprot: I1KID8_SOYBN)	---
Medicago truncatula	Medtr8g030850.1	MTR_8g030850
Solanum tuberosum	PGSC0003DMT400000136	PGSC0003DMT400000136
Solanum lycopersicum	Solyc01g094610.2.1	Solyc01g094610.3

Interestingly, using the N-terminal sequence of the late polarizing RopGEF4 (N4) as query in similar BLAST searches, revealed no hits in the selected plant species. When expanding the target species to all plant species (Viridiplantae), 10 BLAST hits were listed, all among the family of Brassicaceae. In contrast, BLAST searches with the sequence of RopGEF14 N-terminus (N14) revealed hits for all eudicots and monocots selected, but not in mosses or algae.

In order to identify residues in *At*RopGEF3 conserved across identified RopGEF3 orthologs in soy bean, barrel medic, potato and tomato (hereafter referred to as *Gm*RopGEF3, *Mt*RopGEF3, *St*RopGEF3 and *Sl*RopGEF3 respectively), the corresponding full-length sequences were aligned using the multiple sequence alignment program Clustal Omega 1.2.4 (https://www.ebi.ac.uk/Tools/msa/clustalo/; default setting; Fig. 23). The full-length alignment demonstrates again the high degree of conservation of the active PRONE3 domain. However, noticeable are two differing regions in the PRONE3 domain. Firstly, the first linker sequence connecting the PRONE3 subdomains S1 and S2 is longer in *Mt*RopGEF3, *St*RopGEF3 and *Sl*RopGEF3 compared to *Gm*RopGEF3 and *At*RopGEF3. In case of potato and tomato, it is an identical six amino acid peptide at the end of the linker sequence, while it is a completely unrelated eight amino acid peptide in case of barrel medic. Secondly, *Gm*RopGEF3 is completely lacking the PRONE3 subdomain S3 as well as the last and highly conserved six amino acids of S2. This raises the question about the function of PRONE3 subdomain S3 as it seems to be completely dispensable in soy bean. In the N-termini of RopGEF3 orthologs, 13 conserved (≥ 80%), phosphorylatable residues (including serines (S), threonines (T) and tyrosines (Y)) could be identified (S5, S25, T29, S33, S36, S39, Y42, S47, S51, S54, S62, S68, S85 in *At*RopGEF3; Fig. 23, bright red and blue highlights). To find putative phosphorylation sites among these conserved residues, the N-terminal sequence of *At*RopGEF3 was subjected to three prediction tools for phosphorylations: The NetPhos3.1 Server (http://www.cbs.dtu.dk/services/NetPhos/; threshold ≥ 0.5; Blom *et al.,* 1999; Blom *et al.,* 2004), the *Arabidopsis* Protein Phosphorylation Site Database "PhosPhAt" 4.0 (http://phosphat.uni-hohenheim.de/index.html; default setting in prediction tool; Heazlewood *et al.,* 2008; Durek *et al.,* 2010) and the Plant Protein Phosphorylation DataBase P3DB 3.0 (http://www.p3db.org/prediction.php; score range 0-1, cutoff = 0.5; Yao *et al.,* 2014). Considering all sites predicted by at least one of the used prediction tools revealed 21 putative phospho sites in N3 (Fig. 23, highlighted in shades of red and by arrow heads and the corresponding amino acid number). Merging the information from the cross-species alignment and the phospho site predictions yielded 8 conserved (≥ 80%), putative phospho sites in N3 (S5, S25, T29, S47, S54, S62, S68 and S85).

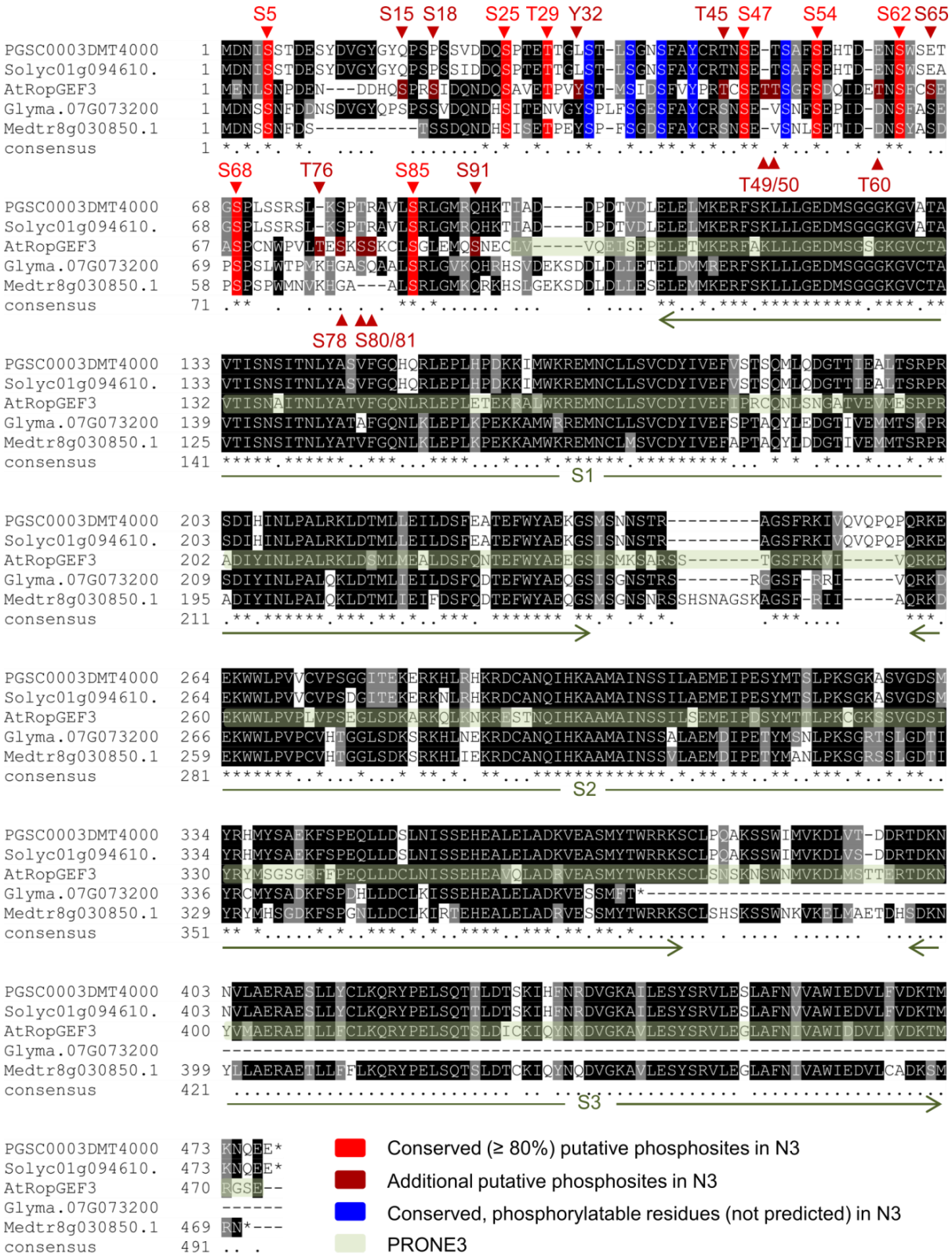

Fig. 23: Identification of conserved, putative phosphoylation sites in RopGEF3 N-terminus by cross-species alignment and *in silio* phospho site prediction. Complete figure legend on next page.

Fig. 23 (previous page)**: Identification of conserved, putative phosphoylation sites in RopGEF3 N-terminus by cross-species alignment and *in silio* phospho site prediction.** Multiple sequence alignment of protein sequences of identified RopGEF3 orthologs by Clustal Omega 1.2.4 (protein sequences obtained from Uniprot (*At*RopGEF) and Phytozome (orthologs)), which was printed and shaded using BoxShade 3.21. Identical residues are highlighted in black, similar residues in grey. Consensus line: Asterisks mark totally identical residues in all sequences; dots mark similar residues at a position. Input sequences include *Arabidopsis thaliana* (At) RopGEF3 sequence and sequences from identified homologs from *Solanum tuberosum* (PGSC0003DMT400000136), *Solanum lycopersicum* (Solyc01g094610.), *Glycine max* (Glyma.07G073200.1) and *Medicago truncatula* (Medtr8g030850.1). Putative phosphorylation sites in RopGEF3 N-terminus (N3) identified by at least one phosphosite prediction tool (NetPhos 3.1, PhosPhAt 4.0, P3DB 3.5) are marked in bright red (conservation among input sequences ≥ 80 %) or dark red (conservation < 80 %). Corresponding amino acid positions are indicated. Conserved, theoretically phosphorylatabe residues, which were not predicted to be phosphorylated by any tool are marked in blue. Sequence of the PRONE domain of RopGEF3 (PRONE3) is highlighted in light green. PRONE3 subdomains S1-3 are indicated by dark green arrows. Note that the phospho site prediction was not performed for the PRONE domain; therefore, no putative phosphorylations are indicated in this domain.

Previously presented results indicated that the N-termini of the early polarizing RopGEF3 and RopGEF14 harbor destabilizing signals, in contrast to the N-terminus of the late polarizing RopGEF4. Based on this, I hypothesized that N3 and N14 share regulatory phospho sites being involved in RopGEF removal from the RHID, which are not present in N4. Pairwise protein sequence alignment of N3 and N14 allows the identification of shared phospho sites, which can be compared to N4 in a separate alignment with N3 (Fig. 24). Putative phosphorylation sites in N14 and N4 were identified using the same prediction tools as mentioned before. Predictions revealed 25 and 19 putative phosphorylation sites in N14 and N4 respectively. Considering the different lengths of the N-termini (N3: 94 amino acids (aa); N4: 84 aa; N14: 127 aa), the number of predicted phospho sites is similar in all N-termini. Comparison of the pattern of putative phosphorylation sites in N-termini of early and late polarizing RopGEFs revealed that numerous phosphorylations are predicted in the middle part of all N-termini (in N3 the region between S47 and T76). However, in two regions of the N-termini the pattern is similar for N3 and N14 and different for N4. In both, N3 and N14 a “serine-isoleucine-aspartic acid (SID)” tripeptide is present at the same position (Fig. 24). The involved serine (S18) was predicted to be phosphorylated in N3 as well as in N14 by all three prediction tools used. S18 is not conserved (≥ 80%) among all RopGEF3 orthologs (Fig. 23), however, it is invariant in *At*RopGEF3, *Gm*RopGEF3 as well as *Mt*RopGEF3. Moreover, similar tripeptides are present in all species at the same or similar positions (*At*RopGEF3: S18-I19-D20; *Gm*RopGEF3: S18-V19-D20; *Mt*RopGEF3: S11-S12-D13; *St*RopGEF3: S20-V21-D22; *Sl*RopGEF3: S20-I21-D22; Fig. 23). The region containing the “SID” tripeptide in N3 is lacking in N4 (Fig. 24B). The second promising putative phospho site shared by N3 and N14 is Y32. Again, this residue is not conserved (≥ 80%) among all RopGEF3 orthologs (Fig. 23), but can be found in *At*RopGEF3, *Gm*RopGEF3 as well as *Mt*RopGEF3. Also here, the region containing Y32 in N3 is lacking in N4. Finally, two residues at the end of N3 and N14 seem to be promising as the end of N4 is not containing

any phosphorylatable residues – strikingly, in contrast to the closely related N3 and also in contrast to N14. S80 in N3 and the corresponding residue in N14 (S93) were both predicted to be phosphorylated by two out of the three used prediction tools. Additionally, despite being not fully identical among the RopGEF3 orthologs, a phosphorylatable residue at the same position is found in soy bean, potato and tomato. Finally, the fully conserved S85 in N3 and the corresponding residue in N14 (S118) are both putative phosphorylation sites. Taken together, the combination of cross-species alignment, *in silico* phospho site predictions and pairwise RopGEF N-termini alignments revealed four promising residues in N3 including S18, Y32, S80 and S85 being putative phospho sites possibly involved in the differential regulation of RopGEF protein abundance at the RHID.

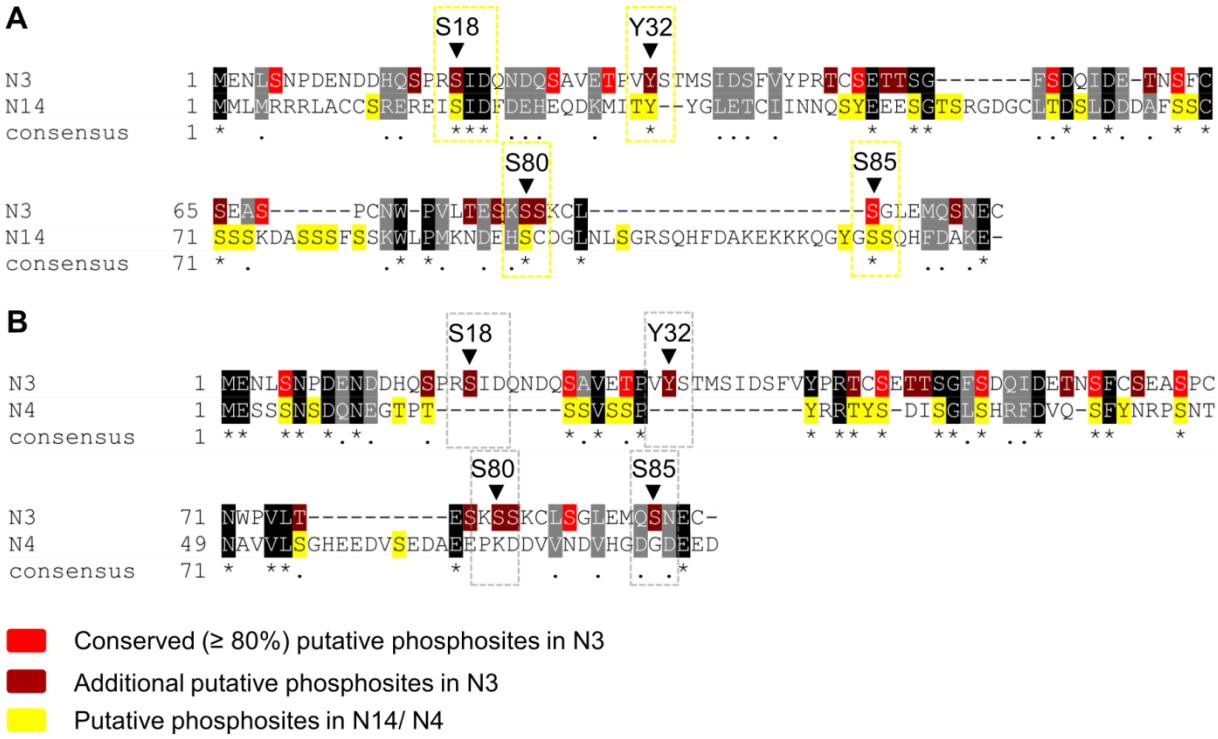

Fig. 24: Putative phospho sites of early and late polarizing RopGEFs differ most at the beginning and the end of RopGEF N-termini. Pairwise protein sequence alignments of N-terminal sequences of RopGEF3 (N3) and RopGEF14 (N14) or RopGEF4 (N4) by Clustal Omega 1.2.4 (protein sequences obtained from Uniprot), which was printed and shaded using BoxShade 3.21. Identical residues are highlighted in black, similar residues in grey. Consensus line: Asterisks mark totally identical residues in all sequences; dots mark similar residues at a position. Putative phosphorylation sites in N3 identified by at least one phospho site prediction tool (NetPhos 3.1, PhosPhAt 4.0, P3DB 3.5) are marked in bright red (conservation among input sequences ≥ 80 %) or dark red (conservation < 80 %). Putative phosphorylation sites in N14 and N4 are highlighted in yellow. (A) Protein sequence alignment of early polarizing RopGEF3 and RopGEF14. Yellow dotted boxes and indicated residues (S18, Y32, S80, S85 in N3) are regions with predicted phosphorylations in both N3 and N14, which are not shared with N4 (grey dotted boxes in (B)). Most noticeable is a shared “SID tripeptide” in N3 and N14 with a potentially phosphorylated serine. (B) Protein sequence alignment of RopGEF3 and the late polarizing RopGEF4. The very beginning and middle part of N3 and N4 are very similar and carry several shared, putative phosphorylation sites. The last fourth of N4 does not contain phosphorylatable residues and therefore also no putative phosphorylation sites.

Finally, I generated stable *A. thaliana* lines endogenously expressing fluorescently-tagged RopGEF3 with phosphomimicking (aspartic acid (D) replacing serine or tyrosine) and nonphosphorylatable (alanine (A) replacing serine or tyrosine) isoforms of these residues in the *ropgef3-1* mutant background. These lines will help to elucidate the relevance of these residues in N3 for RopGEF3 regulation *in planta.* Both, lines with single site mutations as well as RopGEF3 variants with mutations at all four candidate sites were generated and propagated to generation T2.

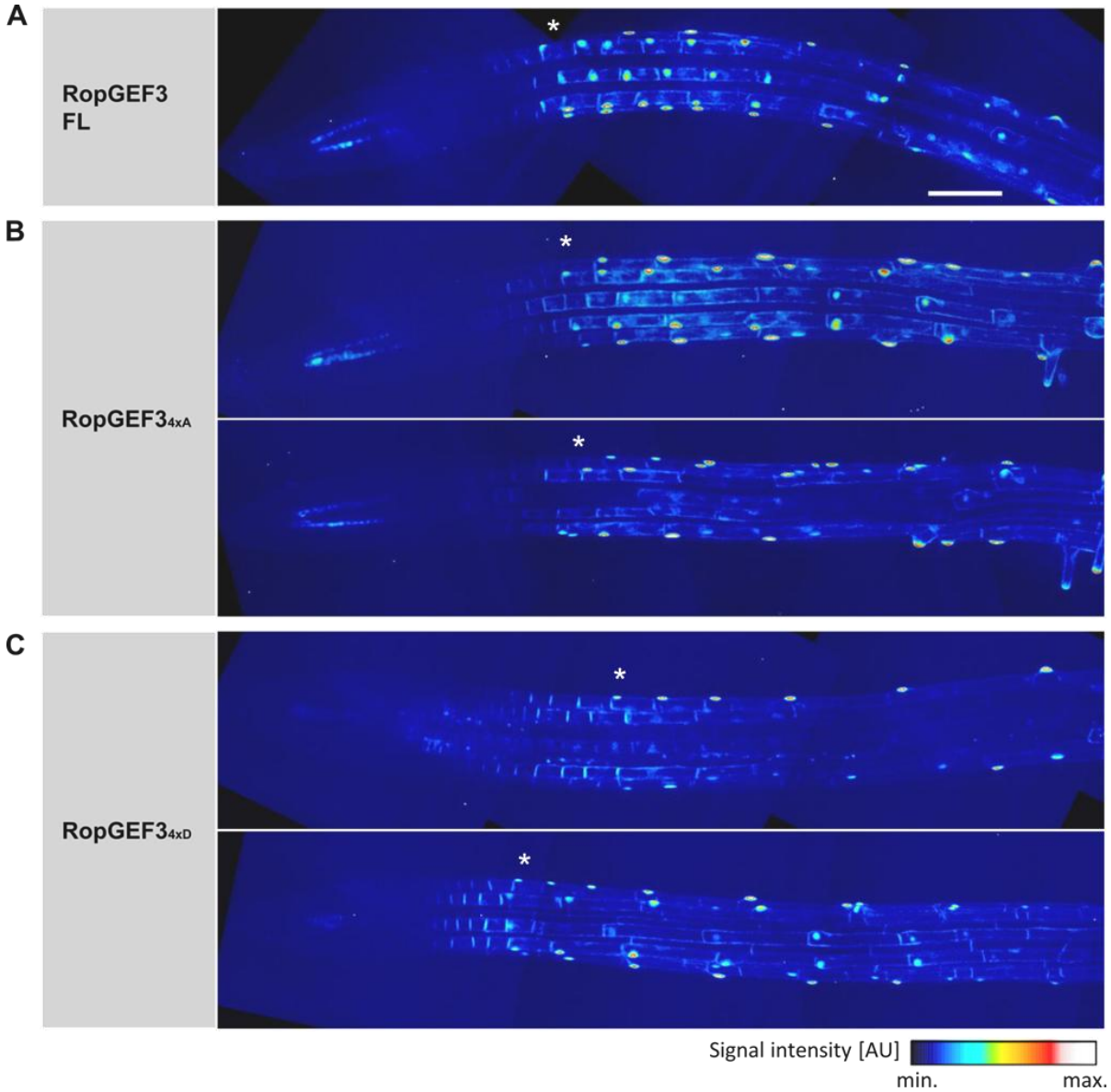

Fig. 25: Mutations of putative phospho sites in N3 might affect RopGEF3 protein stabilization at the RHID. (A-C) Representative z-projections from primary roots of *A. thaliana* lines expressing mCit-RopGEF3 full-length (FL; A), mCit-RopGEF3$_{4xA}$ (B) and mCit-RopGEF3$_{4xD}$ (C) under the endogenous RopGEF3 promoter in the *ropgef3-1* mutant background. In mCit-RopGEF3$_{4xA}$, putative phospho sites including S18, Y32, S80 and S85 are mutated to alanines (A) and serve as nonphosphorylatable isoforms of these residues. In the phosphomimicking mCit-RopGEF3$_{4xD}$ mutant, above mentioned residues are mutated to aspartic acid (D). For each RopGEF3 phospho mutant lines, two individual roots are depicted. Signals are depicted in the pseudo-color LUT 'royal' of ImageJ. Asterisks mark first polarization of corresponding RopGEF3 variants showing that polarization timings are similar. Scale bar, 100 µm.

Initial, qualitative observation of RopGEF3 simultaneously carrying all four phosphomimicking (RopGEF3$_{4xD}$) or nonphosphorylatable (RopGEF3$_{4xA}$) mutations in the N-terminus using confocal microscopy revealed a slight difference to RopGEF3 FL (full-length, without mutations; Fig. 25). While polarization timing did not seem to be altered in both mutant lines, RHID sizes appeared slightly enlarged in RopGEF3$_{4xA}$ possibly indicating a stabilization of the protein at the RHID. In RopGEF3$_{4xD}$, RHID sizes appear rather similar to RopGEF3 FL. However, this requires further quantitative analyses, as well as the investigation of the respective single site mutants.

Taken together, the presented analyses of RopGEF3 N-terminus regarding conservation of single residues and putative phosphorylations provide promising candidate residues possibly being involved in RopGEF3 abundance control in trichoblasts. Future analyses using plant material generated during this thesis and additional experimental approaches will add more evidence to further complement our knowledge on RopGEF regulation and turnover during root hair development.

III. DISCUSSION

Arabidopsis thaliana root hairs and pollen tubes are valuable model systems to study the cellular mechanisms underlying cell polarity establishment. In plants, Rho-of-Plants (ROPs) are well established key regulators of cell polarity, which are activated by ROP guanine nucleotide exchange factors (RopGEFs). While RopGEFs involved in pollen tube growth are largely characterized (Gu *et al.,* 2006; Zhang & McCormick, 2007; Chang *et al.,* 2013; Guan *et al.,* 2013), to date, little is known about RopGEFs regulating root hair growth. ROP2 and ROP4 are considered key regulators of root hair development and polarize early at the Root Hair Initiation Domain (RHID) (Molendijk *et al.*, 2001; Jones *et al.*, 2002; Stanislas *et al.*, 2015; Denninger & Reichelt *et al.,* 2019; Fig. 3); however, processes upstream of ROP activation and the roles of RopGEFs therein are not yet well understood. Furthermore, putative additional roles of RopGEF N-termini besides their RopGEF activity-modulating functions remain largely obscure. In this PhD thesis, I studied the function and regulation of selected trichoblast-expressed RopGEFs during root hair development in *Arabidopsis thaliana*. The focus of this work was the initiation of root hairs prior to ROP activation. Therefore, RopGEF3, the predominant RopGEF being present early at the site of the future root hair (Denninger & Reichelt *et al.,* 2019; Fig. 5), was the central target of research in this PhD thesis. I characterized RopGEF3 function in comparison to other RopGEFs with similar (RopGEF14) or different (RopGEF4) polarization timing at the RHID during root hair development by analyses of mutant and overexpression phenotypes. Thereby, I could provide evidence for a putative task-sharing mechanism among trichoblast-expressed RopGEFs. Additionally, I functionally analyzed RopGEF N-termini by truncations and domain swaps and revealed the possibility that these N-termini are implicated in RopGEF protein stabilization at the RHID, which could be mediated by regulatory phosphorylations (Fig. 26).

4.1 Task sharing between early and late polarizing RopGEFs during root hair development

Previous work from the Grossmann laboratory revealed the successive recruitment of trichoblast-expressed RopGEFs to the RHID: Early polarizing RopGEFs, including RopGEF3 and RopGEF14, localize to the RHID one cell stage before ROP2 was found to be polarized, while late polarizing RopGEFs accumulate at the RHID with bulging (RopGEF4) or later (Denninger & Reichelt *et al.,* 2019). In this thesis, I confirmed the distinct polarization timing of RopGEF3, 4 and 14 at the RHID with new fluorescent marker lines based on the RopGEF coding sequence in the corresponding *ropgef* mutant background (Fig. 5). The differential

timing of early and late polarizing RopGEFs suggested that their specific action at the RHID is required during different phases of root hair development.

To test this hypothesis, I assessed root hair phenotypes of *ropgef* single and double mutants (Fig. 6): Among *ropgef* single mutants, only *ropgef3* mutants showed a delay in bulging and decrease in root hair density. This fits the early and predominant localization of RopGEF3 at the RHID (Fig. 5). Moreover, this phenotype is reminiscent of the *rop2/4* double mutant, in which a large delay in bulging and major decreases in root hair density and length were observed in a more pronounced manner (Fig. 3) underlining the central role of RopGEF3 in root hair formation. This phenotype was confirmed by an additional mutant allele (*ropgef3-4*) and the corresponding rescue line (Fig. 6, 7). Together with the finding that RopGEF3 is necessary and sufficient for ROP2 polarization into polar plasma membrane domains (Denninger & Reichelt *et al.,* 2019; Fig. 8), this data provides convincing evidence for RopGEF3 being involved in early stages of root hair development, more precisely in RHID set-up by ROP2 recruitment. Another evidence for RopGEF3 being upstream of ROP2 was provided by the observation that initial RopGEF3 polarization is not affected by ROP2/4 loss (Fig. 9). Interestingly, around the bulging stage, RopGEF3 polarization continuously reduces in the *rop2/4* mutant background pointing towards a ROP2/4-mediated stabilization of RopGEF3 at the RHID in later stages (Fig. 9). This might be part of a positive feedback mechanism to re-enforce ROP polarization at the RHID providing robustness to the process of root hair initiation, similar to what is proposed in pollen tubes for the formation of the ROP1 cap at the pollen tube apex (Hwang *et al.,* 2010).

Being the second early polarizing RopGEF, I hypothesized that RopGEF14 also impacted bulging timing; however, the *ropgef14-2* mutant did not show a root hair phenotype (Fig. 6, 7). Upon loss of both, RopGEF3 and RopGEF14, however, the delay in bulging as well as the decrease in root hair density was more extreme than in *ropgef3-1* suggesting that RopGEF14 is also involved in root hair initiation, at least when RopGEF3 function is missing (Fig. 6). These findings suggest that RopGEF3 dominates the principal regulation of root hair initiation, while RopGEF14 function is rather supportive and becomes evident only upon RopGEF3 loss. If the exogenous expression of RopGEF3 in the *ropgef3/14* double mutant background would be sufficient to rescue the extended root hair phenotype, this would further confirm the predominant role of RopGEF3 in the initiation of root hairs. Similar to RopGEF3, initial RopGEF14 polarization at the RHID was ROP2/4-independent (Fig. 9) suggesting that also RopGEF14 is upstream of ROP2 polarization. In contrast, in the *ropgef3-1* mutant background, RopGEF14 polarization was abolished in the investigated zone of the primary root, which includes (in the wild type background) the region around bulging (Fig. 9). The extended root hair phenotype of the *ropgef3/14* double mutant suggested, however, that the presence of RopGEF14 does support root hair initiation in

ropgef3-1 to some extent. Additionally, it is likely that this supportive function of RopGEF14 requires its polarized localization at the RHID. Therefore, it is possible that RopGEF14 is not polarized in *ropgef3-1* in the investigated region of the root, but possibly RopGEF14 polarization can happen RopGEF3-independently further up the root. This would allow the mitigation of the delay in bulging by RopGEF14 in the *ropgef3-1* single mutant compared to the *ropgef3/14* double mutant. The observation that initial RopGEF14 polarization is directly or indirectly dependent on the presence of RopGEF3 contradicts the simultaneous polarization timing determined for RopGEF3 and RopGEF14 in corresponding single marker lines (Fig. 5). As the comparison between single marker lines necessarily involves the comparison of two individual roots, subtle timing differences might be difficult to detect. To precisely analyze the temporal relation between RopGEF3 and RopGEF14 polarization at the RHID, a double marker line, carrying fluorescent markers for both RopGEFs under the respective endogenous promoters should be investigated.

In contrast to the early polarizing RopGEFs, RopGEF4, which is expressed later during trichoblast differentiation (Fig. 5, 9) and accumulates at the RHID with the onset of bulging, did not affect root hair initiation and frequency. Instead, RopGEF4 loss caused a reduction in root hair length (Fig. 6, 7) indicating that RopGEF4 is required for efficient root hair elongation. This finding is supported by independent characterizations of *ropgef4* mutants as well as by the corresponding rescue line (Won *et al.*, 2009; Huang *et al.,* 2013; Fig. 7). However, root hairs in the *ropgef4-2* mutant still elongated and generated hairs with a wild type morphology (except for the average length) indicating that tip growth initiation was not impaired. To test whether the short root hairs in *ropgef4-2* are a consequence of premature tip growth arrest or a less efficient tip growth process, root hair growth rates of *ropgef4-2* and Col-0 should be compared by live cell imaging, e. g. using microfluidic imaging platforms (Grossmann *et al.,* 2011). As reduction of root hair length is more pronounced in the *rop2/4* double mutant (Fig. 3) compared to *ropgef4-2*, the involvement of additional RopGEFs in efficient tip growth is likely. A possible candidate might be RopGEF12, for which a similar expression and polarization pattern was observed as for RopGEF4 (Denninger & Reichelt *et al.,* 2019). Recruitment of RopGEF4 to the RHID requires the presence of ROP2/4 (Fig. 9) suggesting that RopGEF4 is downstream of ROP2 polarization in this pathway. In line with the finding that ROP2 polarization relies on RopGEF3 (Denninger & Reichelt *et al.,* 2019), RopGEF4 recruitment to the RHID is also RopGEF3-dependent (Fig. 9). Whether RopGEF3 would be sufficient to ectopically polarize RopGEF4 into a polar domain, a RopGEF3 overexpressing line carrying a RopGEF4 marker under its endogenous promoter should be investigated as it was shown for ROP2 (Fig. 8). Loss of RopGEF4 in addition to loss of one of the early polarizing RopGEFs, revealed a combination of the obtained *ropgef* single mutant phenotypes (Fig. 6). Accordingly, *ropgef3/4* double mutant showed a delay in bulging

and a reduced number of root hairs as the *ropgef3* single mutant and a reduction in root hair length to the same extent as observed in *ropgef4-2*. Similarly, a reduction in root hair length could be observed for the *ropgef4/14* double mutant, while the other parameters investigated did not differ significantly from wild type. Again, these finding suggest that early and late polarizing RopGEFs actually function in distinct processes, namely initiation of root hairs and subsequent tip growth regulation, which are temporally separated.

4.1.1 Exploiting inefficient ROP activators for ROP recruitment?

The finding that RopGEFs are successively recruited to the RHID and affect different phases of root hair development – initiation and tip growth – raises the question about the need for different members of the same, highly conserved protein family in these phases. To address this question, it is important to identify the differences in the molecular requirements of the different developmental phases of root hair growth: In the initiation phase, the master regulators of cell polarity need to be efficiently targeted to the plasma membrane and restricted to the site of the future outgrowth, while the tip growth onset relies on efficient ROP activation. As RopGEF3 was shown to recruit ROP2 into the RHID, but growth was initiated only upon RopGEF4 polarization at the RHID, I hypothesize that early and late polarizing RopGEFs differ in their efficiency to activate ROPs involved in root hair regulation. If the early polarizing RopGEF3 and RopGEF14 would be less potent ROP2 activators, their GTPase-binding ability could be exploited for ROP2 recruitment in the initiation phase and simultaneously premature ROP2 activation would be prevented. Efficient ROP2 activators, potentially including RopGEF4, are only recruited to the RHID, when tip growth is actually requested. If this hypothesis holds true, this would be an elegant way of task sharing among RopGEFs.

The observation that RopGEF3 overexpression induces ectopic RHID-like domains in trichoblasts and other cell types (Fig. 8), yet additional bulges can only be observed in trichoblasts (Denninger & Reichelt *et al.,* 2019), could be used as a tool to investigate the importance of RopGEF4 for tip growth initiation and thus indirectly for ROP activation. Possibly, ectopic RopGEF3 domains polarize RopGEF4 in trichoblasts, thereby allowing ectopic tip growth by ectopic RopGEF4-mediated ROP2 activation, while RopGEF4 expression or polarization in ectopic RopGEF3 domains is not given in other cell types. To test this hypothesis in a more direct way, nucleotide exchange activity of early and late RopGEFs towards ROP2 could be tested *in vitro* by a GEF assay involving fluorescently-labeled guanine nucleotides such as N-Methylanthraniloyl (MANT) GDP as previously performed by Berken *et al.* (2005) and Gu *et al.* (2006; Kanie & Jackson, 2018). Alternatively, a pulldown-based assay involving the protein binding domain of mammalian p21 or ROP effectors such as RIC1 or ICR1, which specifically interact with active ROPs, would allow to

quantify the ROP activation potential of RopGEFs indirectly *in vivo* by assessing the relative amount of active ROPs, e.g. upon RopGEF overexpression (e. g. used in Tao *et al.,* 2002; Duan *et al.,* 2010; Chen *et al.,* 2011; Huang *et al.,* 2013). The advantage of *in vivo* assays is that the proteins are in their endogenous context and specific posttranslational modifications possibly impacting GEF activity are preserved.

If differential ROP activation ability of the early polarizing RopGEF3 and the late polarizing RopGEF4 would be found, this could further be investigated for the involvement of the unstructured N-termini (Fig. 11), which are proposed to contribute to GEF activity regulation (Gu *et al.,* 2006; Zhang & McCormick, 2007; Riley *et al.,* 2011). Therefore, RopGEF chimeric proteins (N14-PRONE3 and N4-PRONE3) generated during this PhD thesis can be investigated for their ROP activation potential and compared to the wild type RopGEFs. However, it was also proposed that PRONE domains differ intrinsically in their ability to activate specific ROPs as PRONE1 expression in pollen tubes caused a ROP-overexpressing phenotype whereas expression of PRONE12 did not (Zhang & McComick, 2007). The authors suspect single amino acid differences in β-arm and structural subdomain 2, which mediate the interaction with ROP GTPases and nucleotide exchange (Thomas *et al.,* 2007), to be responsible for the differential ROP binding affinities of PRONE domains. Therefore, analysis and comparison of GEF activities of N-terminally truncated RopGEF3 and RopGEF4 (PRONE3, PRONE4) in combination with protein sequence alignments of PRONE3 and PRONE4 could provide further insights into the nature of the underlying molecular mechanism.

Additionally, observation of ROP activity sensors in differentiating trichoblasts will help to understand the ROP activation pattern during root hair development. Previously used sensors include a fluorescently-tagged RIC4ΔC fusion protein, which specifically interacts with active ROPs, but lost its effector function due to C-terminal truncation (Hwang *et al.,* 2005), and Ras And Interacting Protein Chimeric Unit (Raichu) sensors, which are GFP-based Förster Resonance Energy Transfer (FRET) probes (Nakamura *et al.,* 2006).

4.1.2 Functional specialization of RopGEF3 and RopGEF4: An evolutionary new invention?

The search of orthologous sequences for RopGEF N-termini in selected model species (see section 2.2.7; Table 2.3) led to an interesting observation. While BLAST results obtained with the N-terminal sequence of RopGEF14 (N14) revealed hits in both monocots and eudicots (but not in mosses or algae), BLAST results for RopGEF3 N-terminus (N3) were restricted to eudicots among the tested species (Table 2.4). For the N-terminus of the late polarizing RopGEF4 (N4) no orthologous sequences could be found in the model species tested. Upon expanding the target species to all plants, BLAST searches revealed orthologs in the family

of Brassicaceae only. Obviously, the analysis of the evolutionary development of protein sequences requires additional investigations using a larger set of target species and proper phylogenetic analyses; however, the above-mentioned observations might allow for some speculation about the functional specialization of these N-terminal RopGEF regions during evolution. Possibly, the RopGEF family (and especially the less conserved variable terminal sequences) diversified continuously in plant kingdom. It is possible that RopGEF14 is evolutionary older than RopGEF3 and RopGEF4 as N14 orthologs were found in monocots as well. In contrast, RopGEF3 potentially evolved only after the monocot-eudicot divergence. The emergence of N3 orthologs in eudicots could represent the need for a further specified RopGEF function in this plant class. Possibly, the functional specification of RopGEFs was further split up in the family of Brassicaceae resulting in the emergence of N4. Based on this, one could further speculate that the putative task-sharing mechanism between RopGEF3 and RopGEF4 might be unique for this plant family.

4.2 PRONE3 is necessary and sufficient for RopGEF3 membrane targeting and polarization timing

After characterization of the distinct roles of early and late polarizing RopGEFs during root hair development, I aimed to investigate the mechanisms underlying the differential polarization timing. Previous work in the Grossmann laboratory using an estradiol-inducible expression system showed that expression of RopGEF3 and RopGEF4 could be induced several cell stages earlier than under the control of the respective endogenous promoter; however, the corresponding polarization timing at the RHID was not altered (Denninger & Reichelt *et al.,* 2019). This indicates that the differential polarization timing is not simply a consequence of promoter activity and suggests that additional factors are required. This could be specific recruitment factors, which polarize prior and independently of corresponding RopGEFs, but also other determinants could contribute such as the differentiation status of the cell. As the active PRONE domain in RopGEFs is highly conserved among the RopGEF protein family (Berken *et al.,* 2005; Gu *et al.,* 2006; Fig. 10), I initially hypothesized that the differential polarization timing of early and late polarizing RopGEFs is mediated via their variable N-termini. These regions have no higher order structure (Fig. 11) and might therefore provide flexible interaction surfaces, which mediate specific and transient bindings as it is often observed for signaling components (Dunker *et al.,* 2005). Therefore, I generated and analyzed a RopGEF3 truncations as well as RopGEF chimeric proteins, in which N3 was exchanged by N4 or N14 (N4-PRONE3, N14-PRONE3). However, PRONE3 and RopGEF chimeric proteins were found to polarize with a similar timing at the RHID (cell stage -5; Fig. 12, 17) as the RopGEF3 wild type protein. For

PRONE3 and N4-PRONE3 this was also reflected in the root hair phenotype since expression of these RopGEF3 variants in the *ropgef3-1* mutant background rescued the delay in bulging (Fig.14, 19). This was different for N14-PRONE3, for which a similar bulging timing was observed as in the *ropgef3-1* mutant (Fig. 19) even though this RopGEF chimera also polarized at the RHID in cell stage -5, similar to RopGEF3 full length (FL), PRONE3 and N4-PRONE3. The reason for this might be the reduced sizes of N14-PRONE3 domains, a feature that is discussed in more detail in the following section. In contrast to PRONE3, RopGEF3 N-terminus alone as well as individual PRONE3 subdomains were mainly localized to the cytosol (Fig. 12, 15). In pollen tubes, targeting of RopGEF1 to the plasma membrane was also shown to require the complete PRONE domain (Gu *et al.,* 2006). In line with the finding that the complete PRONE domain is required for RopGEF nucleotide exchange activity (Berken et *al.,* 2005; Gu *et al.,* 2006), these RopGEF3 truncations were not capable of rescuing the *ropgef3-1* mutant root hair phenotype (Fig. 14, 16). These observations suggest that targeting of RopGEF3 to the plasma membrane as well as the regular RopGEF3 polarization at the RHID requires the complete PRONE3 domain and is independent of the attached N-terminus or the lack of it. The data also suggest that a potential RopGEF3 membrane-targeting factor interacts not only with one of the PRONE subunits, but rather with a protein binding domain composed of a combination of these subdomains or parts of them. As RopGEFs were shown to function as dimers (Thomas *et al.,* 2007; Thomas *et al.,* 2009), the interaction site with the putative membrane-targeting factor could also involve subdomains of both PRONE domains in a RopGEF3 dimer. E. g. RopGEF1 dimerization was shown to be crucial for the interaction with the cytoplasmic kinase AGC kinase 1.5 (AGC1.5) in pollen (Li *et al.,* 2018a). Whether RopGEF3 dimerization is a requirement for membrane association and/ or polarization at the RHID could be investigated by introduction of a dimerization-abolishing point mutation at the position of a conserved leucine in the PRONE domain (Thomas *et al.,* 2009). An alternative explanation for the cytosolic localization of individual PRONE subdomains is that the expression of individual PRONE subdomains results in aberrant folding abolishing the 3D structure or interaction surface required for proper membrane association.

In summary, I found that RopGEF3 membrane targeting and polarization at the RHID involve the full-length PRONE domain and not the N-terminal regions. However, the underlying mechanism remains largely unclear. A recent study in pollen showed that the maintaining polar RopGEF1 distribution at the apex of the pollen tubes requires the phosphorylation of a highly conserved serine within the PRONE domain mediated by the cytoplasmic kinase AGC1.5 (Li *et al.,* 2018a). A similar mechanism involving AGC kinase-mediated PRONE3 phosphorylation could trigger and/ or maintain RopGEF3 polarization at the RHID. The family of AGC protein kinases appears particularly interesting as several family members have

been implicated in polarity control before. For example, the AGCVIII kinase PINOID (PID) belonging to the PIN1-phosphorylating kinases directs PIN1 polarity (Friml *et al.,* 2004; Huang *et al.,* 2010). AGC1.6 was shown to be expressed in trichoblasts (Zhang *et al.,* 2009), however, its expression was only detected in later stages of root hair development, when tip growth was ongoing. Therefore, this particular cytoplasmic kinase might not contribute to the initial RopGEF3 polarization, but maybe to the polarity of late polarizing RopGEFs. In total, 39 AGC kinases are present in the genome of *Arabidopsis thaliana* providing a wide range of candidate kinases to be investigated for mutant phenotypes affecting root hair formation (Bögre *et al.,* 2003). Furthermore, the analysis of RopGEF3 interaction partners will help to elucidate the RopGEF targeting mechanism. A proximity-dependent Biotin identification (BioID) technique is currently established in the Grossmann laboratory, which can be used to identify the RopGEF3 interactome. The particular advantage of such an approach over biochemical pulldown approaches is that low affinity and transient interactions, which might happen at the unstructured RopGEF3 N-terminus (Fig. 11), are more likely to be discovered (Gingras *et al.,* 2019). Based on the finding that membrane targeting and polarization at the RHID is only mediated by PRONE3, revealing the PRONE3 interactome in comparison to the RopGEF3 FL interactome could help to narrow down the candidates for RopGEF3 membrane targeting and RHID recruitment.

Of note is that the factor recruiting RopGEF3 to the plasma membrane is not necessarily identical with the factor/ signal polarizing RopGEF3 at the RHID. The first signal of the fluorescent RopGEF3 marker visible in young trichoblasts is located along the plasma membrane at the rootward cell pole (Denninger & Reichelt *et al.,* 2019; Fig. 9). Two to three cell stages after, the signal accumulates at the RHID; first very close to the cell edge, then the distance to the cell edges increases until the endogenous RopGEF3 domain position is reached (Denninger & Reichelt *et al.,* 2019; Fig. 5, Fig. 9) creating the impression that RopGEF3 may be recruited into the RHID by lateral diffusion through the plasma membrane. Alternatively, RopGEF3 polarization at the RHID might be mediated via vesicle transport as it is shown for polarity of the auxin efflux carrier PIN1 (Geldner *et al.,* 2001; Geldner *et al.,* 2003). To test whether the RopGEF3 marker protein visible at the rootward cell pole is the same that polarizes at the RHID with ongoing trichoblast differentiation, photoconvertible fluorescent tags such as Dendra (Gurskaya *et al.,* 2006) or mEos2 (McKinney *et al.,* 2009) could be employed. The spectral properties of these fluorescent tags can be changed upon exposure to certain light allowing the highlighting of specific subcellular populations of the respective fusion protein.

4.3 N-termini of early and late polarizing RopGEFs differ functionally

Despite the similar polarization timing of PRONE3 and RopGEF chimeras compared to RopGEF3 FL, major differences could be observed for these RopGEF3 variants both, on the subcellular level as well as in terms of root hair morphology. For PRONE3 and N4-PRONE3 polarity indices (PIs) as well as domain sizes were in a similar range as RopGEF3 FL in early stages of root hair development (cell -4). However, with progressing development (in cell stage -1 and +1), PIs and domain diameters increased highly significantly (Fig. 12, 13, 17, 18). N-terminal truncation of RopGEF1 in pollen tubes was also reported to enlarge the RopGEF1 cap all over the pollen tube, which was usually restricted to the apex (Gu *et al.,* 2006). In addition to the increased domain sizes, PRONE3 as well as N4-PRONE3 expression induced ectopic domain formation with a high frequency (Fig. 13, 18). In contrast, N14-PRONE3 polarization degree remained in the range of RopGEF3 FL over the course of root hair development (Fig. 17). However, N14-PRONE3 domains were found to be significantly smaller in later stages (cell stage -1 and +1) compared to RopGEF3 FL, while initial domain sizes resembled RopGEF3 FL as well as PRONE3 and N4-PRONE3 (Fig. 18). The finding that initially, RopGEF3 polarization degree as well as RHID sizes are similar in all RopGEF3 variants, suggests that the initial polarization and domain formation process is mediated via the shared feature of RopGEF3 FL, PRONE3 and RopGEF chimeras, which is the RopGEF3 PRONE domain. The subsequent regulation maintaining RHID properties such as size and position, however, are dependent on the N-terminus.

These different subcellular appearances of RopGEF3 variants lacking the N-terminus of an early polarizing RopGEF (PRONE3, N4-PRONE4) compared to variants containing the N-terminus of an early polarizing RopGEF (RopGEF3 FL, N14-PRONE3) also translated into distinctive root hair phenotypes. While PRONE3 as well as N4-PRONE3 expression in the *ropgef3-1* mutant background rescued the *ropgef3-1* mutant phenotype regarding bulging timing and root hair density, root hair lengths were significantly reduced. In addition, I observed multiple additional hair initiation sites as well as branched root hair tips. Overall, root hairs of PRONE3 and N4-PRONE3 seemed also thicker in diameter (Fig. 14, 19). This root hair phenotype is largely reminiscent of the RopGEF3 overexpression phenotype (Denninger & Reichelt *et al.,* 2019). ROP2 overexpression was found to also induce additional hair initiation sites (Jones *et al.,* 2002) and the *scn1* mutant, lacking a RopGDI (see section 1.1.1), caused multiple bulges and branched hairs as well (Carol *et al.,* 2005) suggesting that this root hair phenotype is caused by increased ROP2 activation. To test this hypothesis, activation of ROPs in PRONE3 or N4-PRONE3 expressing lines could be analyzed semi-quantitatively using the pulldown-based assay mentioned above and compared to the RopGEF3 FL line. In contrast to PRONE3 and N4-PRONE3, expression of

N14-PRONE3 resulted in the formation of wild type-like root hairs with regular length as well as largely regular initiation frequency. However, as mentioned above, the delayed bulging of *ropgef3-1* could not be rescued (Fig. 19). This is likely linked to the decreased diameters of N14-PRONE3 domains, which might initially not be capable of recruiting enough ROPs and therefore fail to initiate bulging timely. However, as root hair density in these lines is in the wild type range (Fig. 19), N14-PRONE3 domains seem to be capable of successfully initiate root hairs in general, potentially with the support of later polarizing RopGEFs.

Taken together, my findings indicate that the N-termini of the early polarizing RopGEF3 and RopGEF14 are functionally related. While the absence of these N-termini (PRONE3) or the presence of the N-terminus of the late polarizing RopGEF4 (N4-PRONE3) lead to oversized RHIDs and RopGEF3 overexpression-like features, the N-termini of RopGEF3 and 14 have a downregulating effect on the size of the RHID. This indicates that N3 and N14 carry destabilizing signals contributing to RopGEF regulation at the RHID, which are not present in the N-terminus of RopGEF4. Moreover, the destabilizing signals in N14 seem to be stronger than in N3 as the N14-PRONE3 chimera creates smaller domains than RopGEF3 FL and cannot fully compensate for the loss of endogenous RopGEF3.

4.4 RopGEF protein stabilization at the RHID is regulated via RopGEF N-termini

RopGEF N-terminal regions were reported to impact the nucleotide exchange activity (Gu *et al.,* 2006; Zhang & McCormick, 2007; Riley *et al.,* 2011), which implies that the root hair phenotypes observed for PRONE3 and N4-PRONE3 might be the consequence of RopGEF hyperactivation leading to increased ROP activation. Whether N3 and N14 actually negatively regulate RopGEF activity in contrast to N4 needs to be tested in subsequent experiments (see section 4.1.1). Additionally, taking into account the alteration of signal intensities at the RHID (PIs) and domain diameters of the different RopGEF3 variants, the hypothesis can be raised that RopGEF N-termini are involved in RopGEF protein stability. Increased RopGEF protein stability could lead to a RopGEF overrepresentation creating the large diameters of PRONE3 and N4-PRONE3 domains and therefore could also result in locally increased ROP activation. To test whether RopGEF3 variants differ in their stabilization at the RHID, I analyzed RopGEF FL, PRONE3, N4-PRONE3 and N14-PRONE3 fluorescent signals at the RHID upon translational inhibition using cycloheximide (CHX) (Fig. 20, 21). In the classical biochemical approach, CHX chases are used to determine protein half lives. In this experimental setup, only the stabilization of these proteins at the RHID could be investigated. However, as the highest proportion of signal was found at the RHID compared to the cytoplasmic background in all lines, this might also reflect actual protein stabilities to some extent. I found that RopGEF3 FL as well as N14-PRONE3 signals at the

RHID decreased faster compared to PRONE3 and N4-PRONE3 in cell stage -1 upon CHX treatment (Fig. 20). This trend became even more pronounced in cell stage +1 (Fig. 21), which might indicate that upon tip growth initiation local protein regulation becomes more dynamic. This data suggests that, indeed, RopGEF variants lacking the N-terminus of one of the early polarizing RopGEFs (PRONE3, N4-PRONE3) are localized more stably at the RHID. In contrast, RopGEF3 FL and N14-PRONE3 are removed faster from the RHID. It is important to be aware that the use of CHX affects protein synthesis unspecifically and therefore, secondary effects might occur. This is why further experiments using alternative experimental approaches are necessary to test whether RopGEF N-termini affect RopGEF protein stability in trichoblasts. As classical pulse-chase approaches involving radioactive labeling of amino acids, which are usually used to determine protein half-lives, are difficult to perform with multicellular organisms, Fluorescence Recovery After Photobleaching (FRAP) experiments could be an alternative. By specifically applying high intensity illumination to the fluorescent RopGEF3 variants at the RHID and subsequent observation of the fluorescent signal, RopGEF turnover rates can be estimated. Another microscopic alternative could involve tandem fluorescent protein timers, which consist of two fluorescent proteins with different maturation times, e.g. the mCherry-sfGFP (monomeric Cherry-superfolder GFP; Zhang *et al.,* 2019). Fusion of these timers to RopGEF3 variants and determination of the ratio of fluorescent intensities allows the comparison of their protein stabilities in trichoblasts. The use of fluorescent timers would also allow the observation of potentially differences in local protein turnover at the RHID before (cell stage -1) and after onset of tip growth (cell stage +1). It should be considered that the fluorescent tag, which is positioned N-terminal in all RopGEF3 variants, might interfere with cellular degradation mechanisms, e. g. with the N-end rule pathway (Tasaki *et al.,* 2013). To control for the impact of the fluorescent tag, microscopic approaches should be performed with C-terminally tagged RopGEF3 variants in addition.

The finding that early and late polarizing RopGEFs are likely subjected to different turnover rates raises the question about the biological meaning of this differential regulation. A higher turnover rate of RopGEF3, which was shown to be decisive for timely root hair formation, might allow trichoblasts to dynamically adjust root hair initiation to given internal signals or growth conditions. For example, lack of the key regulators of root hair development, ROP2 and ROP4, leads to efficient dissolution of RopGEF3 and RopGEF14 domains (Fig. 9). The slower turnover of the late polarizing RopGEF4, which is suspected to contribute to efficient ROP activation, might ensure continuous root hair growth.

4.5 Regulatory, N-terminal phosphorylations might affect RopGEF3 stabilization at the RHID

While regulation of RopGEF nucleotide activity is well studied, not much has been reported about regulation of cellular RopGEF protein abundance. As a consequence, RopGEF-specific degradation pathways remain largely unknown. However, in the context of abscisic acid (ABA) signaling, the mechanism underlying RopGEF1 degradation was characterized (Li *et al.,* 2016; Li *et al.,* 2018b). It was reported that, upon ABA perception, N-terminal phosphorylation triggered RopGEF1 trafficking and vacuolar degradation. Phosphorylation can also mark proteins for the degradation by the Ubiquitin/ Proteasome System (UPS; Hunter, 2007); a mechanism, which was for example shown for the RhoGEF T-LYMPHOMA INVASION AND METASTASIS 1 (Tiam1) in the context of mitogen response (Magliozzi *et al.,* 2014). In addition, other Rho regulators were shown to be subjected to proteasomal degradation as well (Nethe & Hordijk, 2010). Therefore, phosphorylation of RopGEFs as trigger for degradation in the vacuole or the proteasome appeared to be a promising possibility of RopGEF protein abundance regulation. Moreover, I hypothesize that the distinct phenotypes induced by N-termini of early and late polarizing RopGEFs in trichoblasts are the consequence of differential phosphorylations in these regions resulting in different decay rates. First evidence in favor of this hypothesis was provided by the finding that RopGEF3 is indeed phosphorylated *in vivo* (Fig. 22). Whether these phosphorylations are found in the N-terminus and/ or in the active PRONE domain remains to be clarified; especially since RopGEFs were also reported to be phosphorylated in the PRONE domain (Li et *al.* ,2018a).

In order to identify conserved putative phospho sites in the RopGEF3 N-terminus, I first identified RopGEF3 orthologs in selected model plant species (Table 2.4), compared the obtained sequences by cross-species protein sequence alignment and used *in silico* prediction tools for phospho sites (Fig. 23). From the 13 conserved, phosphorylatable residues in RopGEF3 N-terminus, 8 residues were identified as putative pshophorylation sites by the used prediction tools. By comparing of the predicted phospho sites in RopGEF3 N-terminus with the N-termini of the early polarizing RopGEF14 and the late polarizing RopGEF4 four promising candidate residues (S18, Y32, S80 and S85 in N3) were identified. These putative phosphorylation sites in the N-termini of early polarzing RopGEFs might be involved in the rapid turnover of these RopGEFs at the RHID in distinction to the late polarizing RopGEF4, which differs at these sites in the N-terminus. The impact of these putative phospho sites on RopGEF3 regulation in trichoblasts can be investigated by the introduction of phosphomimicking and nonphosphorylatable mutations at the corresponding residues in mCit-RopGEF3 and subsequent microscopic analyses. The corresponding stable *Arabidopsis thaliana* marker lines expressing mCit-RopGEF3 under the endogenous

RopGEF3 promoter and in the *ropgef3-1* mutant background carrying single point mutations or mutations at all candidate residues have been generated during this thesis and will reveal their significance for RopGEF3 regulation. A preliminary analysis of the lines carrying all four phosphomimicking or nonphosphorylatable mutations indicated that dephosphorylation ($RopGEF3_{4xA}$) at these sites might indeed slightly stabilize the protein at the RHID (Fig. 25). However, from these initial results, it seems that the stabilizing effect is much weaker than observed for PRONE3 or N4-PRONE3. An explanation for this could be that not all relevant residues were mutated and central destabilizing phosphorylations at different sites are still present. Alternatively, simultaneous mutations of all candidate residues might distort the results, if single phosphorylations have opposing regulatory effects. RHID sizes in $RopGEF3_{4xD}$ appeared similar to those of RopGEF3 FL or slightly decreased. For both phosphomimicking and nonphosphorylatable mutants, analysis of the corresponding single site mutants will clarify the roles of specific residues. Also, analysis of the resulting root hair phenotypes will help to assess the functionality of these RopGEF3 phospho site mutants.

4.6 Conclusion

In this PhD thesis, I analyzed RopGEFs and their functions during cell polarity establishment in the context of *Arabidopsis thaliana* root hair development, which were in contrast to pollen-expressed RopGEF poorly characterized so far. Additionally, I investigated the impact of the variable N-terminal sequences of trichoblast-expressed RopGEFs on RopGEF subcellular localization and cellular protein abundance, which before have been mainly analyzed for their RopGEF activity-regulating function. In the following the main findings and hypotheses derived from these analyses are summarized and put into the context of root hair initiation (Fig. 26).

Directly after its expression becomes detectable, RopGEF3 is targeted to the plasma membrane of the rootward cell pole via its PRONE domain by an unknown mechanism. In cell stage -5, an incoming polarity cue triggers RopGEF3 polarization at the RHID. This could involve the plant hormone auxin as its involvement in polarization regulation is recognized, even though not completely understood (see section 1.1). I showed that RopGEF14 is polarized at the RHID with a similar timing and in a RopGEF3-dependent manner. I demonstrated that the N-termini of these early polarizing RopGEFs are functionally related and lead to fast removal of RopGEF protein from the RHID, possibly mediated via destabilizing, N-terminal phosphorylations. This rapid turnover of early polarizing RopGEFs might ensure the dynamic adaptation to changing conditions. In cell stage -4, the key regulator of root hair development, ROP2, is polarized at the RHID in a RopGEF3-dependent manner. Moreover, I showed that RopGEF3 polarization is sufficient to polarize ROP2 in

trichoblasts as well as other cell types. I found that, in turn, ROP2 and ROP4 stabilize RopGEF3 and RopGEF14 polarization at the RHID in later stages (cell stage -1, +1) possibly representing a positive feedback mechanism. Based on the observation, that tip growth is only triggered upon RopGEF3-dependent RopGEF4 polarization at the RHID, I postulate that early polarizing RopGEFs, including RopGEF3 and RopGEF14, are inefficient ROP activators. In contrast, RopGEF4 might be a potent ROP activator, which is turned over with a lower rate to ensure robust and continuous ROP activation and root hair growth.

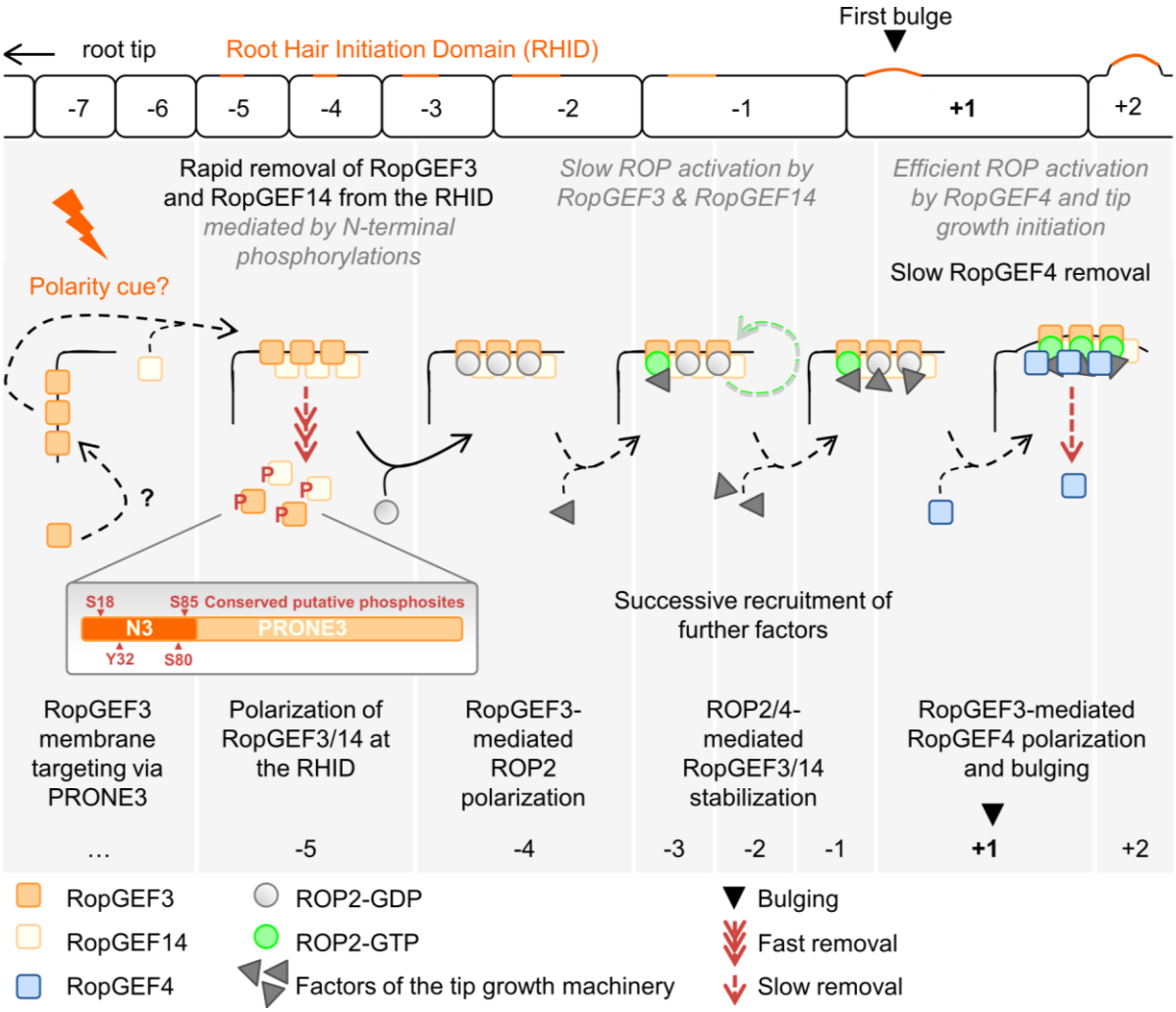

Fig. 26: Overview over the process of root hair initiation and the main findings and hypotheses of this PhD thesis. The upper panel shows the scheme of a trichoblast cell file from cell stage -7 to +2. The bulging cell (cell stage +1) served as reference in this thesis. Main findings of this thesis are written in black, derived hypotheses in grey and italic.

IV. MATERIALS & METHODS

4.1 Materials

4.1.1 *Arabidopsis thaliana* lines

Arabidopsis thaliana lines were obtained from the Nottingham *Arabidopsis* Stock Centre (NASC), collaborators, former members of the Grossmann laboratory or generated during this PhD thesis. All lines used in this thesis are listed in Table 4.1 (mutant lines) and 4.2 (marker lines) with corresponding references.

Table 5: Single and double mutant *Arabidopsis thaliana (At)* lines used in this thesis.

Mutant name	T-DNA ID	Gene name	Gene ID	Reference
ropgef3-1	SALK_079879C	*At*RopGEF3	At4G00460	NASC
ropgef3-4	SALK_021751	*At*RopGEF3	At4G00460	NASC
ropgef3-5	SALK_046978C	*At*RopGEF3	At4G00460	NASC
ropgef4-2	SALK_107520	*At*RopGEF4	AT2G45890	NASC
ropgef14-2	SALK_046067	*At*RopGEF14	AT1G31650	NASC
rop2-1	SALK_055328C	*At*ROP2	AT1G20090	NASC
rop4-1	---	*At*ROP4	AT1G75840	Fu *et al.*, 2005
ropgef3-1xropgef4-2	SALK_079879C SALK_107520	*At*RopGEF3 *At*RopGEF4	At4G00460 AT2G45890	Crossed during this PhD thesis
ropgef3-1xropgef14-2	SALK_079879C SALK_046067	*At*RopGEF3 *At*RopGEF14	At4G00460 AT1G31650	Crossed during this PhD thesis
ropgef4-2xropgef14-2	SALK_107520 SALK_046067	*At*RopGEF4 *At*RopGEF14	AT2G45890 AT1G31650	Crossed during this PhD thesis

Table 6: *Arabidopsis thaliana* marker lines used in this thesis. Endogenous promoters of RopGEF3, 4 and 14 are referred to as pRopGEF3, 4 or 14. Additionally, the CaMV 35S promoter (p35S) was used.

Marker (tag and gene)	Promoter	Plasmid ID	Genetic background	Reference
mCit-RopGEF3 (CDS)	pRopGEF3	pAR033	*ropgef3-1*	This thesis
mCit-RopGEF4 (CDS)	pRopGEF4	pAR035	*ropgef4-2*	This thesis
mCit-RopGEF14 (CDS)	pRopGEF14	pAR037	*ropgef14-2*	This thesis
mCit-RopGEF3 (genomic)	Estradiol-inducible	pPD333 +	Col-0	Philipp Denninger
mCit-RopGEF3 (genomic) + mTurq-ROP2 (genomic)	Estradiol-inducible	pPD333 + pPD042	Col-0	Philipp Denninger
mCit-RopGEF3 (genomic)	pRopGEF3	pPD332	Col-0	Philipp Denninger
mCit-RopGEF4 (genomic)	pRopGEF4	pPD301	Col-0	Philipp Denninger
mCit-RopGEF14 (genomic)	pRopGEF14	pPD305	Col-0	Philipp Denninger
mCit-RopGEF3 (genomic)	pRopGEF3	pPD332	*rop2-1xrop4-1*	This thesis
mCit-RopGEF4 (genomic)	pRopGEF4	pPD301	*rop2-1xrop4-1*	This thesis
mCit-RopGEF14 (genomic)	pRopGEF14	pPD305	*rop2-1xrop4-1*	This thesis
mCit-RopGEF4 (genomic)	pRopGEF4	pPD301	*ropgef3-1*	This thesis
mCit-RopGEF14 (genomic)	pRopGEF14	pPD305	*ropgef3-1*	This thesis
mCit-RopGEF3 N-terminus	pRopGEF3	pAR059	*ropgef3-1*	This thesis
mCit-PRONE3	pRopGEF3	pAR061	*ropgef3-1*	This thesis
mCit-RopGEF3 PRONE subdomain S1	pRopGEF3	pAR079	*ropgef3-1*	This thesis
mCit-RopGEF3 PRONE subdomain S2	pRopGEF3	pAR081	*ropgef3-1*	This thesis
mCit-RopGEF3 PRONE subdomain S3	pRopGEF3	pAR083	*ropgef3-1*	This thesis
mCit-N4-PRONE3	pRopGEF3	pAR063	*ropgef3-1*	This thesis
mCit-N14-PRONE3	pRopGEF3	pAR073	*ropgef3-1*	This thesis
mCit-RopGEF3 S18A/ Y32A/ S80A/ S85A	pRopGEF3	pAR114	*ropgef3-1*	This thesis
mCit-RopGEF3 S18D/ Y32D/ S80D/ S85D	pRopGEF3	pAR116	*ropgef3-1*	This thesis
GFP-LTI6B	p35S	---	Col-0	Cutler *et al.*, 2000

Abbreviations: Cauliflower mosaic virus (CaMV); soding sequence (CDS); monomeric Citrine (mCit); monomeric Turquoise (mTurq); Plant-specific ROP nucleotide exchange (PRONE) domain; RopGEF3 PRONE domain (PRONE3); RopGEF4 N-terminus (N4); RopGEF14 N-terminus (N14); LOW TEMPERATURE INDUCED PROTEIN 6B (LTI6B).

4.1.2 Oligonucleotides and gene synthesis

Oligonucleotides used for cloning and genotyping in this PhD thesis are listed in Table 4.3. Oligonucleotides were designed using the online tool Primer3Plus (http://www.bioinformatics.nl/cgi-bin/primer3plus/primer3plus.cg). A common melting temperature of ~60°C was defined for all oligonucleotides. Oligonucleotides were obtained from Eurofins Genomics (https://www.eurofinsgenomics.eu/). 'oAR' oligonucleotides were desgined during this thesis, 'oPD' oligonucleotides were designed by Philipp Denninger and remaining oligonucleotides were derived from general lab stocks of the Grossmann laboratory.

Table 7: Oligonucleotides used in this thesis.

Oligo ID	Description/ purpose	Sequence (5'→3')
GFP-out-fwd	Sequencing primer for expression vectors	CTGCTGGAGTTCGTGAC
GFP-out-rev	Sequencing primer for expression vectors	ACTTGTGGCCGTTTACG
GG-Entry_fwd	Sequencing primer for entry vectors	GATAACAATTTCACACGAGC
GG-Entry_rev	Sequencing primer for entry vectors	TTGTAAAACGACGGCCAG
GG-Z3_fwd	Sequencing primer for expression vectors	GGCCGCAACCTTAATTAAAC
GG-Z3_rev	Sequencing primer for expression vectors	GTGTAACGTTGGATCTGG
GG-ZP_fwd	Sequencing primer for expression vectors	GGCCTTTTTACGGTTCCT
GG-ZP_rev	Sequencing primer for expression vectors	ACACGACTCGTGTGTGC
HSP18.2Term-out_rev	Sequencing primer for expression vectors	ACAAACTTAAGCACACAAGC
LBb1.3_SALK	Genotyping of T-DNA lines	ATTTTGCCGATTTCGGAAC
oPD0197-LP	*ropgef3-1* genotyping	TCGAATCCAGATGAAAACGAC
oPD0197-RP	*ropgef3-1* genotyping	TCCTGAATGATCCAGTCGAAG
oAR017-fwd	*ropgef3-1* genotyping	CAGACCTTTAAGGAGTGTTTTAAGATT
oAR013-LP	*ropgef3-4* genotyping	AGAAAGGAGCAAAAAGCTTGG
oAR013-RP	*ropgef3-4* genotyping	GATTCATAAAGCTGCAATGGC
oPD181-LP	*ropgef4-2* genotyping	AACCTTCAGCAGGAACACATG
oPD181-RP	*ropgef4-2* genotyping	AGAGTTCTTCGAATTCCGACC
oPD176-LP	*ropgef14-2* genotyping	TGGTAAGACACCGAAACTTGC
oPD176-RP	*ropgef14-2* genotyping	TGCTGATGAGAAGAAGGTTG
oPD104-LP	*rop2-1* genotyping	TCGAATTTGGGTGATTCTCAG
oPD104-RP	*rop2-1* genotyping	TGTGGACTCGAAAGATTCACC
oPD105-LP	*rop4-1* genotyping	ATAGACCATCCTGGTGCAGTG
oPD105-RP	*rop4-1* genotyping	CAAATCCCGAGAGGAATTCTC
oAR018-rev	RopGEF3 CDS N-terminus end; cloning primer	AACAGGTCTCACTGATTAACATTCATT TGATTGCATCTCTAAAC
oAR018B-rev	RopGEF3 CDS N-terminus end; cloning primer	AACAGGTCTCGTCGCTACATTCATTT GATTGCATCTCTAAAC

oAR019A-fwd	RopGEF3 PRONE start; cloning primer	AACAGGTCTCAGGCTCTTGTAGTCCA AGAAATTTCTGAACC
oAR019B-fwd	RopGEF3 PRONE end; cloning primer	AACAGGTCTCGAAGACCTTGTAGTCC AAGAAATTTCTGAACC
oAR019-rev	RopGEF3 PRONE end; cloning primer	AACAGGTCTCACTGATTATTCACTACC TCTCATGGTTTTG
oAR020-fwd	RopGEF4 CDS start; cloning primer	AACAGGTCTCAGGCTATGGAGAGTTC TTCGAATTCC
oAR020-rev	RopGEF4 CDS N-terminus end; cloning primer	AACAGGTCTCGTCTTCTTCGTCTCCA TCTCC
oAR021-fwd	RopGEF4 CDS PRONE start; cloning primer	AACAGGTCTCAGCGACATTGATTCTG CAGA
oAR021-rev	RopGEF4 CDS PRONE end; cloning primer	AACAGGTCTCACTGACTAATCATCTCT GTTTCTCACTGTTC
oAR022-fwd	RopGEF14 CDS N-terminus start; cloning primer	AACAGGTCTCAGGCTATGATGCTGAT GAGAAGAAGGTT
oAR022-rev	RopGEF14 CDS N-terminus end; cloning primer	AACAGGTCTCACAAGCTCCTTAGCAT CAAAATGTTGG
oAR023-fwd	RopGEF3 CDS PRONE start; cloning primer	AACAGGTCTCACTTGTAGTCCAAGAA ATTTCTGAACC
oAR025-fwd	RopGEF3 CDS PRONE S1 start; cloning primer	AACAGGTCTCAGGCTGAACTTGAGAC AATGAAGGAAAGA
oAR025-rev	RopGEF3 CDS PRONE S1 end; cloning primer	AACAGGTCTCACTGATCCTTCTTCTG CATACCAAAA
oAR026-fwd	RopGEF3 CDS PRONE S2 start; cloning primer	AACAGGTCTCAGGCTAGGAAAGAAGA GAAATGGTGGTT
oAR026-rev	RopGEF3 CDS PRONE S2 end; cloning primer	AACAGGTCTCACTGATTTGCGTCTCC ATGTGTACA
oAR027-fwd	RopGEF3 CDS PRONE S3 start; cloning primer	AACAGGTCTCAGGCTGACAAGAACTA TGTTATGGCTGAGA
oAR027-rev	RopGEF3 CDS PRONE S3 end; cloning primer	AACAGGTCTCACTGATCTCATGGTTTT GTCTACATAGAGAA
oAR031-rev	RopGEF4 CDS N-terminus end; cloning primer	AACAGGTCTCACTGAGTCTTCTTCGT CTCCATCTCC

Abbreviations: Forward primer (fwd); reverse primer (rev); left boarder (LB); left primer (LP); right primer (RP); coding sequence (CDS); plant-specific ROP nucleotide exchange (PRONE) domain; subdomain 1-3 (S1-3).

RopGEF3 CDS sequences containing point mutants (phospho mutants with single or multiple mutations) were synthesized by Twist Bioscience as linear DNA fragments with overhangs compatible with the Green Gate cloning system (see section 4.2.1).

4.1.3 Vectors

Vectors used in this thesis are listed in Table 4.4 (including both Green Gate entry and expression vectors). ‘pAR’ vectors were generated during this PhD thesis, ‘pPD’ vectors were generated by Philipp Denninger and ‘pGG’ vectors were derived from general lab stocks of the Grossmann laboratory.

Table 8: Vectors used in this thesis. For Green Gate expression vecors (in pGGZ) the promoter(*) is specified: RopGEF3 endogenous promoter (pRopGEF3; pPD329), RopGEF4 endogenous promoter (pRopGEF4; pPD0063), RopGEF14 endogenous promoter (pRopGEF14; pPD0180) or estradiol-inducible promoter (pPD0161).

Plasmid ID	Insert/ description	Promoter*	Backbone
pGGC000	Empty Green Gate entry vector	---	---
pGGD002	C-decoy	---	pGGD
pGGF001	BASTA resistance	---	pGGF
pGGZ003	Empty Green Gate destination vector	---	---
pPD0059	HSP18.2 terminator	---	pGGE
pPD0063	RopGEF4 promoter	---	pGGA
pPD0160	mCit-GAGAGA	---	pGGB
pPD0161	Ubi-XVE_OlexTATA35S	---	pGGA
pPD0180	RopGEF14 promoter	---	pGGA
pPD0293	RopGEF4 CDS	---	pGGC
pPD0297	RopGEF14 CDS	---	pGGC
pPD0301	mCit-RopGEF4 (genomic)	pRopGEF4	pGGZ
pPD0305	mCit-RopGEF14 (genomic)	pRopGEF14	pGGZ
pPD0329	RopGEF3 promoter	---	pGGA
pPD0331	RopGEF3 CDS	---	pGGC
pPD0332	mCit-RopGEF3 (genomic)	pRopGEF3	pGGZ
pAR033	mCit-RopGEF3 CDS	pRopGEF3	pGGZ
pAR035	mCit-RopGEF4 CDS	pRopGEF4	pGGZ
pAR037	mCit-RopGEF14 CDS	pRopGEF14	pGGZ
pAR039	RopGEF3 CDS N-terminus	---	pGGC
pAR040	RopGEF3 CDS PRONE	---	pGGC
pAR041	RopGEF4 N-terminus with RopGEF3 PRONE	---	pGGC
pAR043	RopGEF14 N-terminus with RopGEF3 CDS PRONE	---	pGGC
pAR046	RopGEF3 PRONE subdomain S1	---	pGGC
pAR047	RopGEF3 PRONE subdomain S2	---	pGGC
pAR048	RopGEF3 PRONE subdomain S3	---	pGGC
pAR059	mCit-RopGEF3 N-terminus	pRopGEF3	pGGZ
pAR061	mCit-RopGEF3 CDS PRONE	pRopGEF3	pGGZ
pAR063	mCit-RopGEF4 CDS N-terminus with RopGEF3 CDS PRONE	pRopGEF3	pGGZ
pAR073	mCit-RopGEF14 CDS N-terminus with RopGEF3 CDS PRONE	pRopGEF3	pGGZ
pAR079	mCit-RopGEF3 CDS PRONE subdomain S1	pRopGEF3	pGGZ
pAR081	mCit-RopGEF3 CDS PRONE subdomain S2	pRopGEF3	pGGZ
pAR083	mCit-RopGEF3 CDS PRONE subdomain S3	pRopGEF3	pGGZ

pAR095	RopGEF4 CDS N-terminus	---	pGGC
pAR097	mCit-RopGEF4 CDS N-terminus	pRopGEF4	pGGZ
pAR113	RopGEF3 CDS S18A/ S80A/ S85A/ Y32A	---	pGGC
pAR114	mCit-RopGEF3 CDS S18A/ S80A/ S85A/ Y32A	pRopGEF3	pGGZ
pAR115	RopGEF3 CDS S18D/ S80D/ S85D/ Y32D	---	pGGC
pAR116	mCit-RopGEF3 CDS S18D/ S80D/ S85D/ Y32D	pRopGEF3	pGGZ

Abbreviations: Heat shock protein (HSP); monomeric Citrine (mCit); coding sequence (CDS); plant-specific ROP nucleotide exchange (PRONE) domain; subdomain 1-3 (S1-3).

4.1.4 Enzymes

All enzymes used in this thesis were obtained from New England Biolabs (Table 4.5).

Table 9: Enzymes used in this thesis.

Enzyme	Catalog number	Reaction buffer
BsaI-HFv2	R3733S	10X Cutsmart
T4 DNA Ligase	M0202S/ L	10X T4 DNA Ligase Buffer
Q5 HiFi DNA Polymerase	M0491S/ L	5X Q5 reaction buffer
Taq DNA Polymerase	M0267S/ L	10X ThermoPol Reaction Buffer
Lambda protein phosphatase	P0753S/ L	50X NEBuffer for Protein MetalloPhosphatases

Abbreviations: High fidelity (HiFi).

4.1.5 Kits

Plasmid DNA was purified using the Nucleospin Plasmid kit (Macherey-Nagel, REF 740588.250). DNA fragments were purified using the Nucleospin Gel and PCR Clean-up kit (Macherey-Nagel, REF 740609.250). Kits were used according to manufacturer's instructions.

4.1.6 Antibodies

For detection of proteins in Western blot following antibodies were used (Table 4.6).

Table 10: Antibodies used in this thesis. Antibody dilutions were made in 1X TBST (see Table 4.7). Primary antibody dilutions were additionally supplied with 0.02% sodium azide.

Antibody	Raised in	Supplier (reference)	Dilution
Anti-GFP (monoclonal)	Rabbit	Invitrogen (G10362)	1:500
Anti-rabbit IgG (H+L), horse radish peroxidase conjugate (polyclonal)	Goat	Promega (W401B)	1:2,000

4.1.7 Media and buffers

Table 11: Recipes for all buffer and media used in this thesis. For critical chemicals the brand is indicated.

Name	Chemical	Final concentration
Plant medium/ agar (pH 5.7)	Murashige and Skoog (MS) Basal Salt Mixture (SERVA)	0.25-0-5X
	Plant agar (Duchefa)	0.8 % (w/v)
	MES hydrate	0.1 % (w/v)
LB medium/ agar	NaCl	10 g/ l
	Trypton	10 g/ l
	Yeast extract	5 g/ l
	Agar	15 g/ l
Extraction buffer (EB) for gDNA isolation (pH 8.0)	Tris	200 mM
	NaCl	100 mM
	EDTA	10 mM
	SDS	1 %
	β-Mercaptoethanol	10 mM
Transformation medium for floral dip	Sucrose	5 % (w/ v)
	Silwet L77/ Gold	0.05 %
6X Protein loading dye	Tris pH 6.8	350 mM
	Glycerol	30 %
	SDS	10%
	Bromphenol blue	0.012
	DTT	600 mM
10X SDS-PAGE running buffer	Glycine	2 M
	Trizma	250 mM
	SDS	1 %
10X Transfer buffer	Glycine	2 M
	Trizma	250 mM
	(+Ethanol in 1X dilution	20%)
10X TBS(T) (pH 7.6)	Tris base	200 mM
	NaCl	1.5 M
	(+Tween20 in 1X dilution	0.1 %)
10X TAE (pH 8.3)	Tris	2 M
	Acetate	1 M
	EDTA	50 mM
Plant lysis buffer	Tris pH 8.0	100 mM
	NaCl	100 mM
	Nonidet P40	10 %
	cOmplete™, EDTA-free protease inhibitor (Roche)	1X

ECL solution – Solution A	Luminol p-Coumaric acid Tris-HCl pH 8.0	2.5 mM 0.4 mM 125 mM
ECL solution – Solution B	Hydrogen peroxide Tric-HCl pH 8.0	0.02 % 100 mM

4.2 Methods

4.2.1 Molecular biology

Vectors cloned in this thesis were generated using the Green Gate cloning system (Lampropoulos *et al.*, 2013).

4.2.1.1 Polymerase chain reaction (PCR) for cloning

Cloning PCRs were performed using Q5 HiFi DNA polymerase (Table 4.5). PCR reactions contained 2-5 ng plasmid DNA as template, 1X Q5 reaction buffer, 400 nM primer forward/ reverse, 100 µM dNTPs and 0.02 U/ µl Q5 HiFi DNA polymerase. PCR reactions were incubated in a cycler machine with the following program: 2 min at 98 °C, 30 cycles of [20 s at 98 °C, 20 s at 60 °C, 30 s per kb at 72 °C], 2 min at 72 °C. PCR fragments were resolved and visualized on a 1-1.5% agarose gel in 1X TAE (Table 4.7) containing 0.03 µl/ ml RotiSafe gel stain (Carl-Roth, #3865). Agarose gels were run at room temperature and 100-180 V. Sizes were estimated by comparison with the 1 kb DNA Ladder (New England Biolabs, #N3232S/L). PCR fragments were purified from PCR reactions using the Nucleospin Gel and PCR Clean-up kit from Macherey-Nagel according to manufacturer's instructions. Purified DNA fragments were eluted in 20 µl MilliQ.

4.2.1.2 Green gate entry vector generation

Purified PCR fragments in 20 µl MilliQ and 100 ng of the empty Green Gate entry vector (pGGC000) were digested with 0.5 U/ µl BsaI-HFv2 (Table 4.5) in 1X Cutsmart buffer for 30-60 min at 37 °C. BsaI-digested DNA fragments were purified using the Nucleospon Gel and PCR Clean-up kit from Macherey-Nagel according to manufacturer's instructions. Purified DNA fragments were eluted in 20 µl MilliQ. Ligation of the digested and purified PCR fragments and vector backbone was performed in 1X T4 ligase buffer with 10 U/ µl T4 DNA ligase (Table 4.5) for 1 h at room temperature. The ligation mix was transformed into competent *Escherichia coli* (*E.coli*) bacteria for plasmid amplification (see section 4.2.1.4).

4.2.1.3 Green gate expression vector generation

Green gate expression vectors were assembled from entry vectors containing the desired promoter (module A), N-tag (module B), coding sequence (module C), C-tag (module D), terminator (module E) and plant resistance gene (module F) as well as the destination vector

pGGZ003 (Lampropoulos *et al.,* 2013). The green gate reaction contained 150 ng of each entry vector as well as the destination vector, 1X Cutsmart buffer, 1 mM ATP, 1.3 U/ µl BsaI-HFv2 and 26.6 U/ µl T4 DNA ligase. The green gate reactions were incubated in a cycler machine with the following program: 30 s at 37 °C, 30 cycles of [1 min at 37 °C, 1 min at 16 °C], 5 min at 50 °C, 5 min at 80 °C. The green gate reactions were then transformed into competent *E.coli* bacteria for plasmid amplification.

4.2.1.4 *E. coli* transformation and selection

For standard plasmid amplification chemically competent DH5α or XL1blue *E. coli* strains were used. For amplification of entry vectors containing the CcdB "killer" gene encoding the cytotoxic protein CcdB, the CcdB-tolerant *E. coli* strain DB3.1 was used. For transformation, 100 µl chemically competent *E. coli* were thawed on ice for 20-30 min. After addition of DNA (20 µl ligation reaction or 1 µl plasmid DNA for retransformations), bacteria were incubated for 45 s at 42 °C. After 2 min incubation on ice, 900 µl non-selective lysogeny broth (LB) medium were added and the bacterial suspension was incubated for 20-60 min at 37 °C while shaking. Bacteria were harvested by centrifugation for 3-5 min at 4,000 rpm, plated on selective LB plates and incubated overnight at 37 °C. Depending on the transformed vector, following antibiotics were used: 100 µg/ ml ampicillin, 50 µg/ ml Kanamycin, 50 µg/ ml streptinomycin.

4.2.1.5 Colony PCR

Transformants were tested by colony PCR for the presence of the desired vector. Colony PCR reactions were performed using Taq DNA polymerase (Table 4.5) and contained the following components: 1X ThermoPol reaction buffer, 100 nM primer forward/ reverse, 80 µM dNTPs and 0.02 U/ µl Taq DNA polymerase. Colonies were picked up with a tooth pick, dipped into the PCR reactions and then transferred on a selective LB replica plate. Replica plates were incubated at 37 °C. PCR reactions were incubated in a cycler machine with the following program: 2 min at 95 °C, 30 cycles of [20 s at 95 °C, 20 s at 60 °C, 60 s per kb at 68 °C], 2 min at 68 °C. PCR fragments were resolved as described in section 4.2.1.1. Positive transformants were picked from the replica plate and used for inoculation of liquid overnight cultures.

4.2.1.6 Plasmid isolation and sequencing

For plasmid amplification, 5 ml selective, liquid LB medium was inoculated with transformed *E. coli* and grown overnight at 37 °C while shaking. Plasmids were isolated from liquid cultures using the Nucleospin Plasmid kit (Macherey-Nagel; see section 4.1.5) according to manufacturer's instructions. Plasmids were eluted in 30-50 µl MilliQ. Plasmids were sequenced with appropriate primers by the custom DNA sequencing service of Eurofins

Genomics (Mix2Seq; https://eurofinsgenomics.eu/de/custom-dna-sequencing/eurofins-services/mix2seq-kits/).

4.2.1.7 Isolation of plant genomic DNA and genotyping

For genomic DNA (gDNA) isolation, rosette leaves of 3-weeks-old *Arabidopsis thaliana* plants were harvested and frozen in liquid nitrogen together with glass beads (2.85-3.45 mm diameter) in 2 ml reaction tubes. Leaf tissue was ground in the TissueLyser II (Quaigen) for 45 s with a shaking frequency of 30 s^{-1}. Tube holders of the machine were precooled at -80 °C prior to use. After addition of 750 µl extraction buffer (EB; Table 4.7) to the pulverized leaf material, samples were incubated at 65 °C for 10 min. Samples were then transferred back to ice and 200 µl 5 M potassium acetate was added. Samples were incubated for at least 20 min on ice and then centrifuged for 10 min at full speed. The clear supernatant was transferred into a new reaction tube and mixed with 1 ml precooled (at –20 °C) isopropanol. Samples were centrifuged for 2 min at full speed. After removal of the supernatant, 500 µl 70 % ethanol were added and samples were centrifuged again. The supernatant was removed again and finally, DNA pellets were dried and resuspended in 50-100 µl MilliQ.

Genotyping PCRs were performed with the Taq DNA polymerase (Table 4.5) and contained the following components: 1 X ThermoPol reaction buffer, 400 nM primer forward/ reverse/ internal (for mutant SALK or SAIL lines), 80 µM dNTPs, and 0.02 U/ µl Taq DNA polymerase. 2 µl of gDNA solution per reaction served as template. PCR reactions were run and evaluated as described in section 4.2.1.1.

4.2.2 Plant handling

4.2.2.1 Seed sterilization

Arabidopsis thaliana seeds were vapor-sterilized with chlorine gas. An amount of seeds corresponding to a volume of 50-100 µl were placed into 2 ml reaction tubes, which were placed with open lids into a sealable container. 50-60 ml fresh sodium hypochlorite solution were mixed with 2-3 ml 37 % HCl and the container was sealed immediately. Seeds were incubated in the resulting chlorine gas for 1.5-2.5 h.

4.2.2.2 Plant growth conditions

Arabidopsis thaliana plants on soil were grown in a plant room under long day conditions (16 h light and 8 h darkness) at 21 °C and 65 % relative humidity. Plants in soil were treated at least once with a nematode solution (Nemaplus from e-Nema). Seedlings were grown on horizontal growth plates (Table 4.7) in a growth chamber under similar conditions.

4.2.2.3 Agrobacterium-mediated *Arabidopsis thaliana* transformation and T1 selection

Chemically competent *Agrobacterium tumefaciens* (strain GV3101-pMP90RK-pSoup) were thawed on ice and incubated with 100-500 ng plasmid DNA for 5 min on ice. Bacteria were then incubated for 5 min in liquid nitrogen and subsequently heat shocked for 5 min at 37 °C. After addition of 900 µl non-selective LB medium, cells were incubated at 28 °C while shaking for 2-4 h. Transformed bacteria were collected by centrifugation at 4,000 rpm for 5 min and plated on selective LB medium containing 50 µg/ ml Kanamycin or 100 µg/ ml Spectinomycin. Selection plates were incubated at 28 °C for 4-5 days.

Plant expression vectors were transformed into 4-6-weeks-old *Arabidopsis thaliana* plants by floral dip (Clough and Bent, 1998). 4-6 colonies of transformed *Agrobacteria tumefaciens* were picked from the selection plate and used for inoculation of 4 ml selective LB medium. The culture was grown overnight at 28 °C while shaking. 100 ml selective LB medium was inoculated with the overnight culture(s) and grown at 28 °C while shaking until OD_{600} 0.6-0.8. Bacteria were harvested by centrifugation for 10 min at 4,000 g. After removal of the supernatant, bacterial pellets were resuspended in 200-250 ml transformation medium (Table 4.7). Plants were dipped into the bacterial suspension for 3-5 min and then covered with plastic bags for 12-24 h. To increase transformation efficiency, the floral dip was usually repeated one week after initial transformation. Plants were then grown until T1 seeds could be harvested.

T1 seeds were collected and dried for 2-3 days at 30 °C. Transformants (usually containing glufosinate-ammonium/ Basta resistance) were selected on soil by treatment with a Basta solution (200 µg/ ml glufosinate-ammonium (BAYER) supplemented with 0.05 % Tween 20) one week after germination. Basta treatment was repeated at least once 2-4 days after the intial treatment. The presence of the desired transgene was verified by genotyping of Basta-resistant T1 plants. Positive transformants were separated into different pots and grown until T2 seeds could be harvested.

4.2.2.4 Induction of gene expression with estradiol

Estradiol-inducible *Arabidopsis thaliana* lines were grown until 7 days after germination (DAG) on regular growth plates (Table 4.7). Gene expression was induced with ½ MS liquid medium containing 20 µM estradiol (from 20 mM estradiol stock in absolute ethanol) supplemented with 0.01 % Silwet L77/ Gold. The estradiol solution was applied 24 h prior to use of the plants using a spray bottle.

4.2.3 Imaging & data analysis

4.2.3.1 Transmitted light imaging and root hair phenotype quantification

For phenotyping, vapor-sterilized seeds were incubated in 0.1 % agarose for 1-3 days in the dark. Seeds were then placed on regular growth plates and grown under standard conditions until 7 DAG. The wild type reference Col-0 was grown on each growth plate to allow normalization of the measurements to the specific Col-0 measurements on the respective plate. Primary roots were imaged using a Nikon SMZ18 stereo microscope, equipped with SHR Plan Apo 0.5X and 2X objectives (Nikon) and an Orca Flash 4.0 sCMOS camera (Hamamatsu). From each primary root three fields of view (FOV) starting from the root tip were acquired with a total magnification of 40X.

Obtained data were evaluated using the image processing program FIJI (Fiji is just ImageJ, version v1.53c; Schindelin *et al.,* 2012). Three parameters were quantified (Fig. 3B): (1) The distance between the first bulge and the primary root tip was measured using the *Segmented Line* tool. (2) Root hair density was determined in the FOV with most root hairs. Primary root length in this FOV was determined using the *Segmented Line* tool and the total root hair number was determined using the *Multi-point* tool. From these values root hair densities were calculated in number of hairs per millimeter primary root. (3) Root hair lengths of 10-20 hairs per primary root were determined using the *Segmented Line* tool and averaged. For example images in figures presented in the Results section, FOV were merged using the *Pairwise Stitching* plugin with the stitching method *Linear Blending* or *Maximum Intensity* (Preibisch *et al.,* 2009). Phenotyping data are presented as box pots, which were generated using the online tool BoxPlotR (http://shiny.chemgrid.org/boxplotr/) created by the Tyers and Rappsilber laboratories.

4.2.3.2 Spinning disk confocal microscopy and image analysis

Confocal images were acquired with a custom-built spinning disk confocal microscope consisting of a microscope stand (Ti-E, Nikon), a motorized stage (Applied Scientific Instrumentation), a spinning disk (CREST Optics, pinhole size 70 µm), a motorized filter wheel (CAIRN Research), a laser launch box (Omicron, 488/ 515/ 561/ 638 nm), two dichroic mirrors (Chroma, quad band (405/ 488/ 561/ 640), triple band (440/ 514/ 561) and an electron-multiplying charge-coupled device (EMCCD) camera (Photometrics). The imaging software used was the Nikon NIS Elements software. Images were acquired using the 20X multi-immersion and the 60X water immersion (Nikon) objectives. Imaging parameters used for different fluorophores and stains used are specified in Table 4.8.

Table 12: Excitation wavelengths and emission filters used for confocal spinning disk imaging.

Fluorophore/ stain	Excitation wavelength [nm]	Emmission filter
mCitrine (mCit)	515	Bandpass 542nm/ 20 (Semrock)
mTurquoise (mTurq)	445	Bandpass 480nm/ 40 (Semrock)
Propidium iodide, chlorophyll	561	Bandpass 605 nm/ 70 (Semrock)

Laser output as well as excitation time were optimized for each line imaged and therefore signal intensities are not comparable by default. However, for RopGEF3 FL, PRONE3, RopGEF chimera and phospho mutant lines these settings were kept identical in order to allow comparison of signal intensities. The same is true for RopGEF3, RopGEF4 or RopGEF14 in different genetic backgrounds (Fig. 9).

The polarity indices (PIs; arbitrary unit (AU)) of fusion proteins in trichoblasts were determined by measurements on original, unprocessed z-stacks acquired with the 20X objective. For this, z-stacks acquired along the primary root were stitched in FIJI as described in section 4.2.3.1. Three regions of interest (ROIs; 3x8 pixels) were measured for the PI calculation of each cell stage (Fig. 5A). The first ROI (ROI_{RHID}) was positioned in the center of the RHID, the second ROI (ROI_{out}) was positioned in the middle between the RHID and the shootward cell edge and the third ROI was positioned outside of the cell as background reference. Mean grey values in these ROIs were measured using the *Multi measure* tool. For ROI_{RHID} and ROI_{out} the maximum values and the corresponding background values were determined. After background subtraction, the ratio between these values was determined (Int_{RHID}/ Int_{out}), which is referred to as polarity index.

Domain sizes (DS; in µm) were determined by calculation of the Full Width Half Max (FWHM) values of intensity profiles along the plasma membrane starting from the rootward cell edge over the RHID using the *Segmented Line* tool (width: 3 pixels). Baseline signal intensity in each cell was determined by averaging the mean grey values along a 20 µm long section of the plasma membrane outside the RHID. This value was subtracted from the maximum value to obtain the peak height and subsequently the half maximum value. Using linear interpolation, the FWHM values were determined.

For example images of single cells small z-projections (3-10 slices) using the *Z project* option in FIJI with the projection type *Max Intensity* were built. Images were processed with a *Gaussian Blur* filter (radius 0-6-0.8) and a subsequent background subtraction (*Rolling ball radius:* 50-100). Images with same acquisition settings were also scaled the same way to allow comparisons of signal intensities. Signals are depicted in the look up table *royal*. In whole root example images, mCitrine signal is depicted in the look up table *yellow* and propidium iodide in *magenta*. For latter channel gamma settings were adjusted individually for each image to optimize the visualization of cell outlines.

4.2.3.3 Propidium iodide staining

In order to highlight cell outlines, seedlings (7 DAG) were stained with 1 µg/ ml propidium iodide in water for 5 min and subsequently washed in MilliQ. Seedlings were then transferred on a microscopic slide with a drop of water and imaged. Fusion proteins (usually with mCit tag) and propidium iodide staining were imaged in sequential scans.

4.2.3.4 Cycloheximide treatment

For the cycloheximide (CHX) treatment, seedlings were grown directly on microscopic slides in small growth chambers filled with agar similar to regular plant growth plates (Table 4.7). First, seedlings were grown horizontally, so that roots penetrated the agar. As soon as primary root tips reached the microscopic slide on the bottom, growth chambers were tilted in a 45° angle so that roots grew along the microscopic slide allowing the observation of growing roots at the microscope. CHX and corresponding mock treatments were performed 7 DAG by adding liquid ½ MS medium with or without 400 µg/ ml CHX into the growth chambers. For evaluation, mean grey values were measured in the center of the RHIDs (3x8 pixels ROI) before and at two times points after treatment (t_1, t_2). The change in fluorescence between t_1 and t_2 was calculated in percentage change per hour. Obtained data are presented in box plots created with BoxPlotR (see section 4.2.3.1).

4.2.3.5 Statistics

Statistical differences in root hair phenotypes and in the CHX experiment were determined by a 2-way ANOVA test performed in R studio. The corresponding script is given below and was kindly provided by Dr. Milan Župunski (University of Novi Sad).

```
library(car)
library(multcomp)
library(ggpubr)
library(ggplot2)
library(rcompanion)
library(lsmeans)
library(xlsx)
install.packages(c("car", "multcomp", "ggpubr", "ggplot2", "rcompanion", "lsmeans", "xlsx"))
mydata <- read.xlsx(choose.files(), sheetName = "Sheet1")
###ANOVA
mydata.an <- aov(mgv ~ genotype, data = mydata) ###mgv is mean gray value
Anova(mydata.an, type = "II")
write.csv(Anova(mydata.an, type = "II"), "anova output.csv")

###Tukey PostHoc test
multi.c <- lsmeans(mydata.an, pairwise~genotype, adjust="tukey")
cld(multi.c[[1]],
```

```
            alpha   = 0.05,
            reversed = TRUE,
            decreasing = TRUE,
            Letters = letters,
            adjust  = "tukey")
write.csv(cld(multi.c[[1]],
          alpha   = 0.05,
          reversed = TRUE,
          decreasing = TRUE,
          Letters = letters,
          adjust  = "tukey"), "tukey comparisons.csv")
```

Statistical differences in domain sizes between RopGEF3 variants and RopGEF3 FL were determined by a two-sided, unpaired Student's t-test assuming unequal variances in Microsoft Excel.

4.2.4 Biochemistry

4.2.4.1 Lambda phosphatase treatment

Arabidopsis thaliana seedlings were grown until 7 DAG on regular growth plates (Table 4.7). Gene expression was induced as described in section 4.2.2.4. 24 h after induction, whole seedlings were harvested from the plates and frozen in liquid nitrogen. Seedlings were pulverized in the reaction tubes by grinding using pre-cooled pistils. After addition of a corresponding amount of plant lysate buffer (Table 4.7; volume = 2x weight of sample in mg), samples were incubated for 10 min at 4 °C on a rotating wheel before being centrifuged at full speed for 20 min and at 4 °C. The supernatant was transferred into a new reaction tube. 40 µl cleared lysate were used per reaction, which contained 1X NEBuffer for Protein MetalloPhosphatases and 1 mM $MnCl_2$. In one reaction tube 1 µl lambda protein phosphatase (Tabe 4.5) was added, while the control reaction contained 1 µl water instead. Samples were incubated for 30 min at 31 °C and after addition of protein loading dye (Table 4.7) for 10 min at 95 °C.

4.2.4.2 SDS-PAGE and Western Blot

Protein samples were separated by sodium dodecyl sulfate polyacrylamide gel electrophoresis (SDS-PAGE). Samples were loaded on 7.5-10 % self-cast polyacrylamid gels and proteins were separated at 120 V and room temperature. Subsequently, proteins were transferred onto a Polyvinylidene fluoride (PVDF) membrane by wet blotting (see Table 4.7 for SDS-PAGE running buffer and transfer buffer). After 90 min transfer at 100 V and 4 °C, the membrane was incubated in 5 % BSA in 1X TBST (Table 4.7) for 1 h at room temperature while shaking. Blocking solution was removed from the membrane by rinsing with 1X TBST. The membrane was incubated with a monoclonal α-GFP antibody overnight at

4°C and after washing with 1X TBST with a secondary antibody at room temperature for 2 h (Table 4.6). Signals were visualized by enhanced chemiluminescence (ECL, Table 4.7). Exposure times for detection were adjusted individually for each membrane depending on signal intensity.

4.2.5 Tools used for *in silico* analyses

Table 13: Online tools used for *in silico* analyses in this thesis. All tools used are listed with the name (including the specific version) and corresponding references.

Tool name	Purpose	Reference
Genevestigator®	Gene expression analysis	Hruz *et al.,* 2008; https://genevestigator.com/
Phytozome 12	BLAST searches	Goodstein *et al.,* 2012; https://phytozome.jgi.doe.gov/pz/portal.html#!search?show=BLAST
Ensembl Plants		Yates *et al.,* 2020; https://plants.ensembl.org/Multi/Tools/Blast
Clustal Omega 1.2.4	Protein sequence alignments	Madeira *et al.,* 2019; https://www.ebi.ac.uk/Tools/msa/clustalo/
BoxShade 3.21	Visualization of conservation in protein sequences	K. Hofmann & M. Baron; https://embnet.vital-it.ch/software/BOX_form.html
Cspritz web server 1.2	Identification of regions of intrinsic disorder in proteins	Walsh *et al.,* 2011; http://old.protein.bio.unipd.it/cspritz/
GPS-Lipid 1.0	Identification of putative lipid modifications in proteins	Ren *et al.,* 2008; Xie *et al.,* 2016; http://lipid.biocuckoo.org/
NetPhos 3.1	Identification of putative phosphorylation sites in proteins	Blom *et al.,* 1999; Blom *et al.,* 2004; http://www.cbs.dtu.dk/services/NetPhos/
PhosPhAt 4.0		Heazlewood *et al.,* 2008; Durek *et al.,* 2010; http://phosphat.uni-hohenheim.de/index.html
P3DB 3.5		Yao *et al.,* 2014; http://www.p3db.org/prediction.php

V. BIBLIOGRAPHY

Adams, A. E. M., Johnson, D. I., Longnecker, R. M., Sloat, B. F., & Pringle, J. R. (1990). CDC42 and CDC43, Two Additional Genes Involved in Budding and the Establishment of Cell Polarity in the Yeast Saccharomyces cerevisiae. *Journal of Cell Biology*, *84*(4), 481–493. https://doi.org/10.1134/s032097251904002x

Aghazadeh, B., Lowry, W. E., Huang, X. Y., & Rosen, M. K. (2000). Structural basis for relief of autoinhibition of the Dbl homology domain of proto-oncogene Vav by tyrosine phosphorylation. *Cell*, *102*(5), 625–633. https://doi.org/10.1016/S0092-8674(00)00085-4

Akamatsu, A., Uno, K., Kato, M., Wong, H. L., Shimamoto, K., & Kawano, Y. (2015). New insights into the dimerization of small GTPase Rac/ROP guanine nucleotide exchange factors in rice. *Plant Signaling and Behavior*, *10*(7), 6–13. https://doi.org/10.1080/15592324.2015.1044702

Asnacios, A., & Hamant, O. (2013). The mechanics behind cell polarity. *Current Opinion in Plant Biology*, *16*(6), 774–779. https://doi.org/10.1016/j.pbi.2013.10.011

Basu, D., Le, J., Zakharova, T., Mallery, E. L., & Szymanski, D. B. (2008). A SPIKE1 signaling complex controls actin-dependent cell morphogenesis through the heteromeric WAVE and ARP2/3 complexes. *Proceedings of the National Academy of Sciences of the United States of America*, *105*(10), 4044–4049. https://doi.org/10.1073/pnas.0710294105

Bender, A., & Pringle, J. R. (1989). Multicopy suppression of the cdc24 budding defect in yeast by CDC42 and three newly identified genes including the ras-related gene RSR1. *Proceedings of the National Academy of Sciences of the United States of America*, *86*(24), 9976–9980. https://doi.org/10.1073/pnas.86.24.9976

Berken, A., Thomas, C., & Wittinghofer, A. (2005). A new family of RhoGEFs activates the Rop molecular switch in plants. *Nature*, *436*(7054), 1176–1180. https://doi.org/10.1038/nature03883

Berleth, T., & Sachs, T. (2001). Plant morphogenesis: Long-distance coordination and local patterning. *Current Opinion in Plant Biology*, *4*(1), 57–62. https://doi.org/10.1016/S1369-5266(00)00136-9

Bi, F., Debreceni, B., Zhu, K., Salani, B., Eva, A., & Zheng, Y. (2001). Autoinhibition Mechanism of Proto-Dbl. *Molecular and Cellular Biology*, *21*(5), 1463–1474. https://doi.org/10.1128/mcb.21.5.1463-1474.2001

Bibikova, T. N., Blancaflor, E. B., & Gilroy, S. (1999). Microtubules regulate tip growth and orientation in root hairs of Arabidopsis thaliana. *Plant Journal*, *17*(6), 657–665. https://doi.org/10.1046/j.1365-313X.1999.00415.x

Bibikova, T. N., Jacob, T., Dahse, I., & Gilroy, S. (1998). Localized changes in apoplastic and cytoplasmic pH are associated with root hair development in Arabidopsis thaliana. *Development*, *125*(15), 2925–2934.

Birnbaum, K., Shasha, D. E., Wang, J. Y., Jung, J. W., Lambert, G. M., Galbraith, D. W., & Benfey, P. N. (2003). A Gene Expression Map of the Arabidopsis Root. *Science*, *302*(5652), 1956–1960. https://doi.org/10.1126/science.1090022

Blom, N., Gammeltoft, S., & Brunak, S. (1999). Sequence and structure-based prediction of eukaryotic protein phosphorylation sites. *Journal of Molecular Biology*, *294*(5), 1351–1362. https://doi.org/10.1006/jmbi.1999.3310

Blom, N., Sicheritz-Pontén, T., Gupta, R., Gammeltoft, S., & Brunak, S. (2004). Prediction of post-translational glycosylation and phosphorylation of proteins from the amino acid sequence. *Proteomics*, *4*(6), 1633–1649. https://doi.org/10.1002/pmic.200300771

Bögre, L., Ökrész, L., Henriques, R., & Anthony, R. G. (2003). Growth signalling pathways in Arabidopsis and the AGC protein kinases. *Trends in Plant Science*, *8*(9), 424–431. https://doi.org/10.1016/S1360-1385(03)00188-2

Borg, S., Pødenphant, L., Jensen, T. J., & Poulsen, C. (1999). Plant cell growth and differentiation may involve GAP regulation of Rac activity. *FEBS Letters*, *453*(3), 341–345. https://doi.org/10.1016/S0014-5793(99)00750-4

Bos, J. L., Rehmann, H., & Wittinghofer, A. (2007). GEFs and GAPs: Critical Elements in the Control of Small G Proteins (DOI:10.1016/j.cell.2007.05.018). *Cell*, *130*(2), 385. https://doi.org/10.1016/j.cell.2007.07.001

Brady, S. M., Orlando, D. A., Lee, J.-Y., Wang, J. Y., Koch, J., Dinneny, J. R., … Benfey, P. N. (2007). Dominant Expression Patterns. *Science*, *318*(5851), 801–806.

Brembu, T., Winge, P., Bones, A. M., & Yang, Z. (2006). A RHOse by any other name: A comparative analysis of animal and plant Rho GTPases. *Cell Research*, *16*(5), 435–445. https://doi.org/10.1038/sj.cr.7310055

Campetelli, A., Bonazzi, D., & Minc, N. (2012). Electrochemical regulation of cell polarity and the cytoskeleton. *Cytoskeleton*, *69*(9), 601–612. https://doi.org/10.1002/cm.21047

Carol, R. J., Takeda, S., Linstead, P., Durrant, M. C., Kakesova, H., Derbyshire, P., … Dolan, L. (2005). A RhoGDP dissociation inhibitor spatially regulates growth in root hair cells. *Nature*, *438*(7070), 1013–1016. https://doi.org/10.1038/nature04198

Cerione, R. A., & Zheng, Y. (1996). The Dbl family of oncogenes. *Current Opinion in Cell Biology*, *8*(2), 216–222. https://doi.org/10.1016/S0955-0674(96)80068-8

Chang, C., Bowman, J. L., & Meyerowitz, E. M. (2016). Field Guide to Plant Model Systems. *Cell*, *167*(2), 325–339. https://doi.org/10.1016/j.cell.2016.08.031

Chang, F., Gu, Y., Ma, H., & Yang, Z. (2013). AtPRK2 promotes ROP1 activation via RopGEFs in the control of polarized pollen tube growth. *Molecular Plant*, *6*(4), 1187–1201. https://doi.org/10.1093/mp/sss103

Chen, M., Liu, H., Kong, J., Yang, Y., Zhang, N., Li, R., … Tao, L. (2011). *RopGEF7* Regulates PLETHORA-Dependent Maintenance of the Root Stem Cell Niche in *Arabidopsis*. *The Plant Cell*, *23*(8), 2880–2894. https://doi.org/10.1105/tpc.111.085514

Chen, R., Hilson, P., Sedbrook, J., Rosen, E., Caspar, T., & Masson, P. H. (1998). The Arabidopsis thaliana AGRAVITROPIC 1 gene encodes a component of the polar-auxin-transport efflux carrier. *Proceedings of the National Academy of Sciences of the United States of America*, *95*(25), 15112–15117. https://doi.org/10.1073/pnas.95.25.15112

Chiou, J. G., Balasubramanian, M. K., & Lew, D. J. (2017). Cell polarity in yeast. *Annual Review of Cell and Developmental Biology*, *33*, 77–101. https://doi.org/10.1146/annurev-cellbio-100616-060856

Clough, S. J., & Bent, A. F. (1998). Floral dip: A simplified method for Agrobacterium-mediated transformation of Arabidopsis thaliana. *Plant Journal*, *16*(6), 735–743. https://doi.org/10.1046/j.1365-313X.1998.00343.x

Cook, D. R., Rossman, K. L., & Der, C. J. (2014). Rho guanine nucleotide exchange factors: Regulators of Rho GTPase activity in development and disease. *Oncogene*, *33*(31), 4021–4035. https://doi.org/10.1038/onc.2013.362

Craddock, C., Lavagi, I., & Yang, Z. (2012). New insights into Rho signaling from plant ROP/Rac GTPases. *Trends in Cell Biology*, *22*(9), 492–501. https://doi.org/10.1016/j.tcb.2012.05.002

Cui, S., Suzaki, T., Tominaga-Wada, R., & Yoshida, S. (2017). Regulation and functional diversification of root hairs. *Seminars in Cell & Developmental Biology*, 1–8. https://doi.org/10.1016/j.semcdb.2017.10.003

Cutler, S. R., Ehrhardt, D. W., Griffitts, J. S., & Somerville, C. R. (2000). Random GFP::cDNA fusions enable visualization of subcellular structures in cells of Arabidopsis at a high frequency. *Proceedings of the National Academy of Sciences of the United States of America*, *97*(7), 3718–3723. https://doi.org/10.1073/pnas.97.7.3718

De Baets, S., Denbigh, T. D. G., Smyth, K. M., Eldridge, B. M., Weldon, L., Higgins, B., … Grierson, C. S. (2020). Micro-scale interactions between Arabidopsis root hairs and soil particles influence soil erosion. *Communications Biology*, *3*(1), 1–11. https://doi.org/10.1038/s42003-020-0886-4

Denninger, P. (2018). *PhD-Thesis: Timing of polar protein accumulation and signaling in Arabidopsis thaliana*.

Denninger, P., Reichelt, A., Schmidt, V. A. F., Mehlhorn, D. G., Asseck, L. Y., Stanley, C. E., … Grossmann, G. (2019). Distinct RopGEFs Successively Drive Polarization and

Outgrowth of Root Hairs. *Current Biology*, *29*(11), 1854-1865.e5. https://doi.org/10.1016/j.cub.2019.04.059

Depuydt, S., Rodriguez-Villalon, A., Santuari, L., Wyser-Rmili, C., Ragni, L., & Hardtke, C. S. (2013). Suppression of Arabidopsis protophloem differentiation and root meristem growth by CLE45 requires the receptor-like kinase BAM3. *Proceedings of the National Academy of Sciences of the United States of America*, *110*(17), 7074–7079. https://doi.org/10.1073/pnas.1222314110

Dettmer, J., & Friml, J. (2011). Cell polarity in plants: When two do the same, it is not the same.... *Current Opinion in Cell Biology*, *23*(6), 686–696. https://doi.org/10.1016/j.ceb.2011.09.006

Dovas, A., & Couchman, J. R. (2005). RhoGDI: Multiple functions in the regulation of Rho family GTPase activities. *Biochemical Journal*, *390*(1), 1–9. https://doi.org/10.1042/BJ20050104

Drubin, D. G., & Nelson, W. J. (1996). Origins of cell polarity. *Cell*, *84*(3), 335–344. https://doi.org/10.1016/S0092-8674(00)81278-7

Duan, Q., Kita, D., Li, C., Cheung, A. Y., & Wu, H.-M. (2010). FERONIA receptor-like kinase regulates RHO GTPase signaling of root hair development. *Proceedings of the National Academy of Sciences*, *107*(41), 17821–17826. https://doi.org/10.1073/pnas.1005366107

Dubrovsky, J. G., Sauer, M., Napsucialy-Mendivil, S., Ivanchenko, M. G., Friml, J., Shishkova, S., … Benková, E. (2008). Auxin acts as a local morphogenetic trigger to specify lateral root founder cells. *Proceedings of the National Academy of Sciences of the United States of America*, *105*(25), 8790–8794. https://doi.org/10.1073/pnas.0712307105

Dunker, A. K., Cortese, M. S., Romero, P., Iakoucheva, L. M., & Uversky, V. N. (2005). Flexible nets: The roles of intrinsic disorder in protein interaction networks. *FEBS Journal*, *272*(20), 5129–5148. https://doi.org/10.1111/j.1742-4658.2005.04948.x

Durek, P., Schmidt, R., Heazlewood, J. L., Jones, A., MacLean, D., Nagel, A., … Schulze, W. X. (2009). PhosPhAt: The Arabidopsis thaliana phosphorylation site database. An update. *Nucleic Acids Research*, *38*(SUPPL.1), 828–834. https://doi.org/10.1093/nar/gkp810

Escobar-Restrepo, J. M., Huck, N., Kessler, S., Gagliardini, V., Gheyselinck, J., Yang, W.-C., & Grossniklaus, U. (2007). The FERONIA Receptor-like Kinase Mediates Male-Female Interactions The FERONIA Receptor-like Kinase Mediates Male-Female Interactions During Pollen Tube Reception Mediates Male-Female Interactions During Pollen Tube Reception. *Science*, *317*(October), 656–660.

Etienne-Manneville, S. (2004). Cdc42 - the centre of polarity. *Journal of Cell Science*, *117*(8), 1291–1300. https://doi.org/10.1242/jcs.01115

Farquhar, L. (1996). *Peterson-Farquhar1996_Article_RootHairsSpecializedTubularCel.pdf*. *62*(MARCH), 1–40.

Feiguelman, G., Fu, Y., & Yalovsky, S. (2017). ROP GTPases structure-function and signaling pathways. In *Plant Physiology*. https://doi.org/10.1104/pp.17.01415

Foreman, J., Demidchik, V., Bothwell, J. H. F., Mylona, P., Miedema, H., Angel Torres, M., … Dolan, L. (2003). Reactive oxygen species produced by NADPH oxidase regulate plant cell growth. *Nature*, *422*(6930), 442–446. https://doi.org/10.1038/nature01485

Friml, J., Yang, X., Michniewicz, M., Weijers, D., Quint, A., Tietz, O., … Offringa, R. (2004). A PINOID-dependent binary switch in apical-basal PIN polar targeting directs auxin efflux. *Science*, *306*(5697), 862–865. https://doi.org/10.1126/science.1100618

Fu, Y., Gu, Y., Zheng, Z., Wasteneys, G., & Yang, Z. (2005). Arabidopsis interdigitating cell growth requires two antagonistic pathways with opposing action on cell morphogenesis. *Cell*, *120*(5), 687–700. https://doi.org/10.1016/j.cell.2004.12.026

Fu, Y., Xu, T., Zhu, L., Wen, M., & Yang, Z. (2009). A ROP GTPase Signaling Pathway Controls Cortical Microtubule Ordering and Cell Expansion in Arabidopsis. *Current Biology*, *19*(21), 1827–1832. https://doi.org/10.1016/j.cub.2009.08.052

Fu, Y., & Yang, Z. (2001). Rop GTPase: A master switch of cell polarity development in plants. *Trends in Plant Science*, *6*(12), 545–547. https://doi.org/10.1016/S1360-1385(01)02130-6

Gälweiler, L., Guan, C., Müller, A., Wisman, E., Mendgen, K., Yephremov, A., & Palme, K. (1998). Regulation of polar auxin transport by AtPIN1 in Arabidopsis vascular tissue. *Science*, *282*(5397), 2226–2230. https://doi.org/10.1126/science.282.5397.2226

Geldner, N., Firml, J., Stierhof, Y. D., Jürgens, G., & Palme, K. (2001). Auxin transport inhibitors block PIN1 and vessicle trafficing. *Nature*, *413*(9), 425-428.

Geldner, N., Anders, N., Wolters, H., Keicher, J., Kornberger, W., Muller, P., … Jürgens, G. (2003). The Arabidopsis GNOM ARF-GEF mediates endosomal recycling, auxin transport, and auxin-dependent plant growth. *Cell*, *112*(2), 219–230. https://doi.org/10.1016/S0092-8674(03)00003-5

Gendre, D., Baral, A., Dang, X., Esnay, N., Boutte, Y., Stanislas, T., … Bhalerao, R. P. (2019). Rho-of-plant activated root hair formation requires arabidopsis YIP4a/b gene function. *Development (Cambridge)*, *146*(5). https://doi.org/10.1242/dev.168559

Gingras, A. C., Abe, K. T., & Raught, B. (2019). Getting to know the neighborhood: using proximity-dependent biotinylation to characterize protein complexes and map organelles. *Current Opinion in Chemical Biology*, *48*(November 2018), 44–54. https://doi.org/10.1016/j.cbpa.2018.10.017

Goodstein, D. M., Shu, S., Howson, R., Neupane, R., Hayes, R. D., Fazo, J., … Rokhsar, D. S. (2012). Phytozome: A comparative platform for green plant genomics. *Nucleic Acids Research*, *40*(D1), 1178–1186. https://doi.org/10.1093/nar/gkr944

Grierson, C., & Schiefelbein, J. (2014). Root Hairs. *The Arabidopsis Book*, *41*(1), 1. https://doi.org/10.1199/tab.0060

Grossmann, G., Guo, W. J., Ehrhardt, D. W., Frommer, W. B., Sit, R. V., Quake, S. R., & Meier, M. (2011). The Rootchip: An integrated microfluidic chip for plant Science. *Plant Cell*, *23*(12), 4234–4240. https://doi.org/10.1105/tpc.111.092577

Grunewald, W., & Friml, J. (2010). The march of the PINs: Developmental plasticity by dynamic polar targeting in plant cells. *EMBO Journal*, *29*(16), 2700–2714. https://doi.org/10.1038/emboj.2010.181

Gu, Y., Fu, Y., Dowd, P., Li, S., Vernoud, V., Gilroy, S., & Yang, Z. (2005). A Rho family GTPase controls actin dynamics and tip growth via two counteracting downstream pathways in pollen tubes. *Journal of Cell Biology*, *169*(1), 127–138. https://doi.org/10.1083/jcb.200409140

Gu, Y., Fu, Y., Dowd, P., Li, S., Vernoud, V., Gilroy, S., & Yang, Z. (2005). A Rho family GTPase controls actin dynamics and tip growth via two counteracting downstream pathways in pollen tubes. *Journal of Cell Biology*, *169*(1), 127–138. https://doi.org/10.1083/jcb.200409140

Gu, Y., Li, S., Lord, E. M., & Yang, Z. (2006). Members of a novel class of Arabidopsis Rho guanine nucleotide exchange factors control Rho GTPase-dependent polar growth. *Plant Cell*, *18*(2), 366–381. https://doi.org/10.1105/tpc.105.036434

Guan, Y., Guo, J., Li, H., & Yang, Z. (2013). Signaling in pollen tube growth: Crosstalk, feedback, and missing links. *Molecular Plant*, *6*(4), 1053–1064. https://doi.org/10.1093/mp/sst070

Gurskaya, N. G., Verkhusha, V. V., Shcheglov, A. S., Staroverov, D. B., Chepurnykh, T. V., Fradkov, A. F., … Lukyanov, K. A. (2006). Engineering of a monomeric green-to-red photoactivatable fluorescent protein induced by blue light. *Nature Biotechnology*, *24*(4), 461–465. https://doi.org/10.1038/nbt1191

Hart, M. J., Evat, A., Evans, T., Aaronsont, S. A., & Cerione, R. A. (1991). *oncogene product*. *354*(November), 311–314.

Hazak, O., Bloch, D., Poraty, L., Sternberg, H., Zhang, J., Friml, J., & Yalovsky, S. (2010). A Rho scaffold integrates the secretory system with feedback mechanisms in regulation of auxin distribution. *PLoS Biology*, *8*(1). https://doi.org/10.1371/journal.pbio.1000282

Hazak, O., Obolski, U., Prat, T., Friml, J., Hadany, L., & Yalovsky, S. (2014). Bimodal regulation of ICR1 levels generates self-organizing auxin distribution. *Proceedings of*

the National Academy of Sciences of the United States of America, *111*(50), E5471–E5479. https://doi.org/10.1073/pnas.1413918111

Heazlewood, J. I., Durek, P., Hummel, J., Selbig, J., Weckwerth, W., Walther, D., & Schulze, W. X. (2008). PhosPhAt : A database of phosphorylation sites in Arabidopsis thaliana and a plant-specific phosphorylation site predictor. *Nucleic Acids Research*, *36*(SUPPL. 1), 1015–1021. https://doi.org/10.1093/nar/gkm812

Hoffman, G. R., & Cerione, R. A. (2000). Flipping the switch: The structural basis for signaling through the CRIB motif. *Cell*, *102*(4), 403–406. https://doi.org/10.1016/S0092-8674(00)00045-3

Hruz, T., Laule, O., Szabo, G., Wessendorp, F., Bleuler, S., Oertle, L., … Zimmermann, P. (2008). Genevestigator V3: A Reference Expression Database for the Meta-Analysis of Transcriptomes. *Advances in Bioinformatics*, *2008*, 1–5. https://doi.org/10.1155/2008/420747

Huang, C., jiao, X., Yang, L., Zhang, M., Dai, M., Wang, L., … Song, C. (2019). ROP-GEF signal transduction is involved in AtCAP1-regulated root hair growth. *Plant Growth Regulation*, *87*(1), 1–8. https://doi.org/10.1007/s10725-018-0448-7

Huang, F., Zago, M. K., Abas, L., van Marion, A., Galván-Ampudia, C. S., & Offringa, R. (2010). Phosphorylation of conserved PIN motifs directs Arabidopsis PIN1 polarity and auxin transport. *Plant Cell*, *22*(4), 1129–1142. https://doi.org/10.1105/tpc.109.072678

Huang, G. Q., Li, E., Ge, F. R., Li, S., Wang, Q., Zhang, C. Q., & Zhang, Y. (2013). Arabidopsis RopGEF4 and RopGEF10 are important for FERONIA-mediated developmental but not environmental regulation of root hair growth. *New Phytologist*, *200*(4), 1089–1101. https://doi.org/10.1111/nph.12432

Huck, N., Moore, J. M., Federer, M., & Grossniklaus, U. (2003). The Arabidopsis mutant feronia disrupts the female gametophytic control of pollen tube receptor. *Development*, *130*(10), 2149–2159. https://doi.org/10.1242/dev.00458

Hunter, T. (2007). The Age of Crosstalk: Phosphorylation, Ubiquitination, and Beyond. *Molecular Cell*, *28*(5), 730–738. https://doi.org/10.1016/j.molcel.2007.11.019

Hwang, J.-U., Wu, G., Yan, A., Lee, Y.-J., Grierson, C. S., & Yang, Z. (2010). Pollen-tube tip growth requires a balance of lateral propagation and global inhibition of Rho-family GTPase activity. *Journal of Cell Science*, *123*(3), 340–350. https://doi.org/10.1242/jcs.039180

Hwang, J. U., Gu, Y., Lee, Y. J., & Yang, Z. (2005). Oscillatory ROP GTPase Activation Leads to the Oscillatory Polarized Growth of Pollen Tubes. *Molecular Biology of the Cell*, *16*, 5385–5399. https://doi.org/10.1091/mbc.E05

Hwang, J. U., Vernoud, V., Szumlanski, A., Nielsen, E., & Yang, Z. (2008). A Tip-Localized RhoGAP Controls Cell Polarity by Globally Inhibiting Rho GTPase at the Cell Apex. *Current Biology*, *18*(24), 1907–1916. https://doi.org/10.1016/j.cub.2008.11.057

Jeon, B. W., Hwang, J. U., Hwang, Y., Song, W. Y., Fu, Y., Gu, Y., … Lee, Y. (2008). The Arabidopsis small G protein ROP2 is activated by light in guard cells and inhibits light-induced stomatal opening. *Plant Cell*, *20*(1), 75–87. https://doi.org/10.1105/tpc.107.054544

Jones, A. R., Kramer, E. M., Knox, K., Swarup, R., Bennett, M. J., Lazarus, C. M., … Grierson, C. S. (2009). Auxin transport through non-hair cells sustains root-hair development. *Nature Cell Biology*, *11*(1), 78–84. https://doi.org/10.1038/ncb1815

Jones, M. A., Raymond, M. J., Yang, Z., & Smirnoff, N. (2007). NADPH oxidase-dependent reactive oxygen species formation required for root hair growth depends on ROP GTPase. *Journal of Experimental Botany*, *58*(6), 1261–1270. https://doi.org/10.1093/jxb/erl279

Jones, M. A., Shen, J.-J., Fu, Y., Li, H., Yang, Z., & Grierson, C. S. (2002). The Arabidopsis Rop2 GTPase is a positive regulator of both root hair initiation and tip growth. *The Plant Cell*, *14*(April), 763–776. https://doi.org/10.1105/tpc.010359

Jungk, A. (2001). Root hairs and the acquisition of plant nutrients from soil. *Journal of Plant Nutrition and Soil Science*, *164*(2), 121–129. https://doi.org/10.1002/1522-2624(200104)164:2<121::AID-JPLN121>3.0.CO;2-6

Kang, E., Zheng, M., Zhang, Y., Yuan, M., Yalovsky, S., Zhu, L., & Fu, Y. (2017). The microtubule-associated protein MAP18 affects ROP2 GTPase activity during root hair growth. *Plant Physiology*, *174*(1), 202–222. https://doi.org/10.1104/pp.16.01243

Kang, P. J., Sanson, A., Lee, B., & Park, H. O. (2001). A GDP/GTP exchange factor involved in linking a spatial landmark to cell polarity. *Science*, *292*(5520), 1376–1378. https://doi.org/10.1126/science.1060360

Kania, U., Fendrych, M., & Friml, J. (2014). Polar delivery in plants; commonalities and differences to animal epithelial cells. *Open Biology*, *4*(4), 140017–140017. https://doi.org/10.1098/rsob.140017

Kanie, T., & Jackson, P. (2018). Guanine Nucleotide Exchange Assay Using Fluorescent MANT-GDP. *Bio-Protocol*, *8*(7). https://doi.org/10.21769/bioprotoc.2795

Kaothien, P., Sung, H. O., Shuai, B., Wengier, D., Cotter, R., Kelley, D., … McCormick, S. (2005). Kinase partner protein interacts with the LePRK1 and LePRK2 receptor kinases and plays a role in polarized pollen tube growth. *Plant Journal*, *42*(4), 492–503. https://doi.org/10.1111/j.1365-313X.2005.02388.x

Kato, J., Kaziro, Y., & Satoh, T. (2000). Activation of the guanine nucleotide exchange factor Dbl following ACK1-dependent tyrosine phosphorylation. *Biochemical and Biophysical Research Communications*, *268*(1), 141–147. https://doi.org/10.1006/bbrc.2000.2106

Kinoshita, T., Caño-Delgado, A., Seto, H., Hiranuma, S., Fujioka, S., Yoshida, S., & Chory, J. (2005). Binding of brassinosteroids to the extracellular domain of plant receptor kinase BRI1. *Nature*, *433*(7022), 167–171. https://doi.org/10.1038/nature03227

Kleine-Vehn, J., & Friml, J. (2008). Polar targeting and endocytic recycling in auxin-dependent plant development. *Annual Review of Cell and Developmental Biology*, *24*, 447–473. https://doi.org/10.1146/annurev.cellbio.24.110707.175254

Kost, B. (2008). *Spatial control of Rho (Rac-Rop) signaling in tip-growing plant cells*. (February), 119–127. https://doi.org/10.1016/j.tcb.2008.01.003

Lampropoulos, A., Sutikovic, Z., Wenzl, C., Maegele, I., Lohmann, J. U., & Forner, J. (2013). GreenGate - A novel, versatile, and efficient cloning system for plant transgenesis. *PLoS ONE*, *8*(12). https://doi.org/10.1371/journal.pone.0083043

Lavy, M., Bloch, D., Hazak, O., Gutman, I., Poraty, L., Sorek, N., … Yalovsky, S. (2007). A Novel ROP/RAC Effector Links Cell Polarity, Root-Meristem Maintenance, and Vesicle Trafficking. *Current Biology*, *17*(11), 947–952. https://doi.org/10.1016/j.cub.2007.04.038

Lemmon, M. A., Ferguson, K. M., & Abrams, C. S. (2002). Pleckstrin homology domains and the cytoskeleton. *FEBS Letters*, *513*(1), 71–76. https://doi.org/10.1016/S0014-5793(01)03243-4

Leyser, O. (2018). Auxin signaling. *Plant Physiology*, *176*(1), 465–479. https://doi.org/10.1104/pp.17.00765

Leyser, O. (2011). Auxin, self-organisation, and the colonial nature of plants. *Current Biology*, *21*(9), R331–R337. https://doi.org/10.1016/j.cub.2011.02.031

Li, E., Cui, Y., Ge, F. R., Chai, S., Zhang, W. T., Feng, Q. N., … Zhang, Y. (2018a). AGC1.5 Kinase Phosphorylates RopGEFs to Control Pollen Tube Growth. *Molecular Plant*, *11*(9), 1198–1209. https://doi.org/10.1016/j.molp.2018.07.004

Li, J., & Chory, J. (1997). A putative leucine-rich repeat receptor kinase involved in brassinosteroid signal transduction. *Cell*, *90*(5), 929–938. https://doi.org/10.1016/s0092-8674(00)80357-8

Li, S., Gu, Y., Yan, A., Lord, E., & Yang, Z. B. (2008). RIP1 (ROP Interactive Partner 1)/ICR1 marks pollen germination sites and may act in the ROP1 pathway in the control of polarized pollen growth. *Molecular Plant*, *1*(6), 1021–1035. https://doi.org/10.1093/mp/ssn051

Li, Y., & Qi, B. (2017). Progress toward understanding protein S-acylation: Prospective in plants. *Frontiers in Plant Science*, *8*(March), 1–20. https://doi.org/10.3389/fpls.2017.00346

Li, Z., Takahashi, Y., Scavo, A., Brandt, B., Nguyen, D., & Rieu, P. (2018b). *Abscisic acid-induced degradation of Arabidopsis guanine nucleotide exchange factor requires calcium-dependent protein kinases*. https://doi.org/10.1073/pnas.1719659115

Li, Z., Waadt, R., & Schroeder, J. I. (2016). Release of GTP Exchange Factor Mediated Down-Regulation of Abscisic Acid Signal Transduction through ABA-Induced Rapid Degradation of RopGEFs. *PLoS Biology*, *14*(5), 1–27. https://doi.org/10.1371/journal.pbio.1002461

Luschnig, C., Gaxiola, R. A., Grisafi, P., & Fink, G. R. (1998). EIR1, a root-specific protein involved in auxin transport, is required for gravitropism in Arabidopsis thaliana. *Genes and Development*, *12*(14), 2175–2187. https://doi.org/10.1101/gad.12.14.2175

Maathuis, F. J. M. (2008). Conservation of protein phosphorylation sites within gene families and across species. *Plant Signaling and Behavior*, *3*(11), 1011–1013. https://doi.org/10.4161/psb.6721

Madeira, F., Park, Y. M., Lee, J., Buso, N., Gur, T., Madhusoodanan, N., … Lopez, R. (2019). The EMBL-EBI search and sequence analysis tools APIs in 2019. *Nucleic Acids Research*, *47*(W1), W636–W641. https://doi.org/10.1093/nar/gkz268

Magliozzi, R., Kim, J., Low, T. Y., Heck, A. J. R., & Guardavaccaro, D. (2014). Degradation of Tiaml by casein kinase 1 and the SCFßTrCP ubiquitin ligase controls the duration of mTOR-S6K signaling. *Journal of Biological Chemistry*, *289*(40), 27400–27409. https://doi.org/10.1074/jbc.M114.575571

Mayer, U., Buttner, G., & Jurgens, G. (1993). Apical-basal pattern formation in the Arabidopsis embryo: Studies on the role of the gnom gene. *Development*, *117*(1), 149–162.

McKinney, S. A., Murphy, C. S., Hazelwood, K. L., Davidson, M. W., & Looger, L. L. (2009). A bright and photostable photoconvertible fluorescent protein. *Nature Methods*, *6*(2), 131–133. https://doi.org/10.1038/nmeth.1296

Mercado-Blanco, J., & Prieto, P. (2012). Bacterial endophytes and root hairs. *Plant and Soil*, *361*(1–2), 301–306. https://doi.org/10.1007/s11104-012-1212-9

Miller, K. E., Kang, P. J., & Park, H. O. (2020). Regulation of Cdc42 for polarized growth in budding yeast. *Microbial Cell*, *7*(7), 175–189. https://doi.org/10.15698/mic2020.07.722

Mionnet, C., Bogliolo, S., & Arkowitz, R. A. (2008). Oligomerization regulates the localization of Cdc24, the Cdc42 activator in Saccharomyces cerevisiae. *Journal of Biological Chemistry*, *283*(25), 17515–17530. https://doi.org/10.1074/jbc.M800305200

Molendijk, A. J., Bischoff, F., Rajendrakumar, C. S. V., Friml, J., Braun, M., Gilroy, S., & Palme, K. (2001). Arabidopsis thaliana Rop GTPases are localized to tips of root hairs and control polar growth. *EMBO Journal*, *20*(11), 2779–2788. https://doi.org/10.1093/emboj/20.11.2779

Muroyama, A., & Bergmann, D. (2019). Plant cell polarity: Creating diversity from inside the box. *Annual Review of Cell and Developmental Biology*, Vol. 35, pp. 309–336. https://doi.org/10.1146/annurev-cellbio-100818-125211

Nagawa, S., Xu, T., & Yang, Z. (2010). RHO GTPase in plants: Conservation and invention of regulators and effectors. *Small GTPases*, *1*(2), 78–88. https://doi.org/10.4161/sgtp.1.2.14544

Nakamura, T., Kurokawa, K., Kiyokawa, E., & Matsuda, M. (2006). Analysis of the spatiotemporal activation of Rho GTPases using raichu probes. *Methods in Enzymology*, *406*(1989), 315–332. https://doi.org/10.1016/S0076-6879(06)06023-X

Nelson, W. J. (2003). Adaptation of core mechanisms to generate cell polarity. *Nature*, *422*(6933), 766–774. https://doi.org/10.1038/nature01602

Nethe, M., & Hordijk, P. L. (2010). The role of ubiquitylation and degradation in RhoGTPase signalling. *Journal of Cell Science*, *123*(23), 4011–4018. https://doi.org/10.1242/jcs.078360

Park, H. O., Chant, J., & Herskowitz, I. (1993). BUD2 encodes a GTPase-activating protein for Budl/Rsrl necessary for proper bud-site selection in yeast. *Nature*, *365*(6443), 269–274. https://doi.org/10.1038/365269a0

Payne, R. J. H., & Grierson, C. S. (2009). A theoretical model for ROP localisation by auxin in arabidopsis root hair cells. *PLoS ONE*, *4*(12). https://doi.org/10.1371/journal.pone.0008337

Pitts, R. J., Cernac, A., & Estelle, M. (1998). Auxin and ethylene promote root hair elongation in Arabidopsis. *Plant Journal*, *16*(5), 553–560. https://doi.org/10.1046/j.1365-313X.1998.00321.x

Preibisch, S., Saalfeld, S., & Tomancak, P. (2009). Globally optimal stitching of tiled 3D microscopic image acquisitions. *Bioinformatics*, *25*(11), 1463–1465. https://doi.org/10.1093/bioinformatics/btp184

Qiu, J. L., Jilk, R., Marks, M. D., & Szymanski, D. B. (2002). The Arabidopsis SPIKE1 gene is required for normal cell shape control and tissue development. *Plant Cell*, *14*(1), 101–118. https://doi.org/10.1105/tpc.010346

Ren, J., Wen, L., Gao, X., Jin, C., Xue, Y., & Yao, X. (2008). CSS-Palm 2.0: An updated software for palmitoylation sites prediction. *Protein Engineering, Design and Selection*, *21*(11), 639–644. https://doi.org/10.1093/protein/gzn039

Riely, B. K., He, H., Venkateshwaran, M., Sarma, B., Schraiber, J., Ané, J. M., & Cook, D. R. (2011). Identification of legume RopGEF gene families and characterization of a Medicago truncatula RopGEF mediating polar growth of root hairs. *Plant Journal*, *65*(2), 230–243. https://doi.org/10.1111/j.1365-313X.2010.04414.x

Roemer, T., Madden, K., Chang, J., & Snyder, M. (1996). Selection of axial growth sites in yeast requires Axl2p, a novel plasma membrane glycoprotein. *Genes and Development*, *10*(7), 777–793. https://doi.org/10.1101/gad.10.7.777

Rossman, K. L., Der, C. J., & Sondek, J. (2005). GEF means go: Turning on Rho GTPases with guanine nucleotide-exchange factors. *Nature Reviews Molecular Cell Biology*, *6*(2), 167–180. https://doi.org/10.1038/nrm1587

Salehin, M., Bagchi, R., & Estelle, M. (2015). ScfTIR1/AFB-based auxin perception: Mechanism and role in plant growth and development. *Plant Cell*, *27*(1), 9–19. https://doi.org/10.1105/tpc.114.133744

Schiefelbein, J. W. (2000). Constructing a Plant Cell. The Genetic Control of Root Hair Development. *Plant Physiology*, *124*(4), 1525–1531. https://doi.org/10.1104/pp.124.4.1525

Schiefelbein, J. W., Shipley, A., & Rowse, P. (1992). Calcium influx at the tip of growing root-hair cells of Arabidopsis thaliana. *Planta*, *187*(4), 455–459. https://doi.org/10.1007/BF00199963

Schiefelbein, J. W., & Somerville, C. (1990). Genetic control of root hair development in Arabidopsis thaliana. *Plant Cell*, *2*(3), 235–243. https://doi.org/10.2307/3869138

Schindelin, J., Arganda-Carreras, I., Frise, E., Kaynig, V., Longair, M., Pietzsch, T., … Cardona, A. (2012). Fiji: An open-source platform for biological-image analysis. *Nature Methods*, *9*(7), 676–682. https://doi.org/10.1038/nmeth.2019

Schmidt, A., & Hall, A. (2002). Guanine nucleotide exchange factors for Rho GTPases : turning on the switch. *Gene Expression Patterns*, *16*, 1587–1609. https://doi.org/10.1101/gad.1003302.GENES

Schmidt, J. E., & Gaudin, A. C. M. (2017). Toward an Integrated Root Ideotype for Irrigated Systems. *Trends in Plant Science*, *22*(5), 433–443. https://doi.org/10.1016/j.tplants.2017.02.001

Shiu, S. H., & Bleecker, A. B. (2001). Receptor-like kinases from Arabidopsis form a monophyletic gene family related to animal receptor kinases. *Proceedings of the National Academy of Sciences of the United States of America*, *98*(19), 10763–10768. https://doi.org/10.1073/pnas.181141598

Snyder, J. T., Rossman, K. L., Baumeister, M. A., Pruitt, W. M., Siderovski, D. P., Der, C. J., … Sondek, J. (2001). Quantitative Analysis of the Effect of Phosphoinositide Interactions on the Function of Dbl Family Proteins. *Journal of Biological Chemistry*, *276*(49), 45868–45875. https://doi.org/10.1074/jbc.M106731200

Stanislas, T., Hüser, A., Barbosa, I. C. R., Kiefer, C. S., Brackmann, K., Pietra, S., … Grebe, M. (2015). Arabidopsis D6PK is a lipid domain-dependent mediator of root epidermal planar polarity. *Nature Plants*, *1*(November), 1–9. https://doi.org/10.1038/nplants.2015.162

Takeuchi, H., & Higashiyama, T. (2016). Tip-localized receptors control pollen tube growth and LURE sensing in Arabidopsis. *Nature*, *531*(7593), 245–248. https://doi.org/10.1038/nature17413

Tao, L. Z., Cheung, A. Y., & Wu, H. M. (2002). Plant Rac-like GTPases are activated by auxin and mediate auxin-responsive gene expression. *Plant Cell*, *14*(11), 2745–2760. https://doi.org/10.1105/tpc.006320

Tasaki, T., Sriram, S. M., Park, K. S., & Kwon, Y. T. (2012). The N-End rule pathway. *Annual Review of Biochemistry*, *81*(1), 261–289. https://doi.org/10.1146/annurev-biochem-051710-093308

Thomas, C., Fricke, I., Scrima, A., Berken, A., & Wittinghofer, A. (2007). Structural Evidence for a Common Intermediate in Small G Protein-GEF Reactions. *Molecular Cell*, *25*(1), 141–149. https://doi.org/10.1016/j.molcel.2006.11.023

Thomas, C., Fricke, I., Weyand, M., & Berken, A. (2009). 3D structure of a binary ROP-PRONE complex: The final intermediate for a complete set of molecular snapshots of the RopGEF reaction. *Biological Chemistry*, *390*(5–6), 427–435. https://doi.org/10.1515/BC.2009.049

Thomas, C., Weyand, M., Wittinghofer, A., & Berken, A. (2006). Purification and crystallization of the catalytic PRONE domain of RopGEF8 and its complex with Rop4 from Arabidopsis thaliana. *Acta Crystallographica Section F: Structural Biology and Crystallization Communications*, *62*(6), 607–610. https://doi.org/10.1107/S1744309106018689

Vernoud, V., Horton, A. C., Yang, Z., & Nielsen, E. (2003). Analysis of the Small GTPase Gene Superfamily of Arabidopsis 1. *Plant Physiology*, *131*(March), 1191–1208. https://doi.org/10.1104/pp.013052.GTPase

Vetter, I. R., & Wittinghofer, A. (2001). The guanine nucleotide-binding switch in three dimensions. *Science*, Vol. 294, pp. 1299–1304. https://doi.org/10.1126/science.1062023

Vieten, A., Sauer, M., Brewer, P. B., & Friml, J. (2007). Molecular and cellular aspects of auxin-transport-mediated development. *Trends in Plant Science*, *12*(4), 160–168. https://doi.org/10.1016/j.tplants.2007.03.006

Volgger, M., Lang, I., Ovečka, M., & Lichtscheidl, I. (2010). Plasmolysis and cell wall deposition in wheat root hairs under osmotic stress. *Protoplasma*, *243*(1), 51–62. https://doi.org/10.1007/s00709-009-0055-6

Vroemen, C. W., Langeveld, S., Mayer, U., Ripper, G., Jürgens, G., Van Kammen, A., & De Vries, S. C. (1996). Pattern formation in the arabidopsis embryo revealed by position-specific lipid transfer protein gene expression. *Plant Cell*, *8*(5), 783–791. https://doi.org/10.2307/3870281

Walsh, I., Martin, A. J. M., Di Domenico, T., Vullo, A., Pollastri, G., & Tosatto, S. C. E. (2011). CSpritz: Accurate prediction of protein disorder segments with annotation for

homology, secondary structure and linear motifs. *Nucleic Acids Research*, *39*(SUPPL. 2), 190–196. https://doi.org/10.1093/nar/gkr411

Wang, H., Chevalier, D., Larue, C., Cho, S. K., & Walkera, J. C. (2007). The Protein Phosphatases and Protein Kinases of Arabidopsis thaliana. *The Arabidopsis Book*, *1996*. https://doi.org/10.1199/tab.0106

Wang, Y., Zhang, W. Z., Song, L. F., Zou, J. J., Su, Z., & Wu, W. H. (2008). Transcriptome analyses show changes in gene expression to accompany pollen germination and tube growth in arabidopsis. *Plant Physiology*, *148*(3), 1201–1211. https://doi.org/10.1104/pp.108.126375

Weizmann, Y., Willner, I., Schmidt, J. J., Montemagno, C. D., Vogel, V., Block, S. M., … Schliwa, M. (2006). *References and Notes 1.* (May).

Wisniewska, J., Xu, J., Seifartová, D., Brewer, P. B., Růžička, K., Blilou, L., … Friml, J. (2006). Polar PIN localization directs auxin flow in plants. *Science*, *312*(5775), 883. https://doi.org/10.1126/science.1121356

Won, S. K., Lee, Y. J., Lee, H. Y., Heo, Y. K., Cho, M., & Cho, H. T. (2009). cis-element- and transcriptome-based screening of root hair-specific genes and their functional characterization in Arabidopsis. *Plant Physiology*, *150*(3), 1459–1473. https://doi.org/10.1104/pp.109.140905

Wu, G., Li, H., & Yang, Z. (2000). Arabidopsis RopGAPSs are a novel family of Rho GTPase-activating proteins that require the Cdc42/Rac-interactive binding motif for Rop-specific GTPase stimulation. *Plant Physiology*, *124*(4), 1625–1636. https://doi.org/10.1104/pp.124.4.1625

Wu, G., Gu, Y., Li, S., & Yang, Z. (2001). A genome-wide analysis of Arabidopsis Rop-interactive CRIB motif-containing proteins that act as Rop GTPase targets. *Plant Cell*, *13*(12), 2841–2856. https://doi.org/10.1105/tpc.13.12.2841

Xie, Y., Zheng, Y., Li, H., Luo, X., He, Z., Cao, S., … Ren, J. (2016). GPS-Lipid: A robust tool for the prediction of multiple lipid modification sites. *Scientific Reports*, *6*(June), 1–9. https://doi.org/10.1038/srep28249

Yan, A., Xu, G., & Yang, Z. B. (2009). Calcium participates in feedback regulation of the oscillating ROP1 Rho GTPase in pollen tubes. *Proceedings of the National Academy of Sciences of the United States of America*, *106*(51), 22002–22007. https://doi.org/10.1073/pnas.0910811106

Yang, Z. (2008). Cell Polarity Signaling in Arabidopsis. *Annu. Rev. Cell Dev. Biol.*, 551–575. https://doi.org/10.1146/annurev.cellbio.23.090506.123233

Yang, Z. (2002). Small GTPases: versatile signaling switches in plants. *The Plant Cell*, *14 Suppl*, S375–S388. https://doi.org/10.1105/tpc.001065.S376

Yang, Z., & Lavagi, I. (2012). Spatial control of plasma membrane domains: ROP GTPase-based symmetry breaking. *Current Opinion in Plant Biology*, *15*(6), 601–607. https://doi.org/10.1016/j.pbi.2012.10.004

Yao, Q., Ge, H., Wu, S., Zhang, N., Chen, W., Xu, C., … Xu, D. (2014). P3DB 3.0: From plant phosphorylation sites to protein networks. *Nucleic Acids Research*, *42*(D1), 1206–1213. https://doi.org/10.1093/nar/gkt1135

Yates, A. D., Achuthan, P., Akanni, W., Allen, J., Allen, J., Alvarez-Jarreta, J., … Flicek, P. (2020). Ensembl 2020. *Nucleic Acids Research*, *48*(D1), D682–D688. https://doi.org/10.1093/nar/gkz966

Yu, F., Qian, L., Nibau, C., Duan, Q., Kita, D., Levasseur, K., … Luan, S. (2012). FERONIA receptor kinase pathway suppresses abscisic acid signaling in Arabidopsis by activating ABI2 phosphatase. *Proceedings of the National Academy of Sciences*, *109*(36), 14693–14698. https://doi.org/10.1073/pnas.1212547109

Yu, Y., Song, J., Tian, X., Zhang, H., Li, L., & Zhu, H. (2018). Arabidopsis PRK6 interacts specifically with AtRopGEF8/12 and induces depolarized growth of pollen tubes when overexpressed. *Science China Life Sciences*, *61*(1), 100–112. https://doi.org/10.1007/s11427-016-9107-3

Zhang, H., Linster, E., Gannon, L., Leemhuis, W., Rundle, C. A., Theodoulou, F. L., & Wirtz, M. (2019). Tandem fluorescent protein timers for noninvasive relative protein lifetime measurement in plants. *Plant Physiology*, *180*(2), 718–731. https://doi.org/10.1104/pp.19.00051

Zhang, Y., He, J., & McCormick, S. (2009). Two Arabidopsis AGC kinases are critical for the polarized growth of pollen tubes. *Plant Journal*, *58*(3), 474–484. https://doi.org/10.1111/j.1365-313X.2009.03792.x

Zhang, Y., & McCormick, S. (2007). A distinct mechanism regulating a pollen-specific guanine nucleotide exchange factor for the small GTPase Rop in Arabidopsis thaliana. *Proceedings of the National Academy of Sciences*, *104*(47), 18830–18835. https://doi.org/10.1073/pnas.0705874104

Zheng, Z. L., & Yang, Z. (2000). The Rop GTPase: An emerging signaling switch in plants. *Plant Molecular Biology*, *44*(1), 1–9. https://doi.org/10.1023/A:1006402628948

Zhu, K., Debreceni, B., Bi, F., & Zheng, Y. (2001). Oligomerization of DH Domain Is Essential for Dbl-Induced Transformation. *Molecular and Cellular Biology*, *21*(2), 425–437. https://doi.org/10.1128/mcb.21.2.425-437.2001

VI. APPENDIX

1.4 List of abbreviations

Common abbreviation and units are used as accepted. More specific abbreviations used on this thesis are introduced in the text and listed in alphabetical order below.

A. thaliana; *Arabidopsis*; *At*	*Arabidopsis thaliana*
ABA	Abscisic acid
AU	Arbitrary unit
Axl2	AXIAL BUDDING 2
BAM3	BARELY ANY MERISTEM 3
BioID	Biotin identification
BLAST	Basic Local Alignment Search Tool
BRI1	BRASSINOSTEROID INSENSITIVE 1
Bud5	BUD SITE SELECTION PROTEIN 5
CA	Constitutively active
Ca^{2+}	Calcium
Cdc24/ 42p	CELL DIVISION CONTROL 24/ 42
CDS	Coding sequence
CHX	Cycloheximide
Col-0	Colambia-0 ecotype
CRIB	Cdc24/ Rac-Interactive Binding
CRISPR	Clustered Regularly Interspaced Short Palindromic Repeats
*Cr*RLK1L	*Catharanthus roseus* RLK1-like
DAG	Days after germination
Dbl	Diffuse B-cell lymphoma
DH	Dbl Homology
DN	Dominant negative
DOCK	DEDICATOR OF CYTOKINESIS
DS	Domain size
E. coli	*Escherichia coli*
F-actin	Filamentous actin/ actin microfilaments
FER	FERONIA
FL	Full length
FOV	Field of view
FRAP	Fluorescent Recovery After Photobleaching
FRET	Förster Resonance Energy Transfer
FWHM	Full Width at Half Maximum
GAP	GTPase-activating protein
GDI	Guanine nucleotide-dissociation inhibitor
GDP	Guanosine diphosphate
GEF	Guanine nucleotide exchange factor
GFP	Green fluorescent protein
Gm	*Glyine max*

GTP	Guanosine-5’-triphosphate
GTPase	Guanosine triphosphostases
HVR	Hypervariable region
ICR1	INTERACTOR OF CONSTITUTIVELY ACTIVE ROP 1
KPP	KINASE PARTNER PROTEIN
LB	Lysogeny broth
LRR	Leucine-Rich Repeat
LTI6B	LOW TEMPERATURE INDUCED PROTEIN 6B
MANT	N-Methylanthraniloyl
mCit/ mCherry/ mTurq	Monomeric Citrine/ Cherry/ Turquoise
Mt	*Medicago truncatula*
N3/ N4/ N14	N-terminus of RopGEF3/4/14
NASC	Nottingham *Arabidopsis* Stock Centre
PH	Pleckstrin Homology
PI	Polarity index
PID	PINOID
PIN	PIN-FORMED
PRK	POLLEN-SPECIFIC RECEPTOR-LIKE KINASE
PRONE3/4/14	Plant-specific Rop Nucleotide Exchanger of RopGEF3/4/14
Raichu	Ras And Interacting Protein Chimeric Unit
RBH	Reciprocal Best Hit
REN	ROP1 ENHANCER
RHID	Root Hair Initiation Domain
RIC	ROP-INTERACTIVE CRIB MOTIF-CONTAINING
RLK	Receptor-like kinase
ROI	Region of interest
ROP	Rho-Of-Plants
ROS	Reactive oxygen species
Rsr1	RAS-RELATED PROTEIN 1
RTK	Receptor tyrosine kinases
S1-3	PRONE subdomains 1-3
SCN	SUPERCENTIPEDE
SEC3A	EXOCYST COMPLEX COMPONENT SEC3A
SEM	Standard error of the mean
sfGFP	Superfolder GFP
Sl	*Solanum lycopersicum*
SPK1	SPIKE1
St	*Solanum tuberosum*
TAIR	The *Arabidopsis* Information Resource
T-DNA	Transfer DNA
Tiam1	T-LYMPHOMA INVASION AND METASTASIS 1
UPS	Ubiquitin/ Proteasome System
WS	Wassilewskija

1.5 List of figures

1.6 List of tables

VII. ACKNOWLEDGEMENTS/ DANKSAGUNGEN

At the end, I would like to thank everyone, who accompanied, supported and advised me during the four years of my PhD.

I would like to thank Prof. Dr. Guido Grossmann for offering this PhD project to me and for the scientific guidance and discussions throughout this project. I am grateful that you made the completion of this PhD project possible and for your advices and feedback on this thesis.

I also thank Prof. Dr. Karin Schumacher and Prof. Dr. Marius Lemberg for the yearly TAC meetings, scientific discussion and critical advices on my project. Furthermore, I would like to thank Dr. Sebastian Wolf for completing my examination commission. I would also like to thank Dr. Jan-Felix Evers for providing access to the spinning disk microscope.

A very special thanks goes to my PhD fellows, who sweetened my everyday PhD life and created so many great and fun memories of the PhD time. The best thing about my PhD is that I met you and we got though this together.

One big thanks goes to Philipp, who introduced me into the methods of plant science and who laid the foundation for this project. Another special thanks goes to Vanessa Aphaia Fiona and Rik for being wonderful, always helpful colleagues. Despite not being official members of the Grossmann lab, Linda and Alan from the Evers lab were at least as close as actual team members and I am really happy that we had this great neighborhood on the 4th floor. Thank you for all the nice breaks in the kitchen and the bakery, for the nice and hilarious conversations, for the fun evenings we spent together and for your support in every aspect! Then I would like to thank Marjourette and Milan. It was very enriching that you joined the lab and I thank you for always being so kind and supportive.

A superspecial thank you goes to Nina! Thank you for becoming my friend and for your company in our little beaks. I enjoyed our great machine gun conversations so much (finally somebody, who can keep up with my speaking rate), they really made my days! Thank you for your open ears, for your positive aura and your support.

Of course, there are many more people, who supported me in one way or the other, therefore, a comprehensive thank you goes to the Schumacher lab, the Raissig lab and the whole COS community.

Ganz besonderer Dank gilt auch denjenigen, die mich außerhalb des PhDs unterstützt und immer wieder geerdet haben.

Dazu möchte ich mich zuerst bei der Freunde-Gang für die vielen schönen Feiern, Geburtstage, Urlaube, Badminton-, Tischtennis- und Spiele-Abende und Events in allen möglichen Konstellationen bedanken. Die Zeit mit euch ist wunderbar und hat mich während der Doktorarbeit immer wieder aufgebaut und die Sonnenseite des Lebens spüren lassen. Für die Zukunft wünsche ich mir, dass das immer so bleibt!

Besonders möchte ich mich bei Tibi bedanken für die schöne gemeinsame Zeit, für unsere Mittagessen im Bräu Stüble mit Kuchen und Espresso, die meine Freitage gerettet haben, für die vielen Spaziergänge, Gespräche mit gutem Essen und die chilligen Abende. Danke, Tibi!

Als nächstes möchte ich mich bei meinen Baschdl-Mädels bedanken, mit denen ich den ein oder anderen kreativen Abend verbringen durfte. Es ist so schön, dass wir die kreative Leidenschaft teilen und ich freue mich auf mehr Bastelprojekte mit euch. Jetzt ist die Doktorarbeit geschafft, jetzt gibt es kein Halten mehr, Mädels!

Ein weiterer Dank geht an meine Freundin Verena und ihre Mäuschen. Vielen Dank für die schönen Sonntagsbrunches und Ausflüge, die sich immer wie Urlaub angefühlt haben. Danke für deine Unterstützung, liebe Verena!

Schließlich möchte ich mich von Herzen bei meiner Familie bedanken. Liebe Mutti, lieber Daddy, liebe Schwesti, danke, dass ihr da seid! Ich danke euch, für eure unermüdliche Unterstützung und Hilfe in jeglicher Form. Danke, dass ihr mich mit Grundnahrungsmitteln und Eierlikör versorgt habt, danke für eure Besuche und die schöne Zeit bei euch, in der ich immer wieder neue Kraft tanken konnte.

Und zum Schluss geht ein ganz besonderer Dank an meinen Mann. Du bist ein wunderbarer Mensch, Ole. Du erlebst alle Hochs und Tiefs näher mit, als du vielleicht manchmal möchtest, und dafür danke ich dir. Ich bin froh, dich an meiner Seite zu wissen.